NASA TECHNICAL MEMORANDUM

NASA TM X-62,029

NASA TM X-62,029

AERODYNAMIC CHARACTERISTICS OF A LARGE-SCALE MODEL WITH A SWEPT WING AND AUGMENTED JET FLAP

Michael D. Falarski and David G. Koenig

Ames Research Center
and
U.S. Army Air Mobility R&D Laboratory
Moffett Field, Calif. 94035

July 1971

AERODYNAMIC CHARACTERISTICS OF A LARGE-SCALE MODEL WITH A SWEPT WING AND AUGMENTED JET FLAP

BY

Michael D. Falarski and David G. Koenig

Ames Research Center
and
U. S. Army Air Mobility R&D Laboratory

SUMMARY

This report presents data of tests of a large-scale swept augmentor wing model in the 40- by 80-foot wind tunnel. The data includes longitudinal characteristics with and without a horizontal tail as well as results of preliminary investigation of lateral-directional characteristics. The augmentor flap deflection was varied from 0° to 70.6° at isentropic Jet Thrust coefficients of 0 to 1.47. The tests were made at a Reynolds number from 2.43×10^6 to 4.1×10^6.

INTRODUCTION

The augmentor wing concept is being studied as one means for attaining STOL performance in turbofan powered aircraft. Initial tests on an unswept wing model in the 40- by 80-foot wind tunnel were reported on in reference 1. Another series of tests with the same model but with a modified augmentor configuration and with the model equipped with wing mounted engines are reported in reference 2.

The tests reported herein initiate the investigation of the application of the augmentor to a swept wing. The wing configuration of the model used was swept 27-1/2° at the quarter chord line but was similar to the unswept wing in aspect ratio, taper ratio, and spanwise extent of the augmentor. The tests were made out of ground effect for flap settings from 0° to 70° with and without a horizontal tail. A major portion of the tests were made at zero sideslip but a small amount of lateral stability and control data were obtained.

The tests were made in cooperation with the Defense Research Board of Canada and the De Havilland Aircraft of Canada Limited.

NOTATION

A	thrust augmentation ratio of jet augmentor, J_A/J_I
b	wing span, m(ft)
BLC	boundary layer control
c	chord, m(ft)
$\bar{c}$	mean aerodynamic chord, m(ft)
C_D	drag coefficient, $\frac{\text{drag}}{qS}$
C_{D_m}	total momentum drag coefficient due to gas generator and compressor gas flow
$C_{J_{AI}}$	isentropic augmentor jet force coefficient, (see text) $\frac{\text{isentropic force}}{qS}$
C_{J_I}	total isentropic jet thrust coefficient, $C_{J_{AI}} + C_{\mu_{aI}} + C_{\mu_{FI}}$
C_ℓ, C_R	rolling moment coefficient, $\frac{\text{rolling moment}}{qSb}$
C_L	lift coefficient, $\frac{\text{lift}}{qS}$
C_m	pitching moment coefficient, $\frac{\text{pitching moment}}{qS\bar{c}}$
C_n	yawing moment coefficient, $\frac{\text{yawing moment}}{qSb}$
$C_{T_{JP}}$	jet pipe thrust coefficient, $\frac{\text{thrust}}{qS}$
C_Y	side force coefficient, $\frac{\text{side force}}{qS}$
$C_{\mu_{aI}}$	isentropic aileron BLC coefficient, $\frac{\text{isentropic BLC force}}{qS}$
$C_{\mu_{FI}}$	isentropic fuselage BLC coefficient, $\frac{\text{isentropic BLC force}}{qS}$
d	distance between trailing edge of flap and shroud, m(ft) (see fig. 2(e))
i_t	horizontal tail incidence, positive with trailing edge down, deg

J_A	augmentor jet force at q = 0, n/m^2(psf)
J_I	isentropic jet force at q = 0, n/m^2(psf)
q	free-stream dynamic pressure, n/m^2(psf)
S	wing area, sq m(sq ft)
t	airfoil thickness, m(ft)
x	chordwise station, m(ft)
y	airfoil ordinate, m(ft)
Z_{JP}	distance between moment center and line of action of Jet-pipe residual thrust, m(ft)
α,AL	model angle of attack, deg
β	angle of sideslip of plane of symmetry, deg
δ_a	aileron deflection (δ_a = 45/60 means left aileron at 45°, right aileron at 60°) positive with trailing edge down, deg
δ_e	elevator deflection, positive with trailing edge down, deg
δ_f	augmentor flap deflection, positive with trailing edge down, deg (see figure 2(e))
δ_{ID}	augmentor intake door deflection, positive with leading edge down, deg (see figure 2(e))
δ_{JP}	deflection of jet pipes relative to fuselage datum plane, deg
δ_s	slat deflection, positive with leading edge down, deg (see figure 2(c))
δ_{SP}	spoiler deflection, trailing edge up, deg (see figure 2(k))
Δ_d	augmentor throttling, reduction in distance between trailing edge of flap and shorud in percent of d.
θ	augmentor jet angle relative to wing chord plane, deg

SUBSCRIPTS

a	aileron
A	augmentor
f	flap
F	fuselage
JP	jet-pipe
I	isentropic
L	left
R	right
s	slat
u	uncorrected
V	Viper
w	wing

MODEL AND APPARATUS

Basic Model

The model is shown installed in the wind tunnel in figure 1. Geometric details are shown in figure 2 and reference dimension are listed in table I - III. The air for the augmentor and BLC systems on the model was supplied by a pump consisting of a J-85 coupled pneumatically to two turbocompressors that were modified Viper engines. The turbocompressors supplied air for the augmentor and ailerons.

The wing and horizontal tail planform geometry are presented in figure 2(b) and 2(d). The wing leading edge slat geometry is presented in figure 2(c). To increase the maximum lift coefficient the right tip slat was modified during the test. The modification consisted of reducing the slat gap to .019c and increasing the overlap to .006c for the outboard 24.5% semispan.

Augmentor Flap

The geometry of the augmentor flap cross section is shown in figure 2(e). The augmentor is an ejector system consisting of a trailing edge primary nozzle (figure 2(f)) through which the compressed air is delivered, (lower) flap, (upper) shroud, and intake door. The secondary air is entrained from the wing upper surface, the slot between the intake door and shroud, and the tertiary gap between the wing lower surface and flap. The mixed jet is ejected downward between the flap and the shroud. The angle of the intake door was optimized for each flap deflection. During a series of tests the tertiary gap was sealed to determine its effect on augmentor performance (see figure 2(e)).

The ducting for the primary air and aileron BLC is shown in figures 2(g) and 2(h). Figure 2(h) shows the variation of duct diameter with wing span which was designed to maintain in duct mach number of .36.

Fuselage BLC

The fuselage BLC installation is shown in figure 2(j). It was located just aft of the wing leading edge in the part of the wing spanning the fuselage for the purpose of preventing airflow separation at the wing fuselage juncture by energizing the fuselage boundary layer. The BLC air was provided by J-85 compressor bleed air.

Aileron BLC

The geometry of the aileron BLC system is shown in figure 2(k). The system was fed through an extension of the augmentor primary air duct. Aileron blowing was therfore coupled with the augmentor output. Airflow to the aileron was approximately 5% of total turbo-compressor output.

Lateral Control System

The model was equipped with several methods for lateral control:

Ailerons.- Lift requirements for landing and takeoff resulted in symmetrical drooping of the BLC aileron by as much as 45°. Lateral control was obtained by differentially deflecting the ailerons.

Spoilers.- Upper wing panel type spoilers were installed on the left wing for lateral control as shown in figure 2(k). The spoilers were 11.2% of wing chord, located ahead of the aileron.

Augmentor Throttling.- A flap plate was installed on the lower portion of the flap of the outer 50% of the port wing augmentor as shown in figure 2(e).

This simulates a deflected aft portion of the flap to reduce the augmentor exit area and affect a local throttling of the augmentor eflux to create a rolling moment.

TEST

Test procedure consisted primarily of varying angle of attack at constant C_{J_I}. The angle of attack range was -8 to 30°. Sideslip range was from -6 to 11°. Augmentor flap deflection was varied from 0° (the shroud was left in its normal position) to 70.6°.

The position of the augmentor intake door was optimized at each flap deflection. The ailerons were normally deflected 30°. For each flap deflection tests were made at several $C_{J_{I's}}$.

DATA REDUCTION

For all force and moment data, the effects of compressor residual jet thrust, and the intake momentum drag of the fuselage mounted J85 and Viper engines, have been subtracted from the measured values. Forces and moments are referred to the stability axes. The corrections made for thrust and ram drag are as follows:

$$C_L = C_{L_u} - C_{T_{JP}} \text{ Sin } (\alpha u - \delta_{JP})$$

$$C_{D_{net}} = C_{Du} + C_{T_{JP}} \text{ Cos } (\alpha u - \delta_{JP}) - C_{D_{mJ85}} - C_{D_{MV}}$$

$$C_{m_{net}} = C_{m_u} - C_{T_{JP}} \frac{Z_{JP}}{\bar{c}}$$

Wind tunnel boundary corrections were based upon the "aerodynamic C_L", computed as follows:

$$C_{L_{AERO}} = C_{L_U} - C_{J_A} (A_{net}) \sin (\Theta + \alpha_u) \qquad \text{(Augmentor)}$$

$$-C\mu_{aL} \sin (\delta_{aL} + \alpha_u) \frac{Sa}{S} \qquad \text{(Aileron BLC, left)}$$

$$-C\mu_{aR} \sin (\delta_{aR} + \alpha_u) \frac{Sa}{S} \qquad \text{(Aileron BLC, right)}$$

$$-C\mu_F \sin\alpha_u \left(\frac{S_F}{S}\right) \qquad \text{(Fuselage BLC)}$$

Thus the following boundary corrections were made:

$$\alpha = \alpha_u + .458\, C_{L_{AERO}}$$

$$C_D = C_{D_u} + .00799\, C_{L_{AERO}}^{\ 2}$$

$$C_m = C_{m_u} + .023\, C_{L_{AERO}} \qquad \text{(tail on only)}$$

The moment center used for data computation was located longitudinally at 0.25 $\bar{c}$ and vertically 0.20 $\bar{c}$ below the wing chord datum.

The $C_{J_{AI}}$ is the force coefficient computed on the basis of the measured mass flow and total pressure in the duct prior to discharge (see figure 2(g) for measuring station). Based on previous tests of a similar nozzle (ref. 1 and 2), the nozzles losses are expected to be 5 to 10 percent, and therefore the nozzle force coefficient would be 5 to 10 percent lower than $C_{J_{AI}}$.

PRESENTATION OF DATA

The longitudinal aerodynamic characteristics of the model are presented in figures 3 to 26. Data with and without the horizontal tail are presented in these figures. An index to the figures is given in Table IV.

The lateral-directional characteristics of the model are presented in figures 27 to 39. The data includes the effect of spoilers, augmentor throttling, and differential aileron deflection. An index to these figures is shown in Table V.

REFERENCES

1. Koenig, D. G.; Corsiglia, V. R.; Morelli, J. P.: Aerodynamic Characteristics of a Large Scale Model with an Unswept Wing and Augmented Jet Flap. NASA TN D-4610, 1968.
2. Cook, A. M.; Aiken, T. N.: Low Speed Aerodynamic Characteristics of a Large Scale STOL Transport Model With an Augmented Jet Flap. NASA TM X-62017, 1971.

TABLE I. - WING REFERENCE DIMENSION

Wing area, sq m(sq ft)	21.36(230.0)
Aspect ratio	8.0
Span, m(ft)	13.08(42.895)
Taper ratio	0.30
Sweep at 1/4 chord, deg	27.5
Airfoil section	RAE 104
Root chord, m(ft)	2.515(8.25)
Tip chord, m(ft)	0.755(2.475)
Root thickness, percent	12 1/2
Tip thickness, percent	10 1/2
Augmentor span limits, Inner, m(ft) (percent)	1.111(3.645)(12.34)
Augmentor span limits, Outer, m(ft) (percent)	4.575(15.01)(70.0)
Wing area spanned by one augmentor, sq m(sq ft)	6.75(72.62)
Wing area spanned by one aileron, sq m(sq ft)	1.997(21.50)
Wing area spanned by fuselage, sq m(sq ft)	3.88(41.77)
Flap hinge axis, percent chord	68.543
Aileron hinge axis, percent chord	68.0
Incidence, camber, twist	0
Mean aerodynamic chord, m(ft)	1.793(5.880)

NOTE: All chords are measured in streamwise direction.

TABLE II. - TAIL REFERENCE DIMENSION

Horizontal Tail

Gross area, sq m(sq ft)	55.77(60.0)
Aspect ratio	4.5
Span, m(ft)	5.005(16.432)
Taper ratio	0.40
Sweep at 1/4 chord, deg	25
Airfoil section	RAE 104 with modified l.e.
Thickness/Chord ratio, percent	10
Root chord, m(ft)	1.591(5.22)
Tip chord, m(ft)	0.635(2.082)
Elevator hinge axis, percent chord	60
Elevator travel, deg	±30
Tailplane incidence, deg	±12
Tailplane arm, m(ft)	6.804(22.32)
Tailplane volume coefficient	0.990
Mean aerodynamic chord, m(ft)	1.114(3.654)

Vertical Fin

Fin arm, m(ft)	5.361(17.603)
Fin volume coefficient	0.07476

TABLE III. - COORDINATES OF R.A.E. 104 AIRFOIL(t/c max.=.10)

X/C	Y/C 100	X/C	Y/C 100
0	0	0.35	4.9300
0.001	0.3441	0.36	4.9488
0.002	0.4863	0.38	4.9775
0.003	0.5953	0.4	4.9946
0.004	0.6870	0.42	5.0000
0.005	0.7676	0.44	4.9937
0.006	0.8404	0.45	4.9862
0.007	0.9072	0.46	4.9756
0.0075	0.9387	0.48	4.9454
0.008	0.9692	0.5	4.9027
0.009	1.0274	0.52	4.8468
0.01	1.0824	0.54	4.7769
0.012	1.1842	0.55	4.7363
0.0125	1.2083	0.56	4.6917
0.014	1.2776	0.58	4.5802
0.016	1.3642	0.6	4.4650
0.018	1.4452	0.62	4.3113
0.02	1.5215	0.64	4.1370
0.025	1.6960	0.65	4.0438
0.03	1.8522	0.66	3.9473
0.035	1.9945	0.68	3.7452
0.04	2.1256	0.7	3.5331
0.05	2.3617	0.72	3.3128
0.06	2.5709	0.74	3.0861
0.07	2.7592	0.75	2.9708
0.075	2.8468	0.76	2.8545
0.08	2.9307	0.78	2.6103
0.09	3.0881	0.8	2.3819
0.1	3.2336	0.82	2.1437
0.12	3.4945	0.84	1.9055
0.14	3.7222	0.85	1.7864
0.15	3.8254	0.86	1.6673
0.16	3.9224	0.88	1.4202
0.18	4.0992	0.9	1.1910
0.2	4.2556	0.92	0.9528
0.22	4.3936	0.925	0.8932
0.24	4.5149	0.94	0.7146
0.25	4.5697	0.95	0.5955
0.26	4.6208	0.96	0.4764
0.28	4.7124	0.975	0.2977
0.3	4.7905	0.98	0.2382
0.32	4.8556	0.9875	0.1489
0.34	4.9082	1.0	0

TABLE IV. - INDEX OF DATA FIGURES; LONGITUDINAL

FIGURE	EFFECT	β	δ_f	δ_a	δ_s	SLAT MOD.	HORIZ. TAIL	FUS. BLC	C_{J_I}
3a	Tertiary seal	0	41.1	30	60	ON	OFF	OFF	1.47
b	↓	↓	↓	↓	↓	↓	↓	↓	.77
c	↓	↓	↓	↓	↓	↓	↓	↓	.36
d	↓	↓	↓	↓	↓	↓	↓	↓	↓
4a	↓	↓	70.6	↓	↓	↓	↓	↓	1.10
b	↓	↓	↓	↓	↓	↓	↓	↓	↓
5	δID	↓	↓	45	↓	OFF	↓	↓	.77
6	δa	↓	31.8	↓	↓	ON	↓	↓	.18, .77
7	↓	↓	41.1	↓	↓	↓	↓	↓	.77
8a	↓	↓	70.6	↓	↓	OFF	↓	↓	.77
b	↓	↓	↓	↓	↓	↓	↓	↓	.77, 1.10
c	↓	↓	↓	↓	50	↓	↓	↓	1.10
9a	↓	↓	↓	↓	60	↓	ON	↓	.77
b	↓	↓	↓	↓	↓	ON	↓	↓	↓
10a	FUS.BLC	↓	↓	15	↓	OFF	OFF	≃	↓
b	↓	↓	↓	45	↓	↓	↓	↓	1.10
c	↓	↓	↓	30	50	↓	↓	↓	1.10
d	↓	↓	↓	↓	60	ON	ON	↓	.77, 1.47
11a	↓	↓	↓	↓	50, 60	OFF	OFF	OFF	1.10
b	↓	↓	↓	↓	60	ON	↓	↓	↓
12a	δ_s	↓	↓	↓	↓	OFF	ON	↓	0
b	↓	↓	↓	↓	↓	↓	↓	↓	.77
13a	δ_e	↓	↓	↓	60	↓	↓	↓	1.10
b	↓	↓	↓	↓	↓	ON	↓	↓	.77
c	↓	↓	↓	↓	↓	↓	↓	↓	1.10
d	↓	↓	↓	↓	↓	ON, OFF	↓	↓	.77, 1.10
14	↓	↓	41.1	↓	↓	ON	↓	↓	.77
15	i_t	↓	↓	↓	↓	↓	↓	↓	1.10
16	C_{J_I}	↓	70.6	↓	↓	OFF	OFF	↓	.77
17	↓	↓	0	4	50	↓	↓	↓	↓
18	↓	↓	31.8	30	60	ON	↓	↓	↓
19a	↓	↓	41.1	↓	↓	OFF	↓	↓	↓
b	↓	↓	↓	↓	↓	ON	↓	↓	↓
20	↓	↓	51.1	↓	↓	OFF	↓	↓	↓
21	↓	↓	61.2	↓	↓	↓	↓	↓	↓
22a	↓	↓	70.6	↓	↓	↓	↓	↓	↓
b	↓	↓	↓	↓	↓	ON	↓	↓	↓
23	↓	↓	31.8	↓	↓	↓	ON	↓	↓
24	↓	↓	41.1	↓	↓	↓	↓	↓	↓
25	↓	↓	51.1	↓	↓	↓	↓	↓	↓
26a	↓	↓	70.6	↓	↓	OFF	↓	↓	↓
b	↓	↓	↓	↓	↓	↓	↓	↓	↓
c	↓	↓	↓	↓	↓	ON	↓	↓	↓

TABLE V. - INDEX OF DATA FIGURES: LATERAL-DIRECTIONAL.

FIGURE	EFFECT	β	δ_f	δ_a	δ_s	SLAT MOD.	HORIZ. TAIL	FUS. BLC	C_{J_I}
27a	δa	0	41.1	45/15	60	ON	ON	OFF	.77
b	↓	↓	↓	≈/30	↓	↓	↓	↓	↓
28a	↓	↓	70.6	45/15	↓	↓	↓	↓	↓
b	↓	↓	↓	≈/30	↓	↓	↓	↓	↓
c	↓	↓	↓	↓	↓	↓	↓	↓	.77,1.10
29	δa, α	↓	↓	45/15	↓	↓	↓	↓	.77
30	augmentor	↓	41.1	30	↓	↓	↓	↓	.77,1.10
31a	throttling	↓	↓	↓	↓	↓	↓	↓	↓
b	↓	↓	↓	≈/30	↓	↓	↓	↓	.77
32	↓	↓	70.6	30	↓	↓	↓	↓	.77,1.10
33a	↓	↓	↓	≈/30	↓	↓	↓	↓	.77
b	↓	↓	↓	30	↓	↓	↓	↓	↓
34a	δSP	↓	↓	↓	↓	↓	↓	↓	.77
b	↓	↓	↓	↓	↓	↓	↓	↓	.77,1.10
c	↓	↓	↓	≈/30	↓	↓	↓	↓	.77
35a	↓	↓	↓	30	↓	↓	↓	↓	.77
b	↓	↓	↓	↓	↓	↓	↓	↓	1.10
36a	$\beta,\alpha = 0$	↓	↓	↓	↓	↓	↓	↓	≈
b	$\beta,\alpha = 12$	↓	↓	↓	↓	↓	↓	↓	↓
c	β, α	↓	↓	↓	↓	↓	↓	↓	.77
d	↓	↓	↓	↓	↓	↓	↓	↓	↓
e	β	-6, +6	↓	↓	↓	↓	↓	↓	↓
37a	β, α= 4	↓	41.1	↓	↓	↓	↓	↓	≈
b	β, α=12	↓	↓	↓	↓	↓	↓	↓	↓
c	β, α	↓	↓	↓	↓	↓	↓	↓	.77
38	i_t	-6,0,+6	↓	↓	↓	↓	↓	↓	↓
39	TAIL	0	↓	↓	↓	↓	ON,OFF	↓	↓

(a) Top View

Figure 1.- Photographs of the model installed in the Ames 40- by 80-foot wind tunnel.

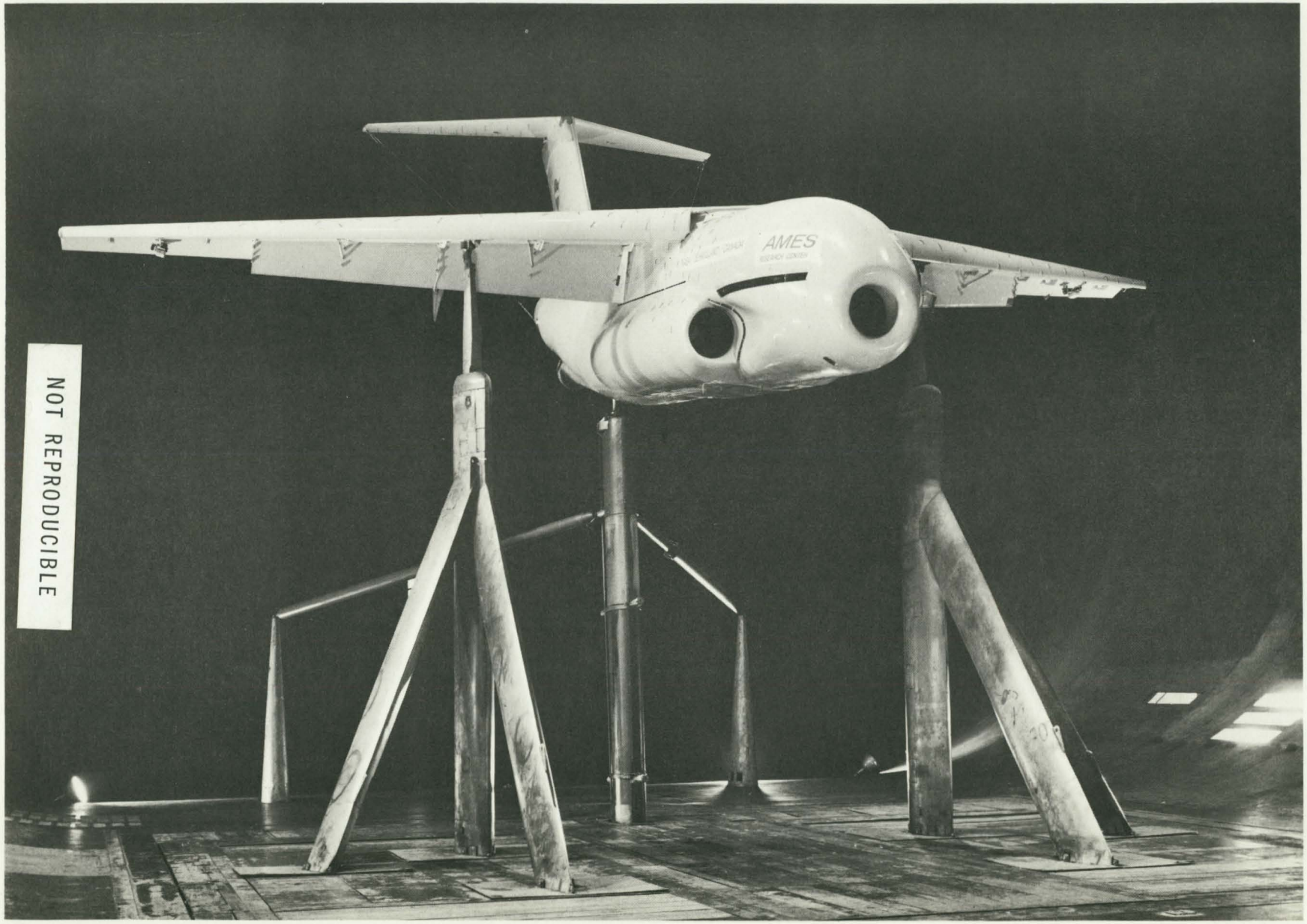

(b) Three-quarter front view
Figure 1.- Continued.

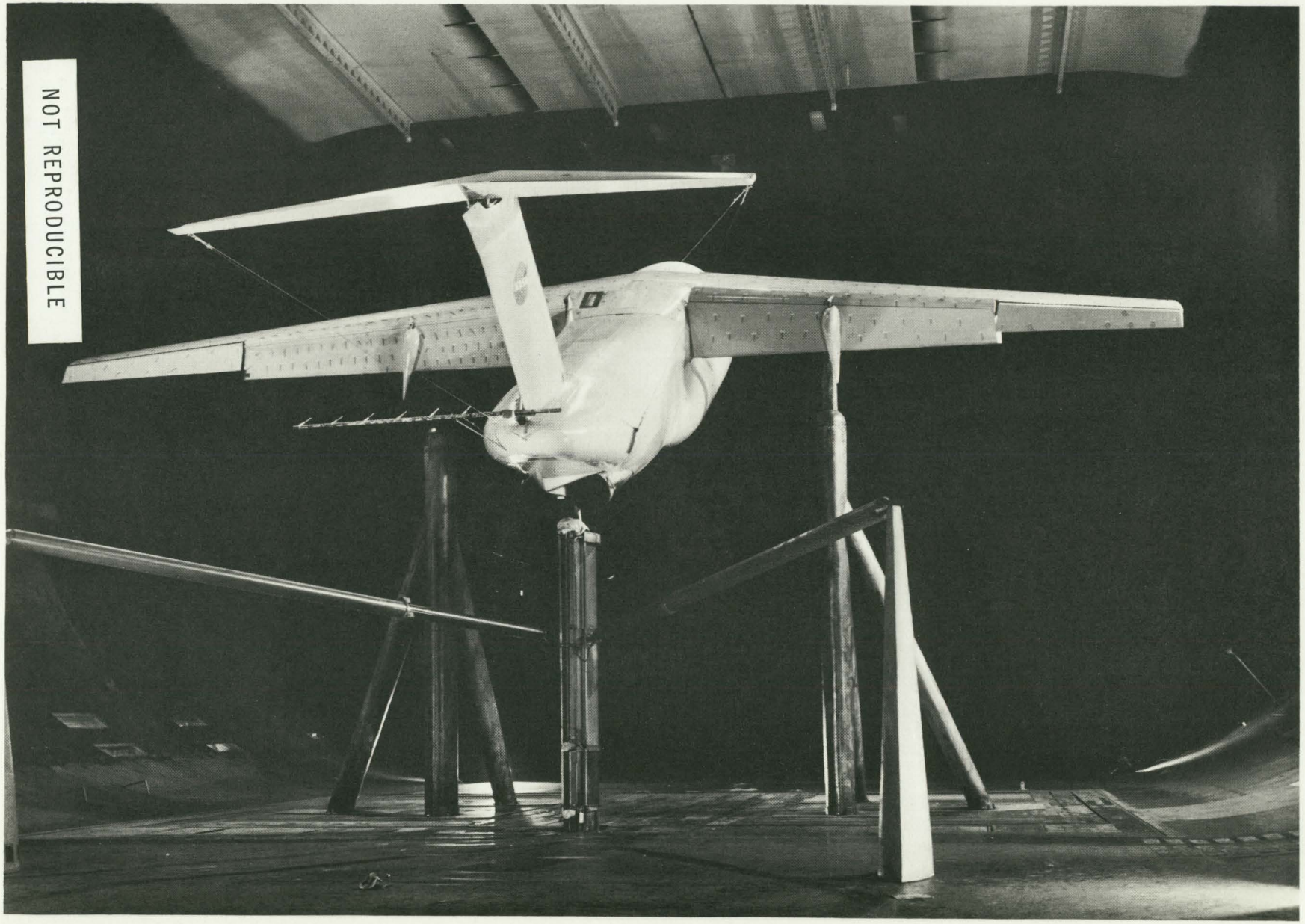

(c) Three-quarter rear view
Figure 1.- Concluded.

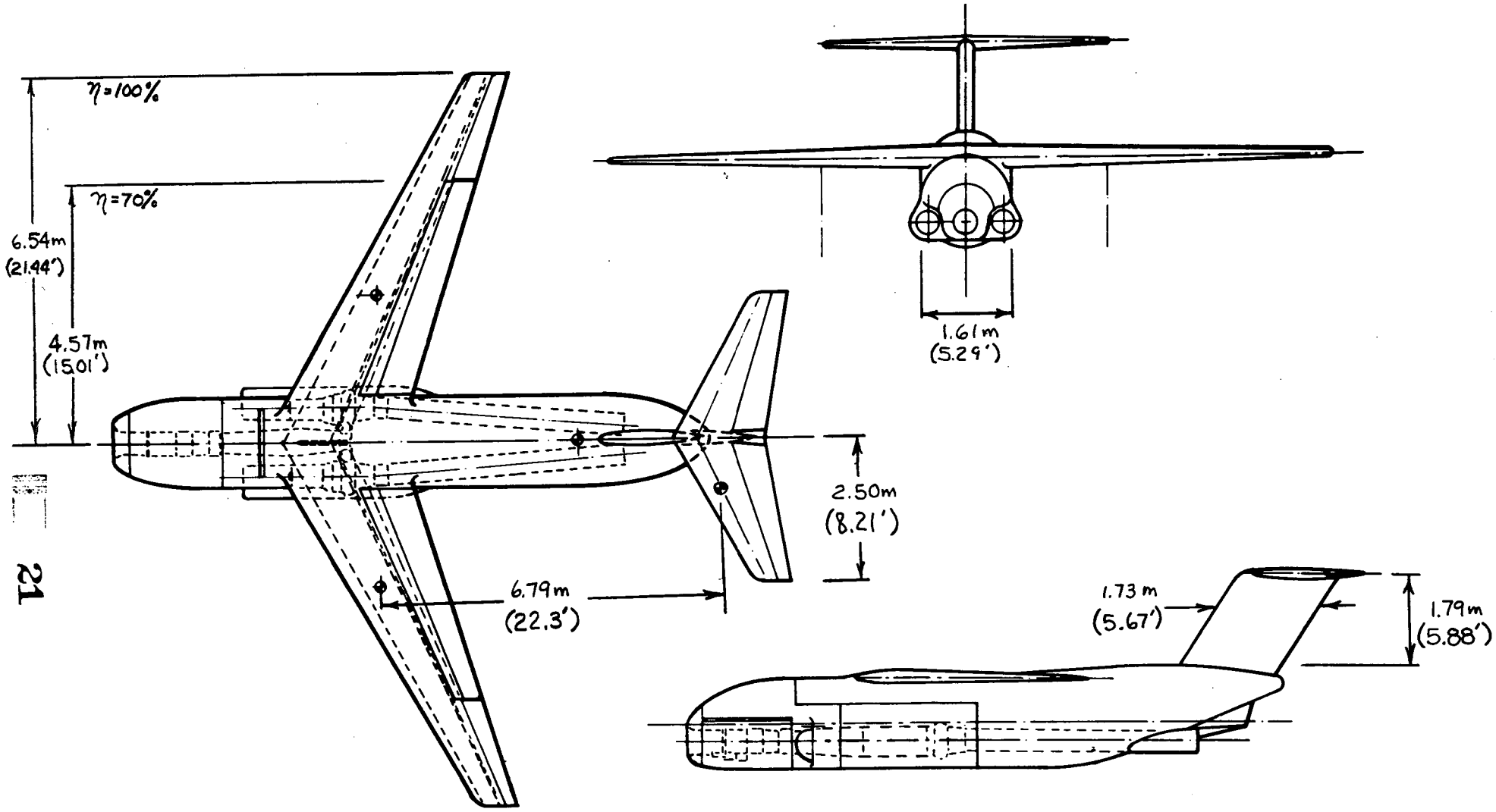

(a) General arrangement

Figure 2.- Geometric details of the model.

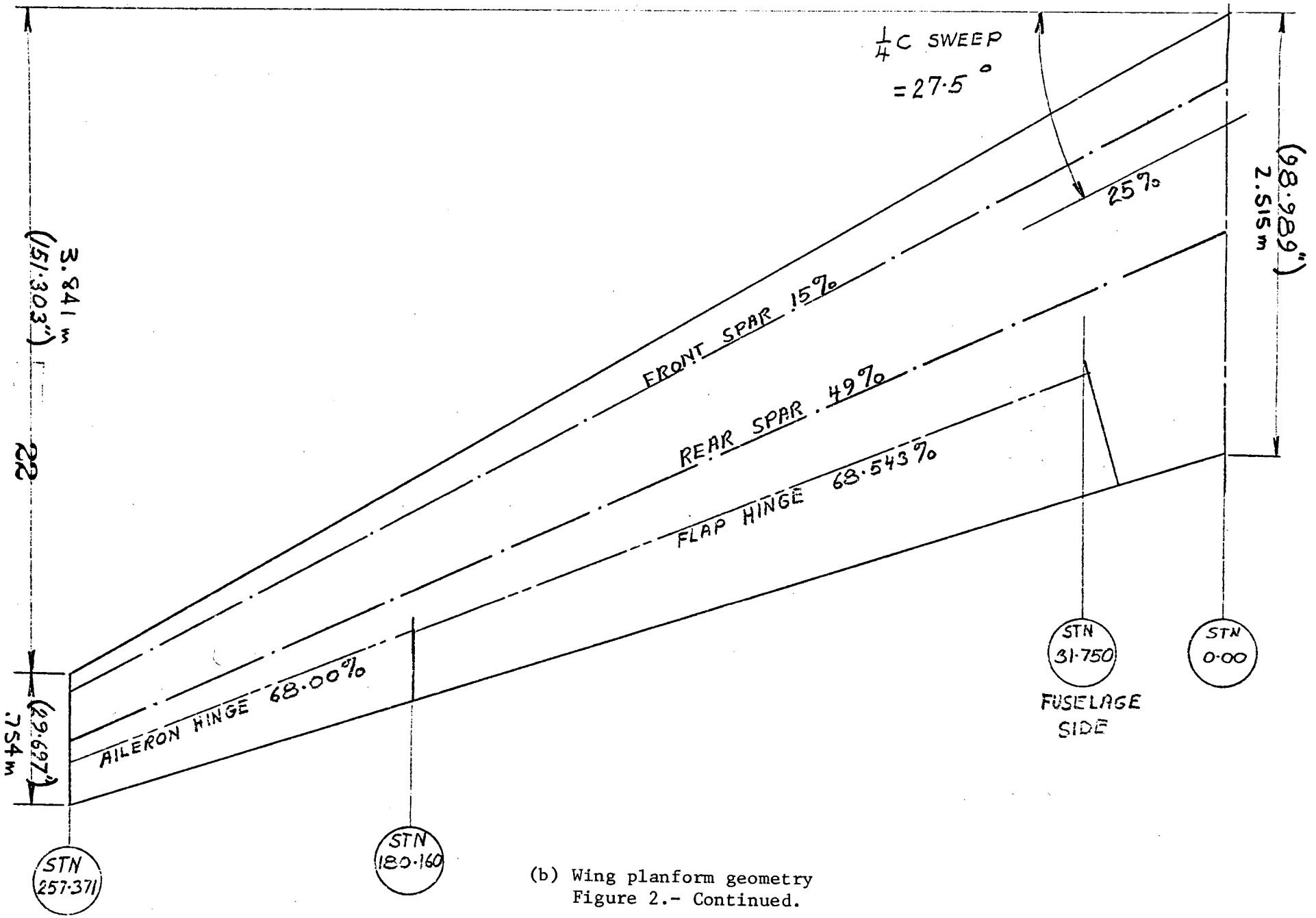

(b) Wing planform geometry
Figure 2.- Continued.

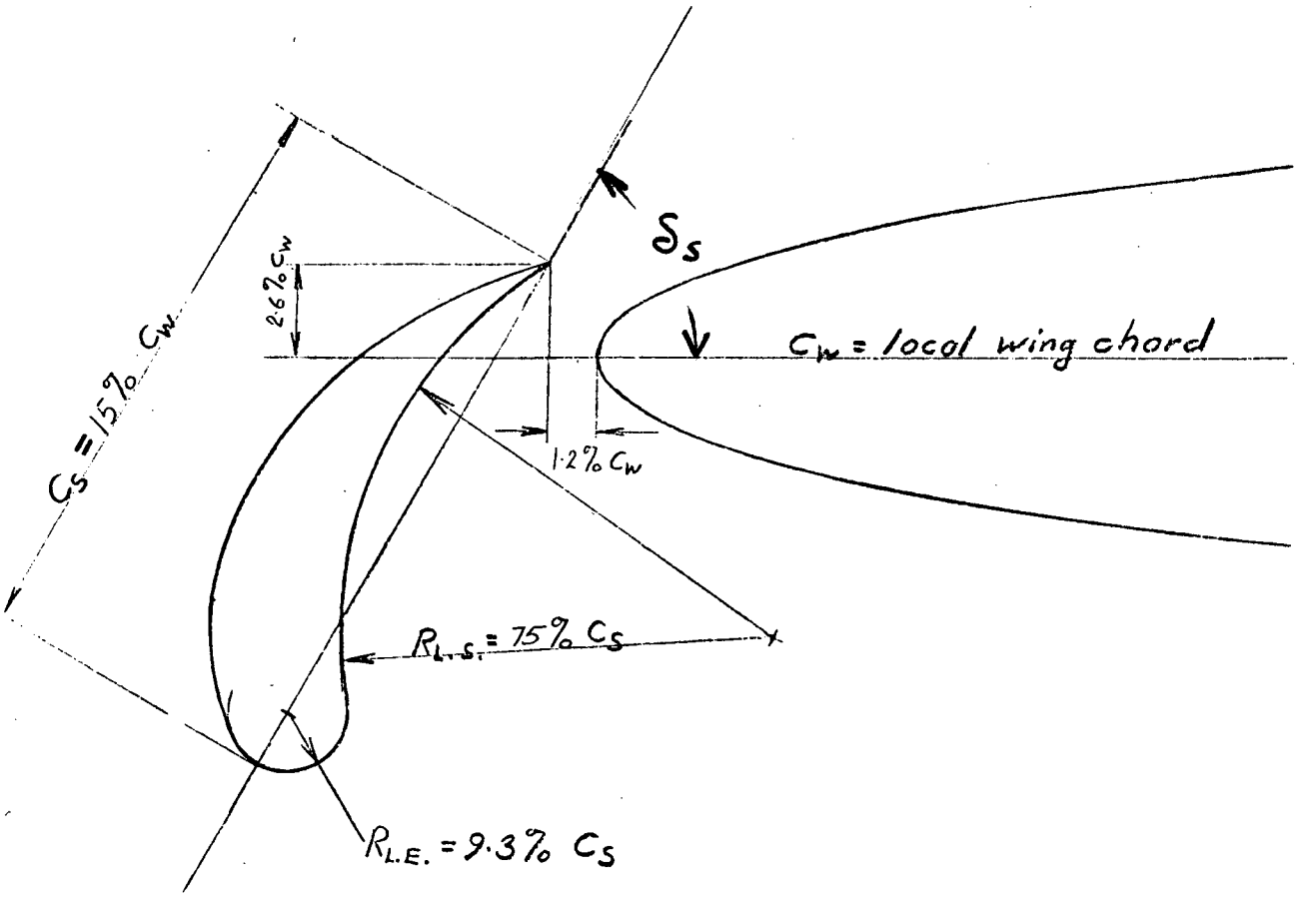

SLAT CO-ORDINATES	
x/c_s	y/c_s
	Upper
0.025	0.0667
0.05	0.1000
0.10	0.1520
0.15	0.1843
0.20	0.2088
0.25	0.2255
0.30	0.2375
0.40	0.2500
0.50	0.2476
0.60	0.2265
0.70	0.1941
0.80	0.1431
0.90	0.0794
1.00	0.0000
L/E RADIUS = 9.314% c_s	

(c) Leading edge slat geometry
Figure 2.- Continued.

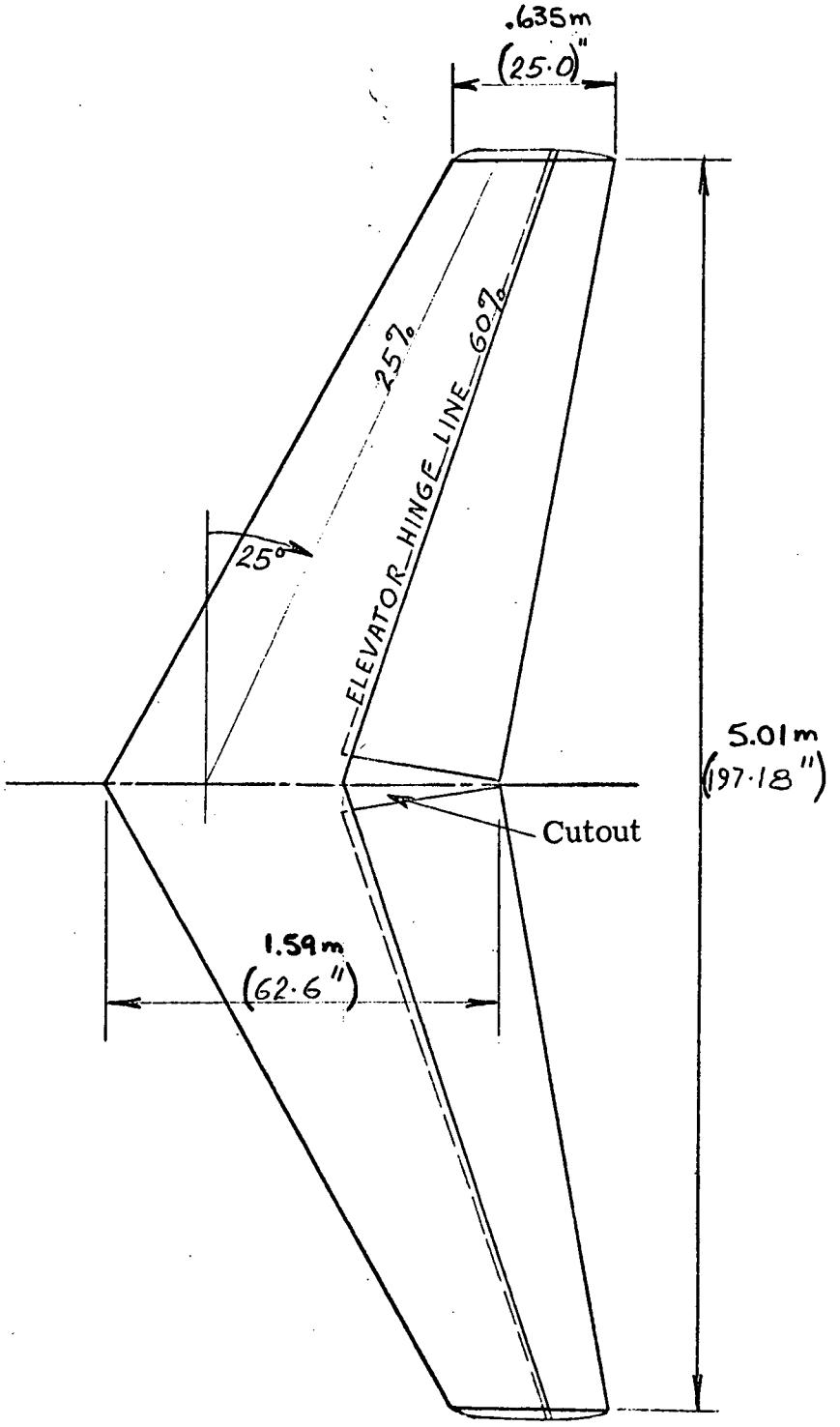

Elevator Travel = $\pm$ 30°

Tailplane Incidence = $\pm$ 12°

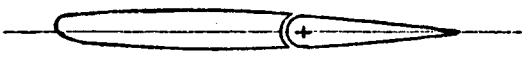

RAE 104 10% $\frac{t}{c}$

(with modified L.E.)

(d) Horizontal tail geometry
Figure 2.- Continued.

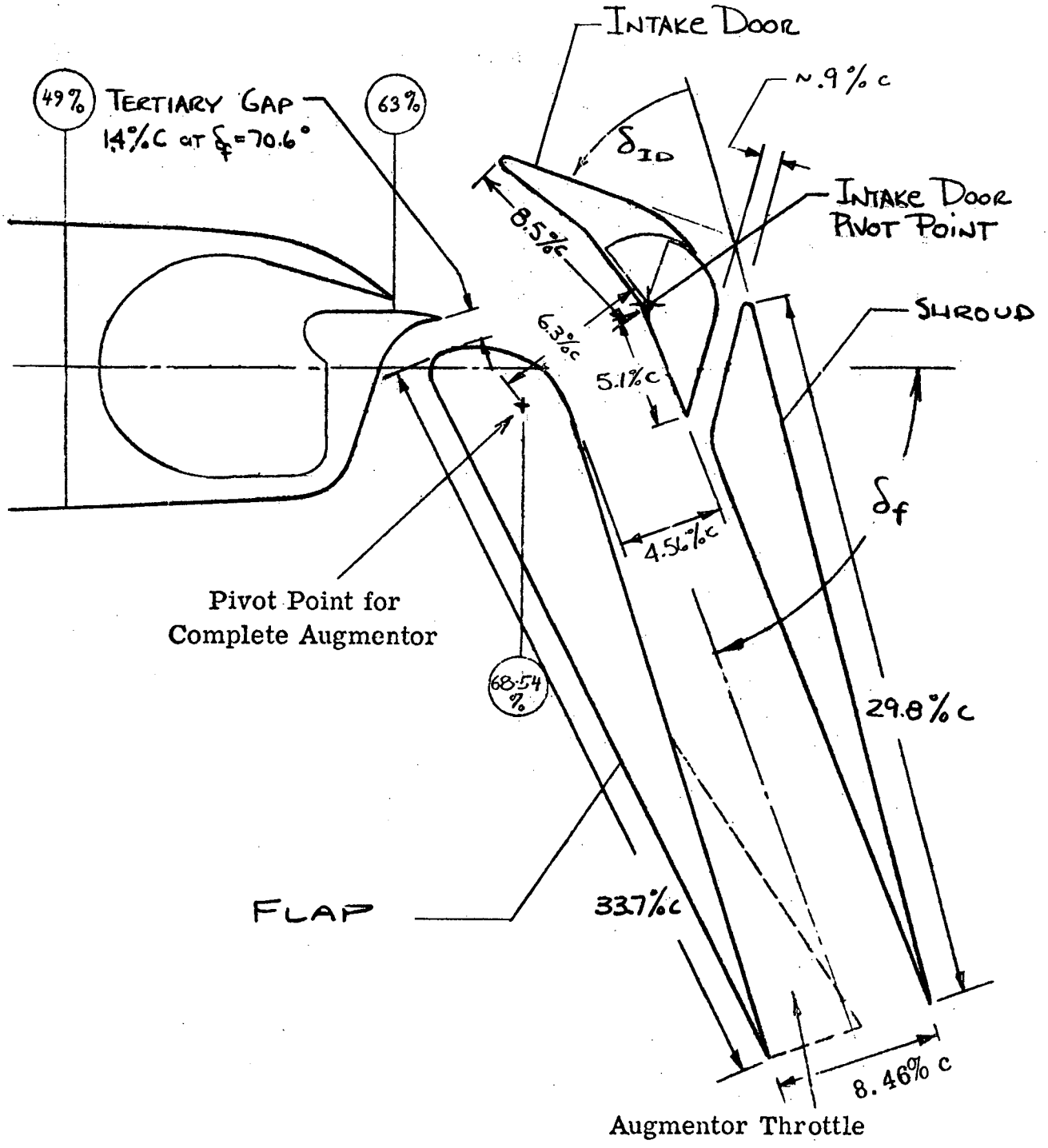

(e) Streamwise section of augmentor flap
Figure 2.- Continued.

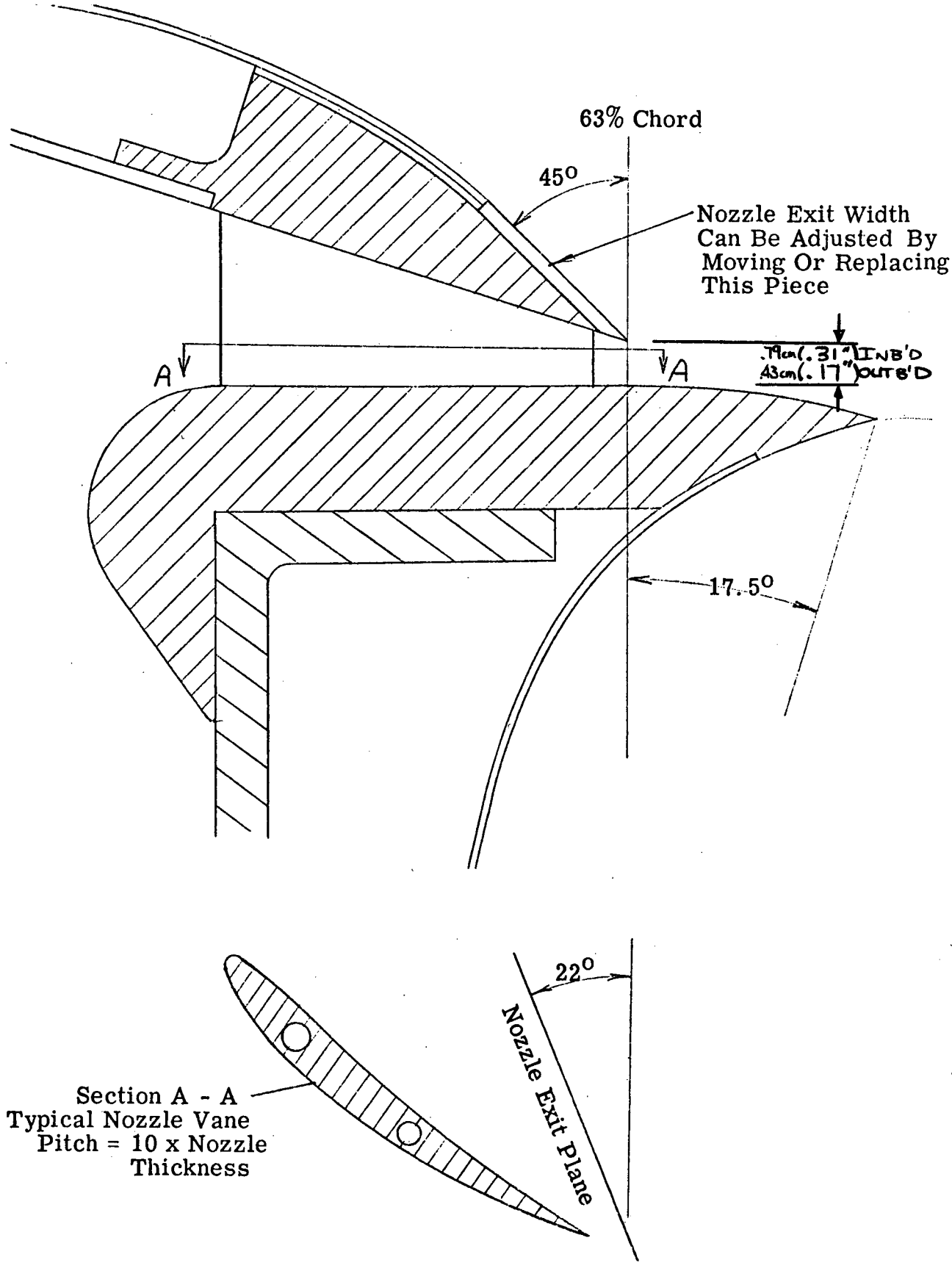

(f) Augmentor nozzle cross section

Figure 2.- Continued.

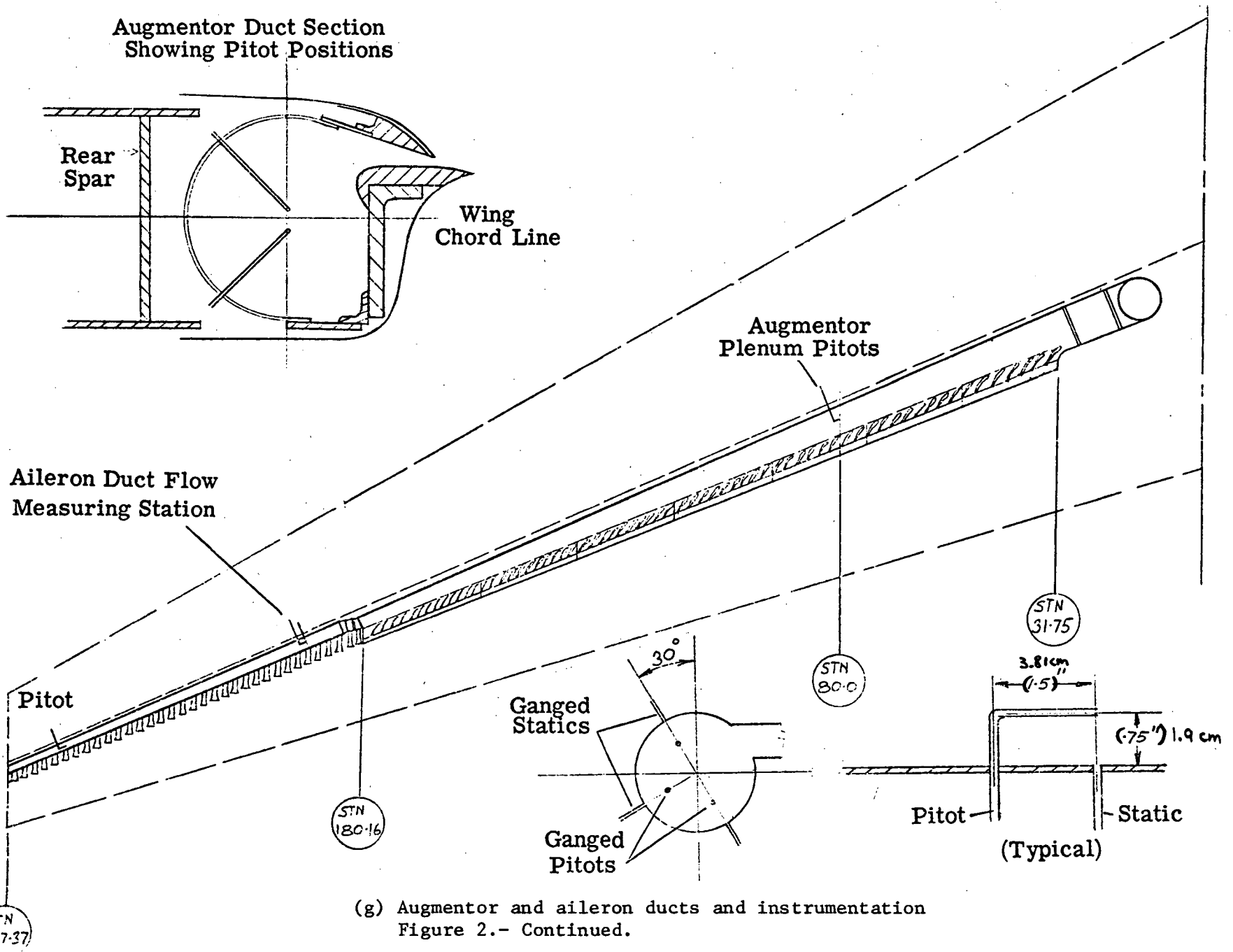

(g) Augmentor and aileron ducts and instrumentation
Figure 2.- Continued.

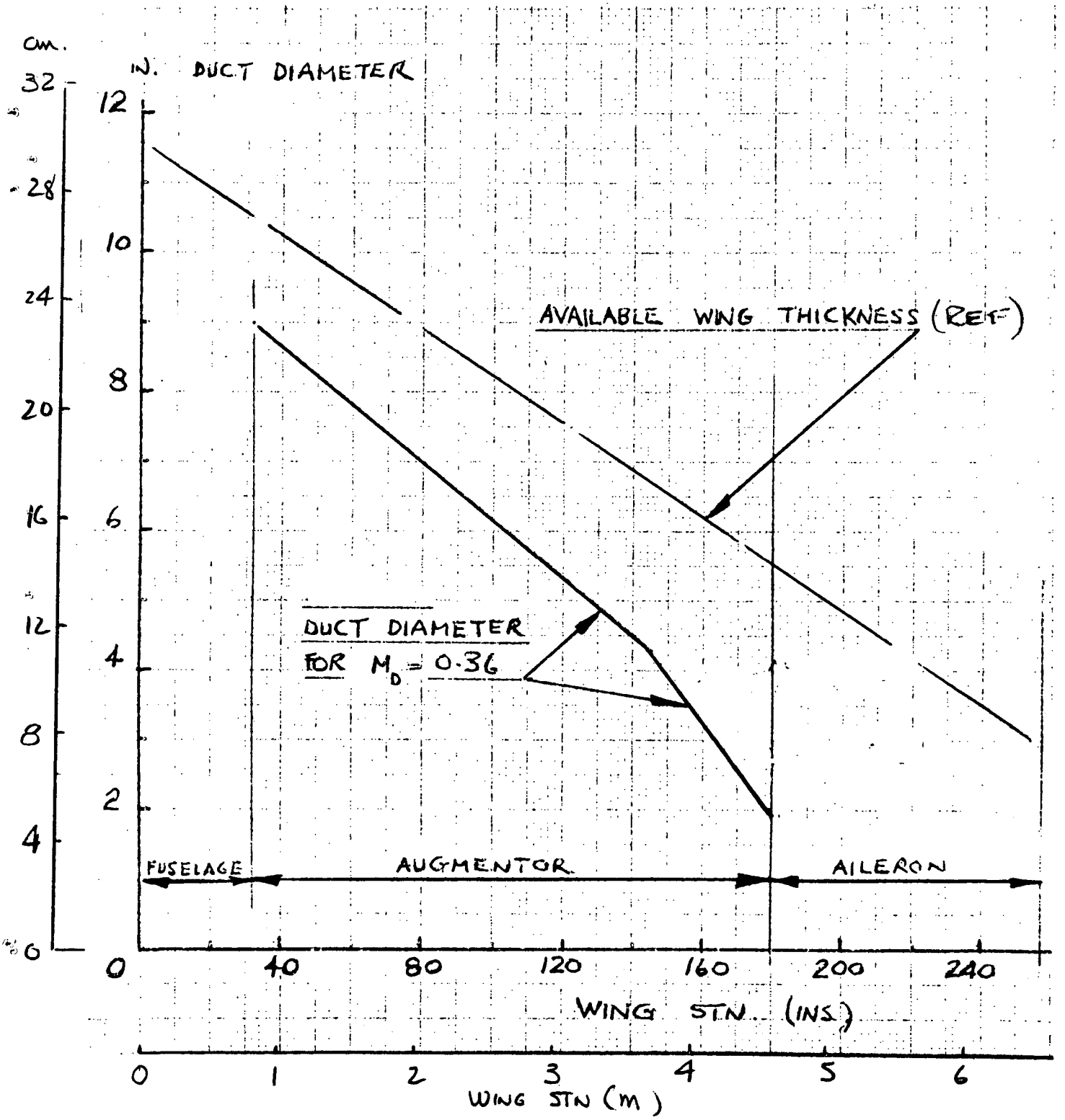

(h) Augmentor duct size to produce streamwise flow at nozzle exit
Figure 2.- Continued.

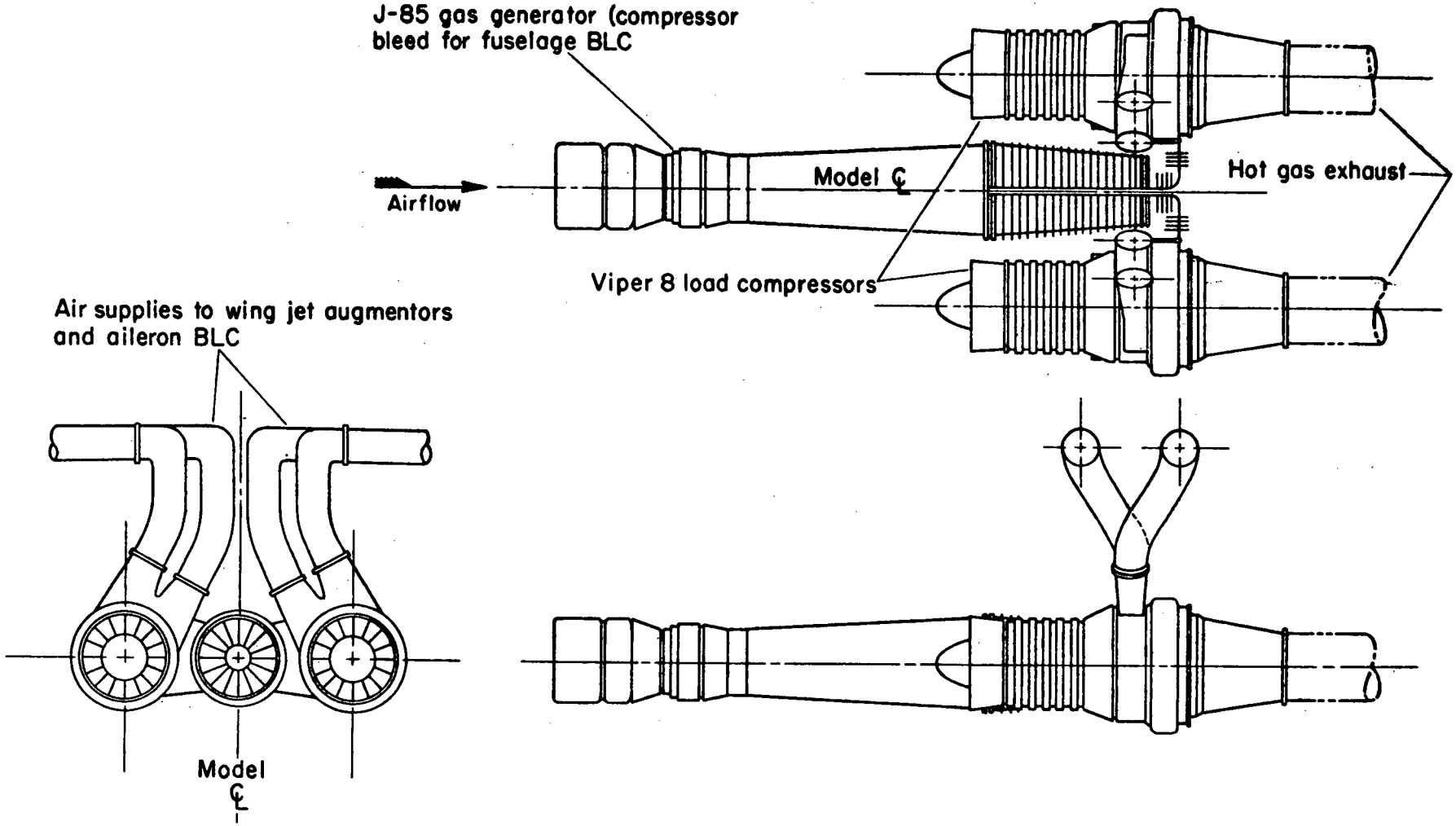

(i) Augmentor air compressor system.

Figure 2.- Continued.

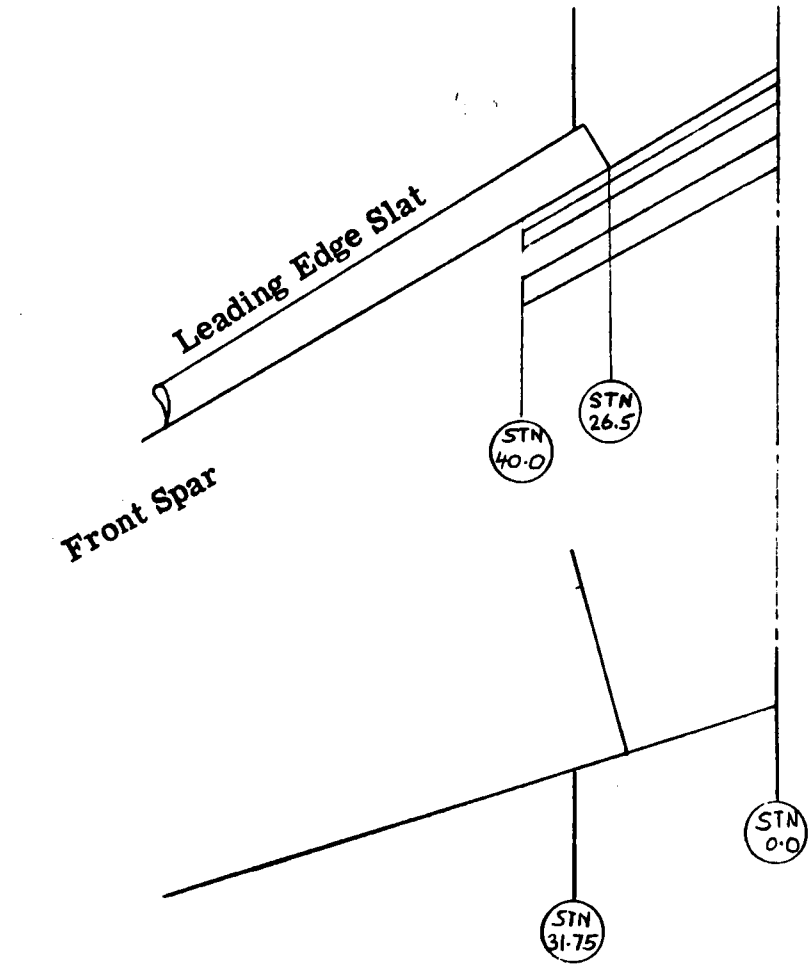

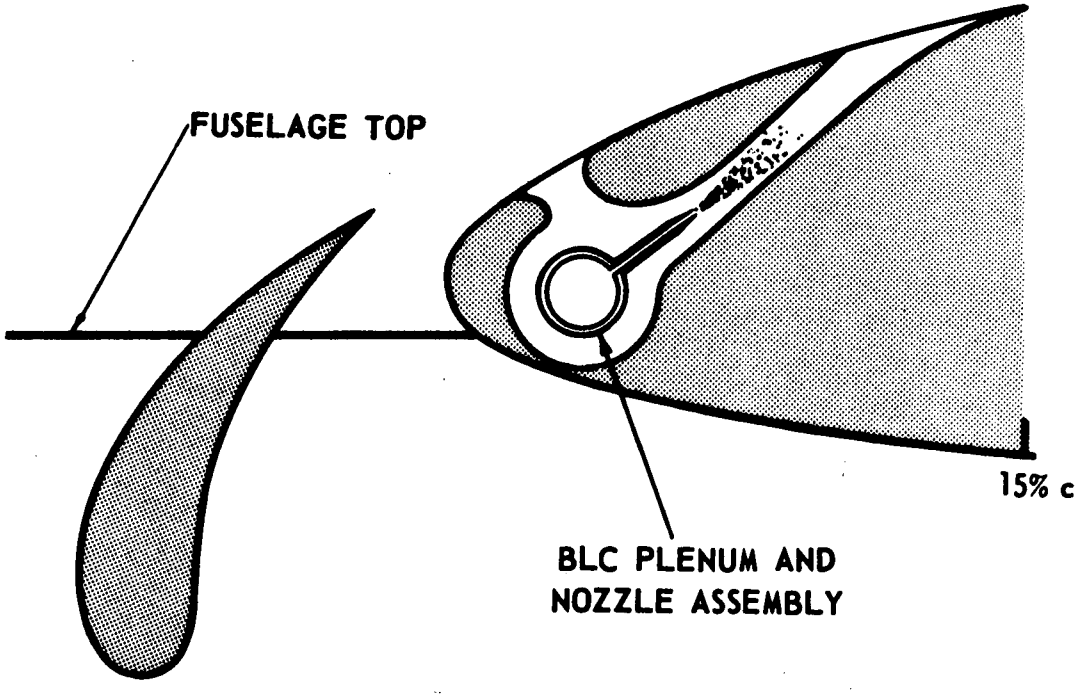

(j) Fuselage BLC geometry
Figure 2.- Continued.

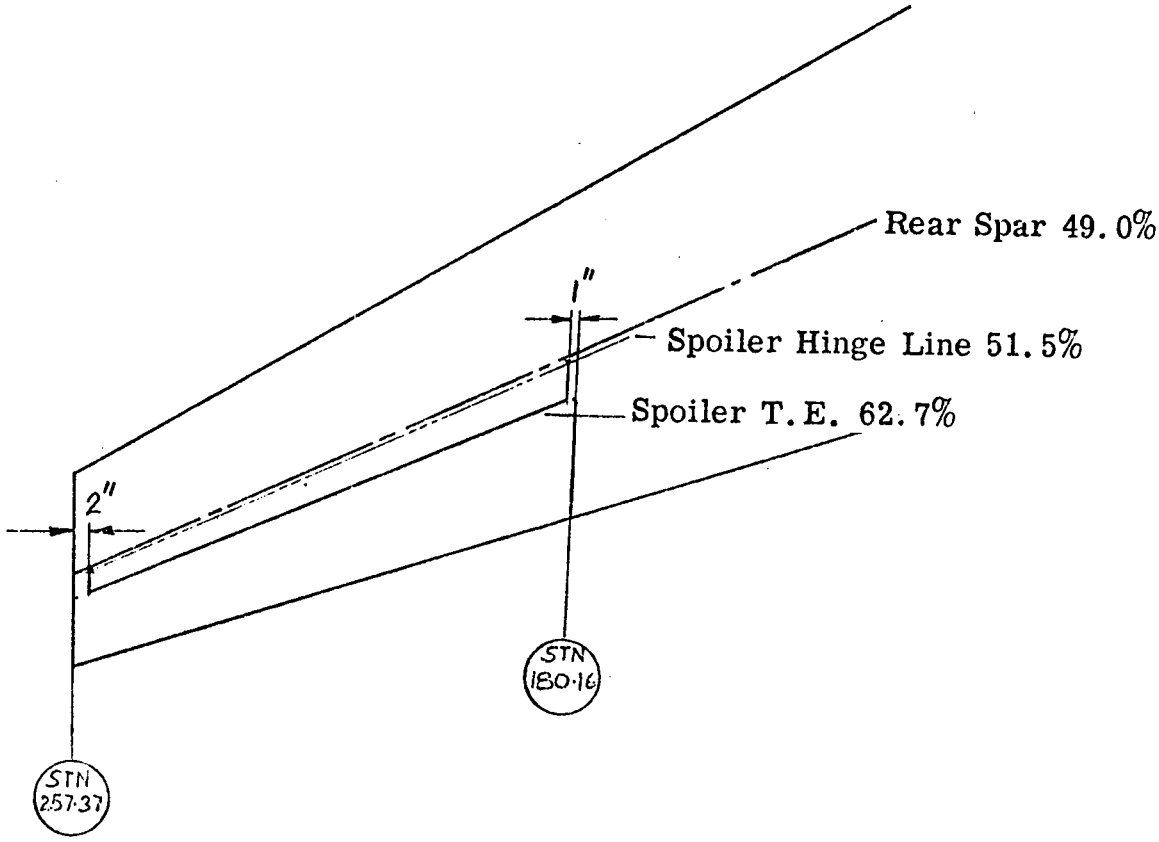

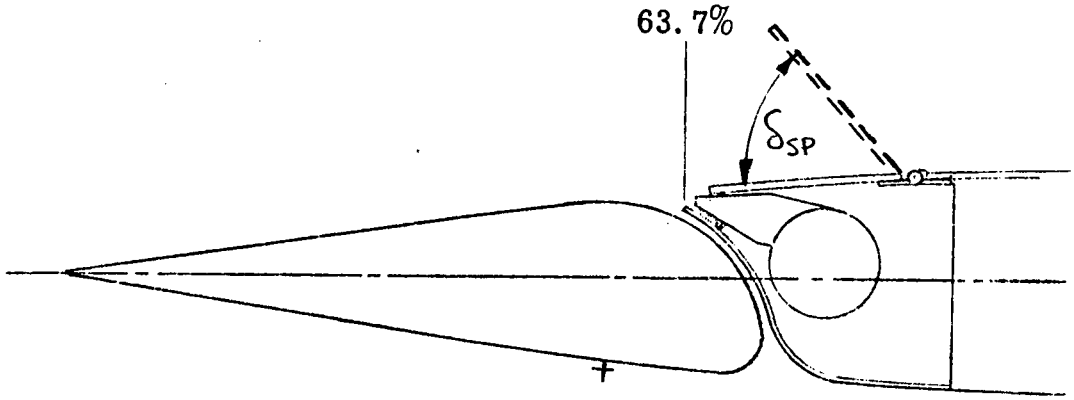

(k) Aileron blowing and lift spoiler geometry
Figure 2.- Concluded.

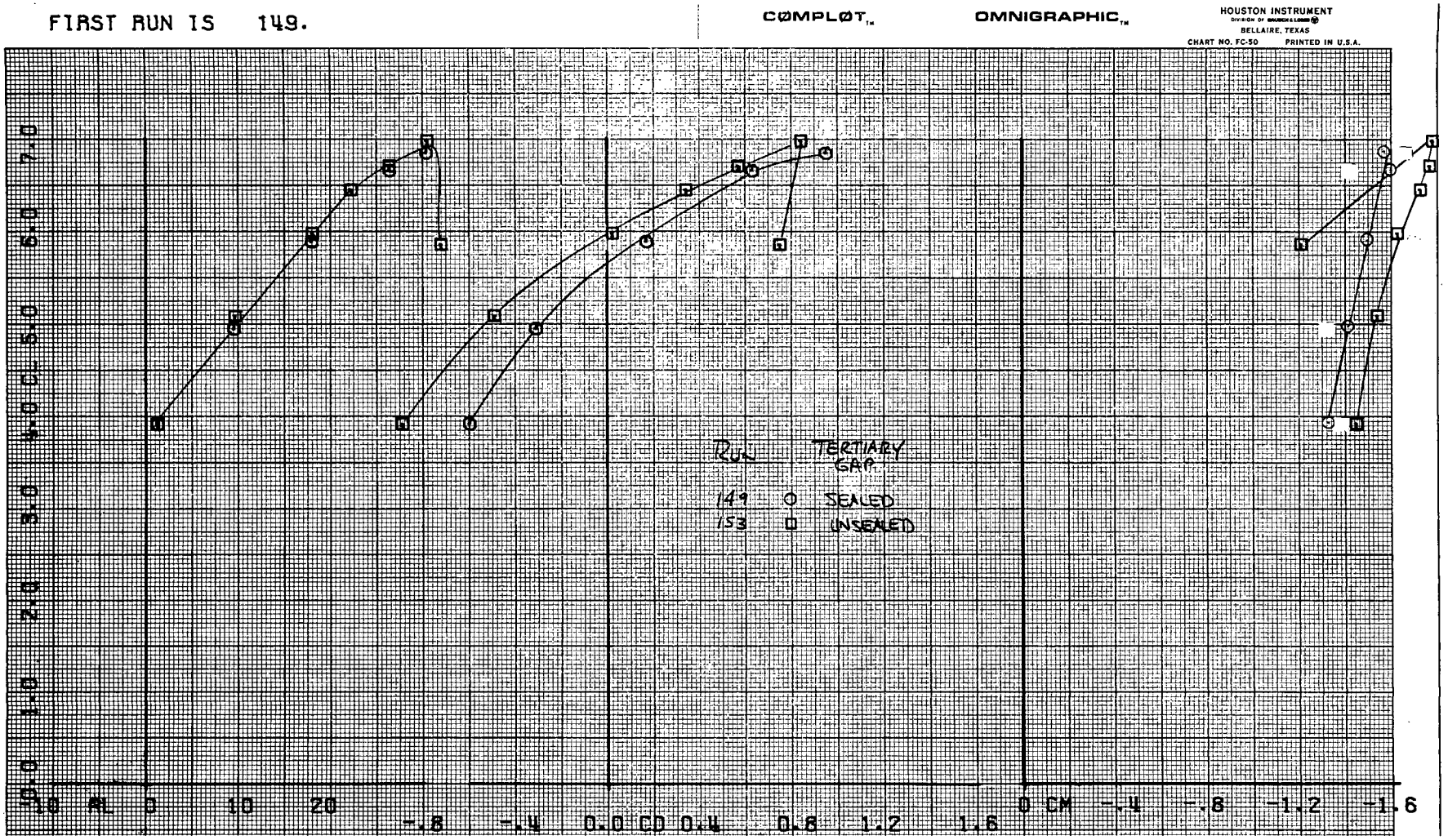

(a) $C_{J_I} = 1.47$

Figure 3.- Effect of sealing the augmentor tertiary gap on the longitudinal aerodynamic characteristics with horizontal tail removed; $\delta_f = 41.1°$ and $\delta_s = 60°$ (mod to stb'd)

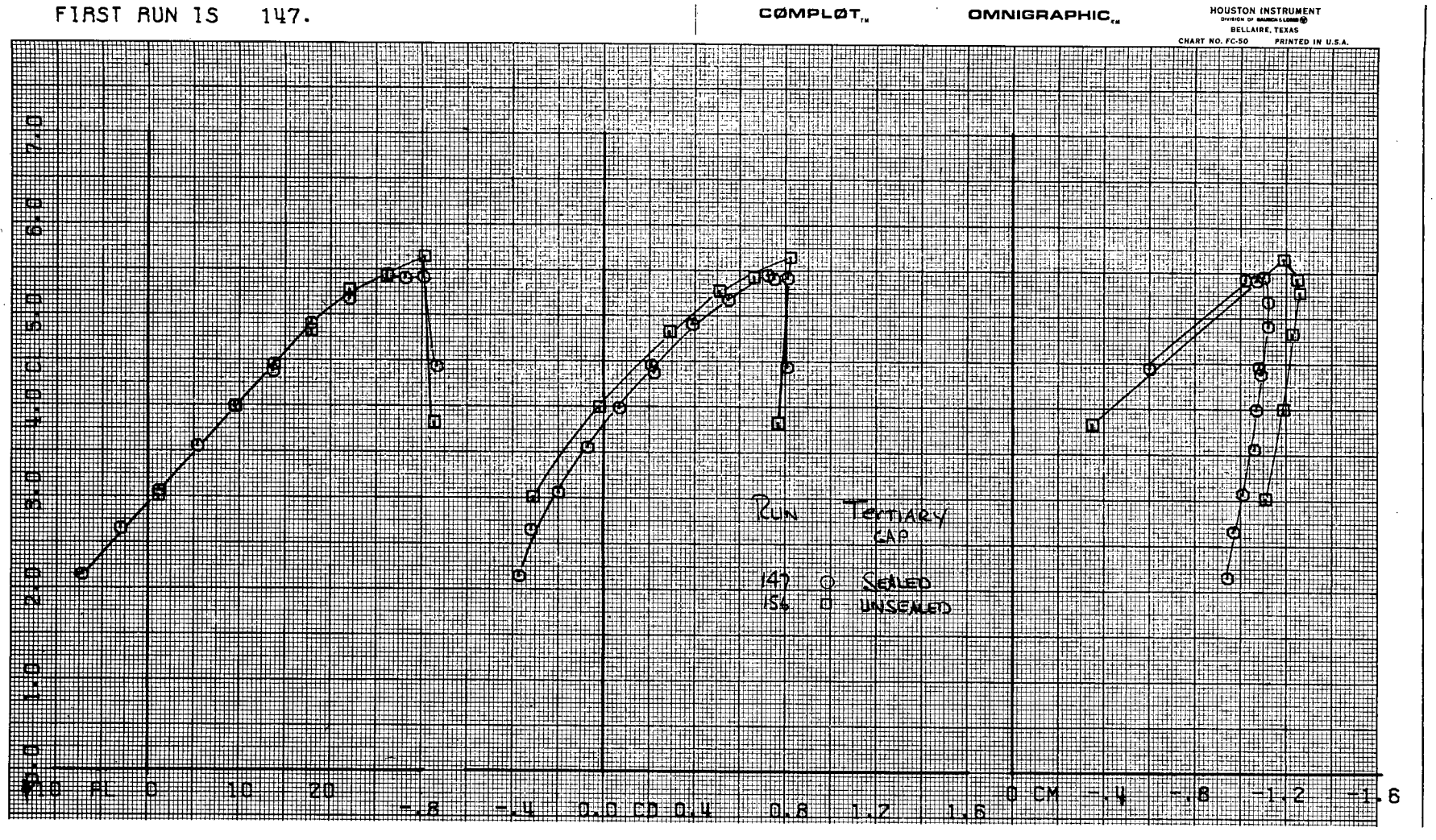

(b) C_{J_I} = .77

Figure 3 .- Continued.

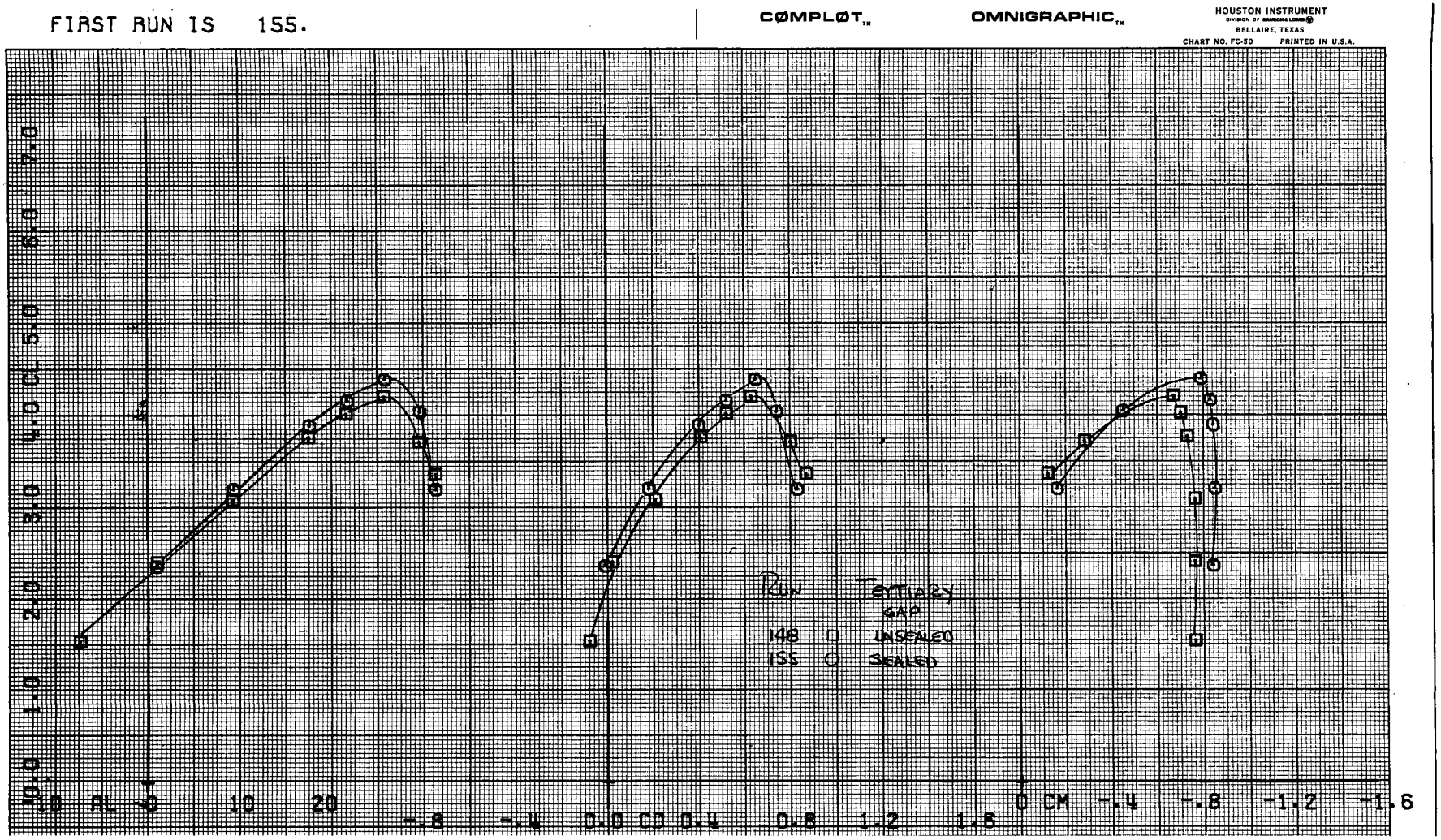

(c) $C_{J_I} = .36$

Figure 3 .- Continued.

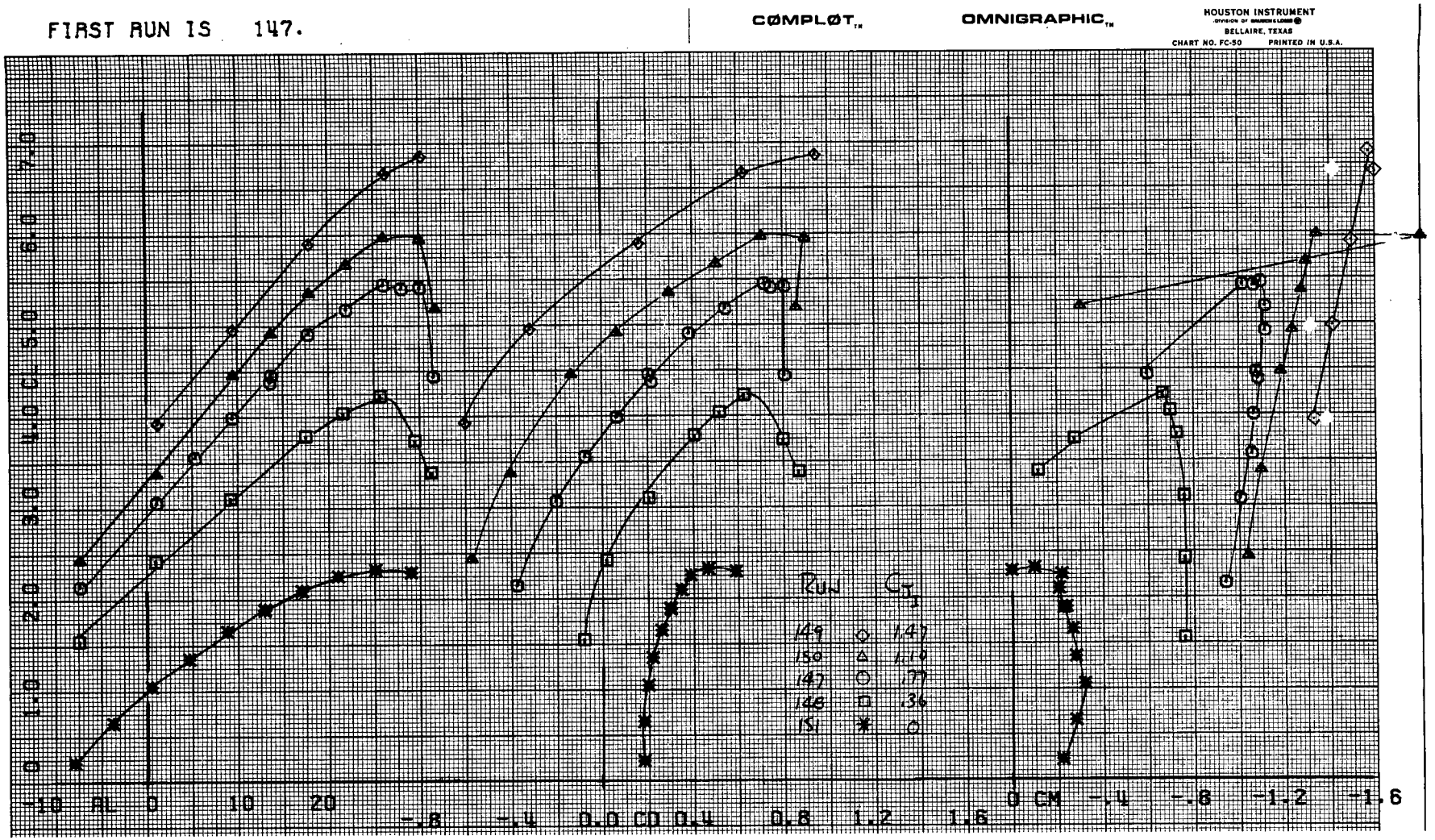

(d) Effect of C_{J_I} with tertiary gap sealed

Figure 3 .- Concluded.

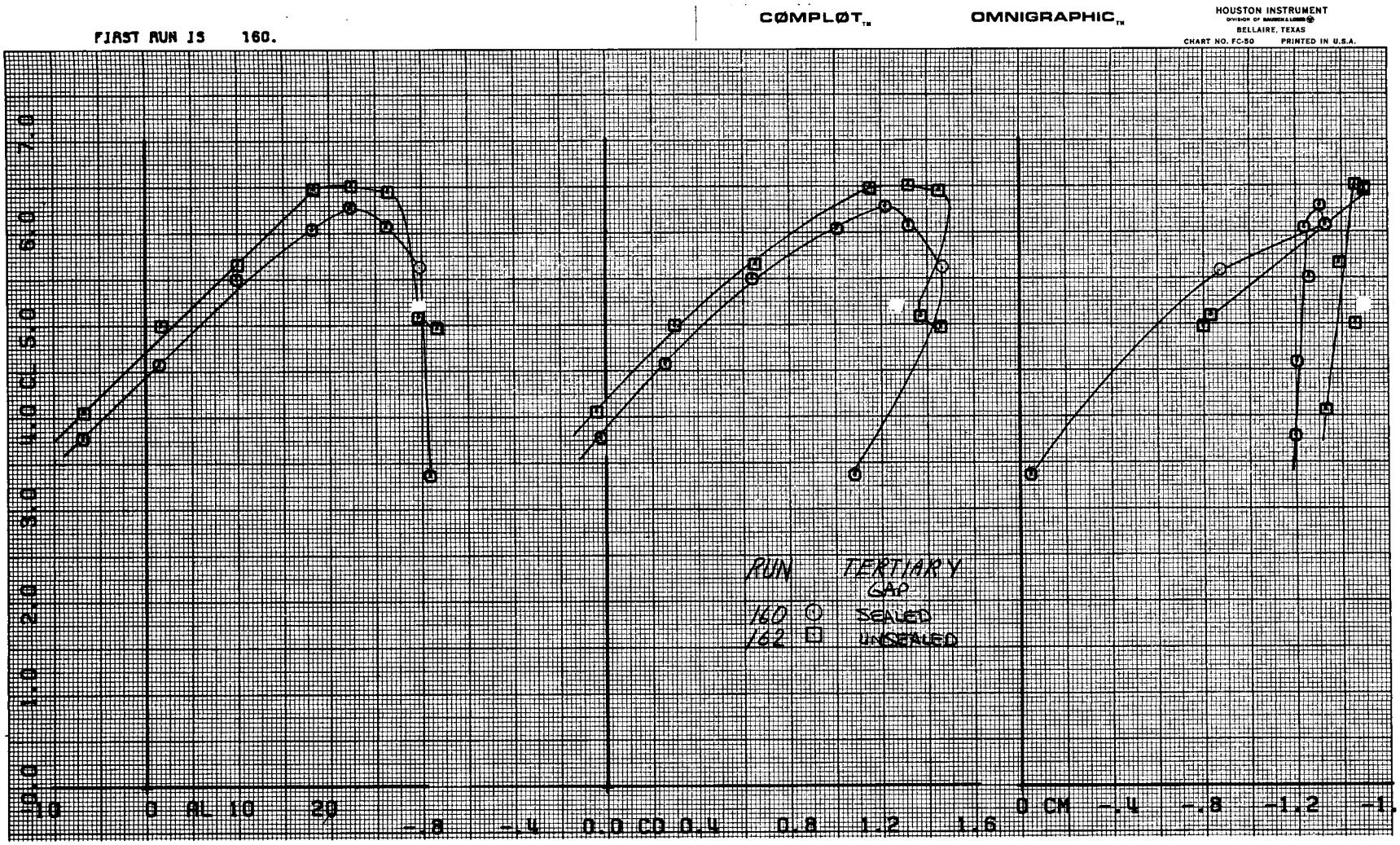

(a) $C_{J_I} = 1.10$

Figure 4.- Effect of sealing augmentor tertiary gap on longitudinal aerodynamic characteristics with horizontal tail removed; $\delta_f = 70.6°$ and $\delta_s = 60°$ (mod to stb'd)

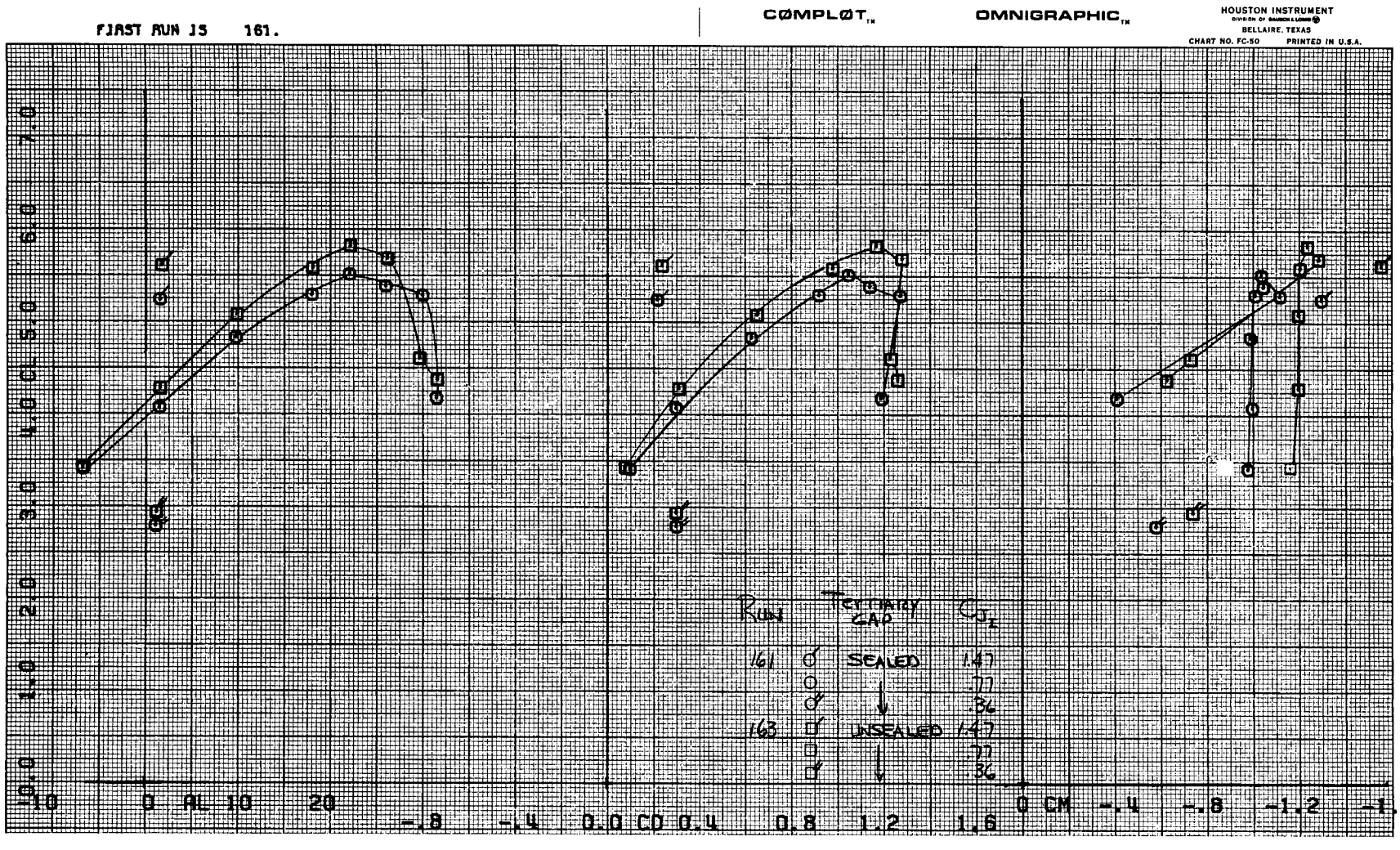

(b) C_{J_I} = .36, .77 and 1.47

Figure 4.- Concluded.

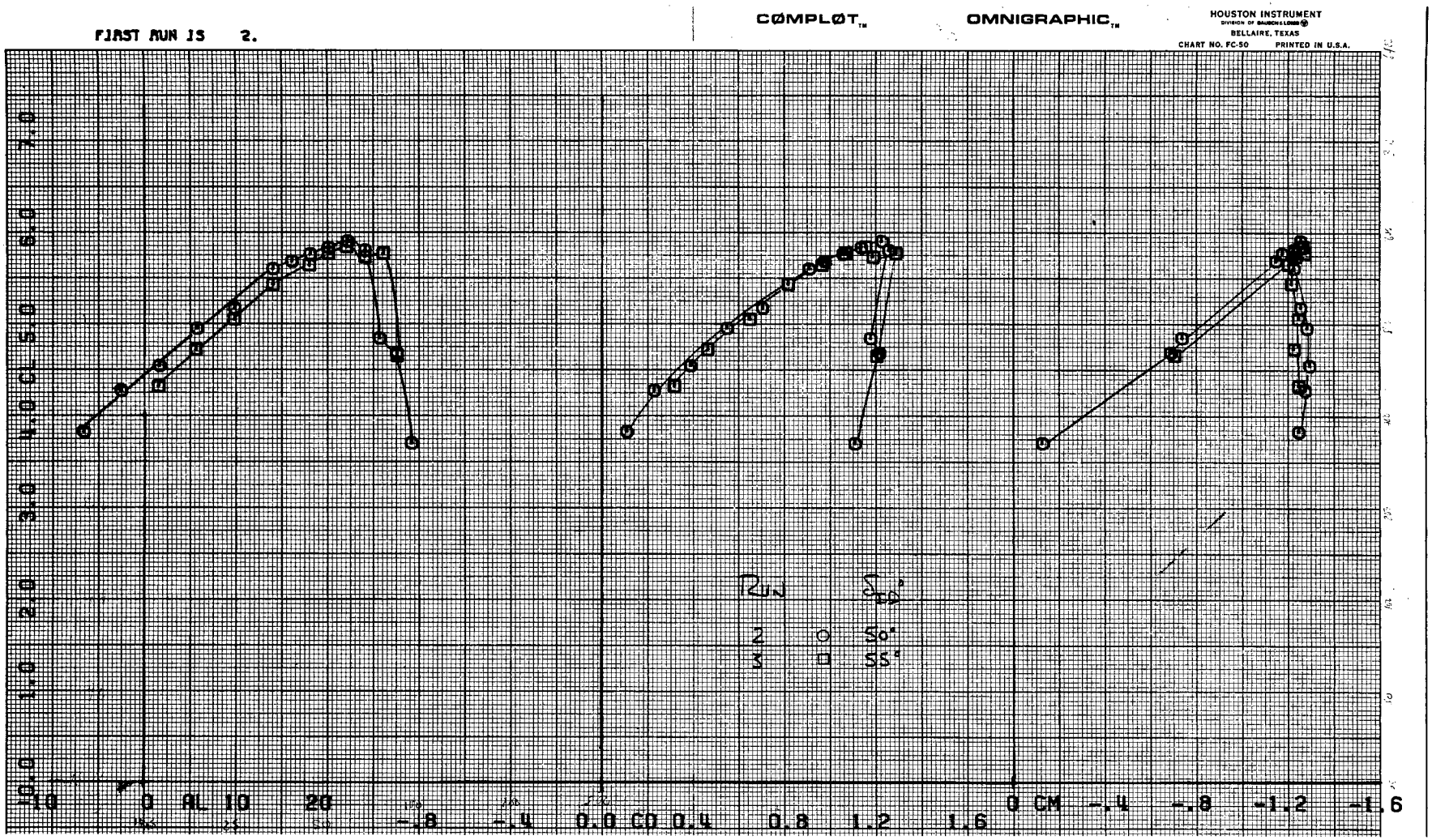

Figure 5.- Effect of augmentor intake door deflection on longitudinal aerodynamic characteristics with horizontal tail removed;

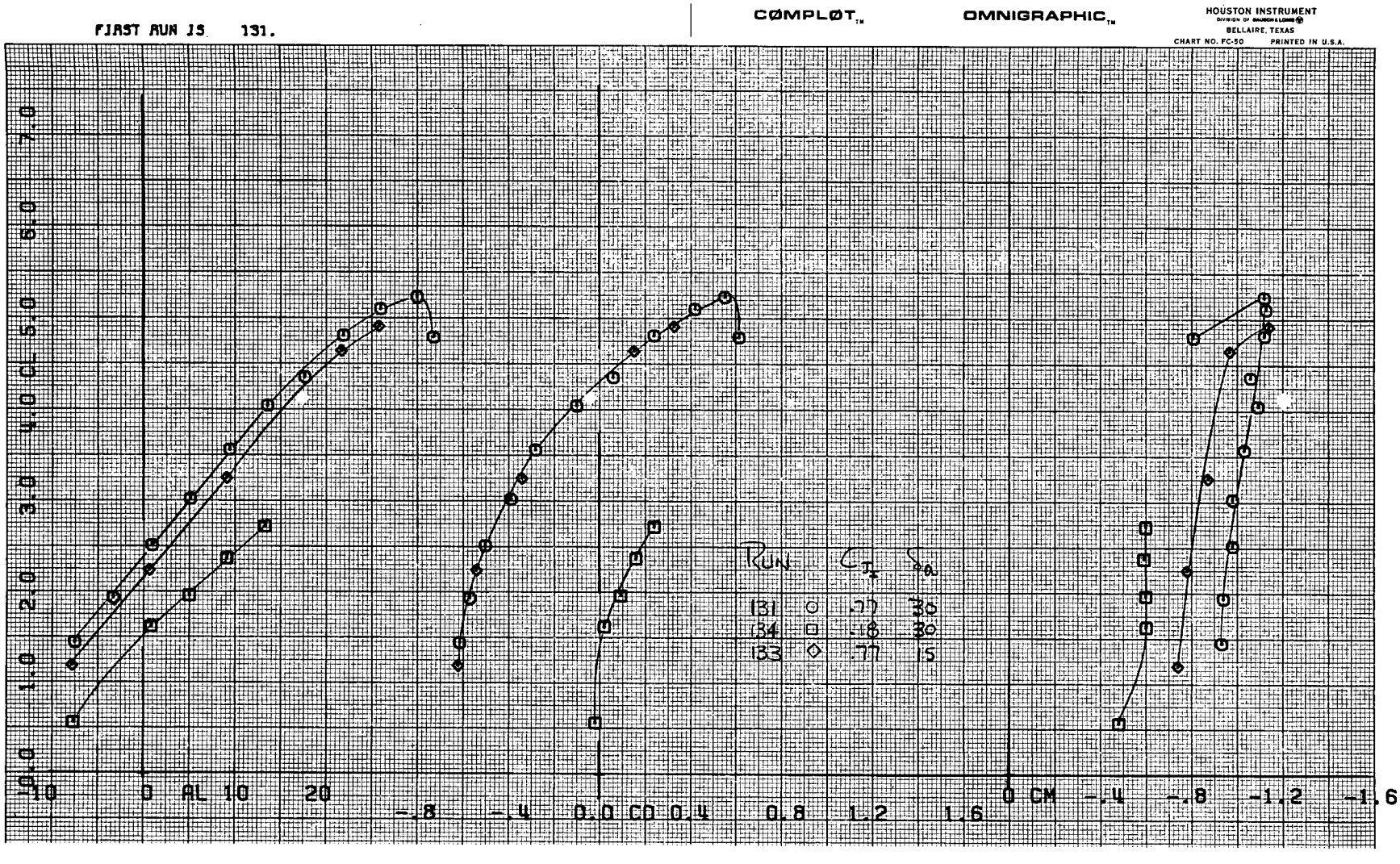

Figure 6.- Effect of symmetrical aileron deflection on longitudinal aerodynamic characteristics with horizontal tail removed; $\delta_f = 31.8°$, $\delta_s = 60°$ (mod to stb'd).

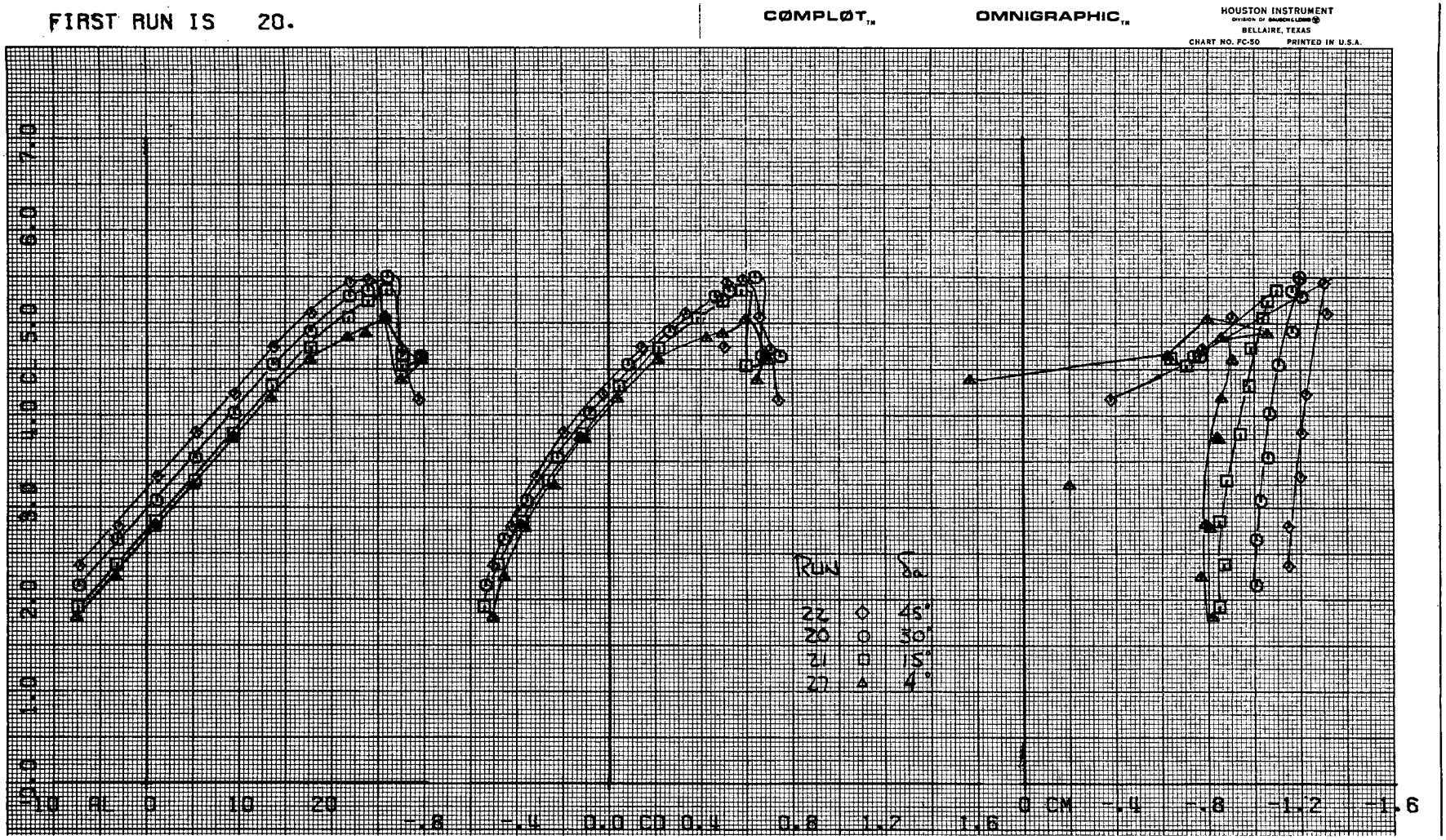

Figure 7.- Effect of symmetrical aileron deflection on longitudinal aerodynamic characteristics with horizontal tail removed; $\delta_f = 41.1°$, $\delta_s = 60°$(mod to stb'd).

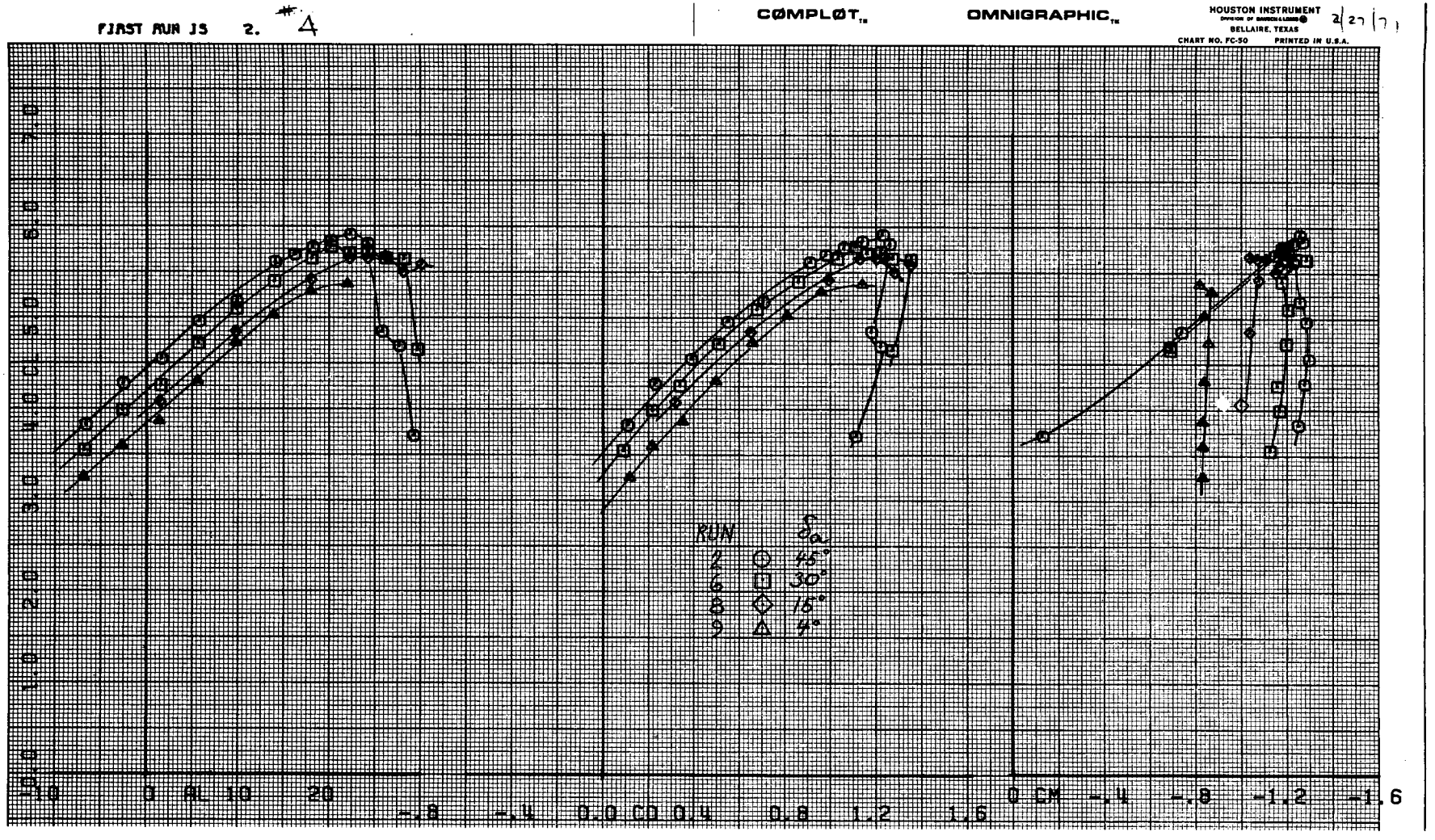

(a) $C_{J_I} = .77, \delta_s = 60°$

Figure 8.- Effect of symmetrical aileron deflection on longitudinal aerodynamic characteristics with horizontal tail removed; $\delta_f = 70.6°$.

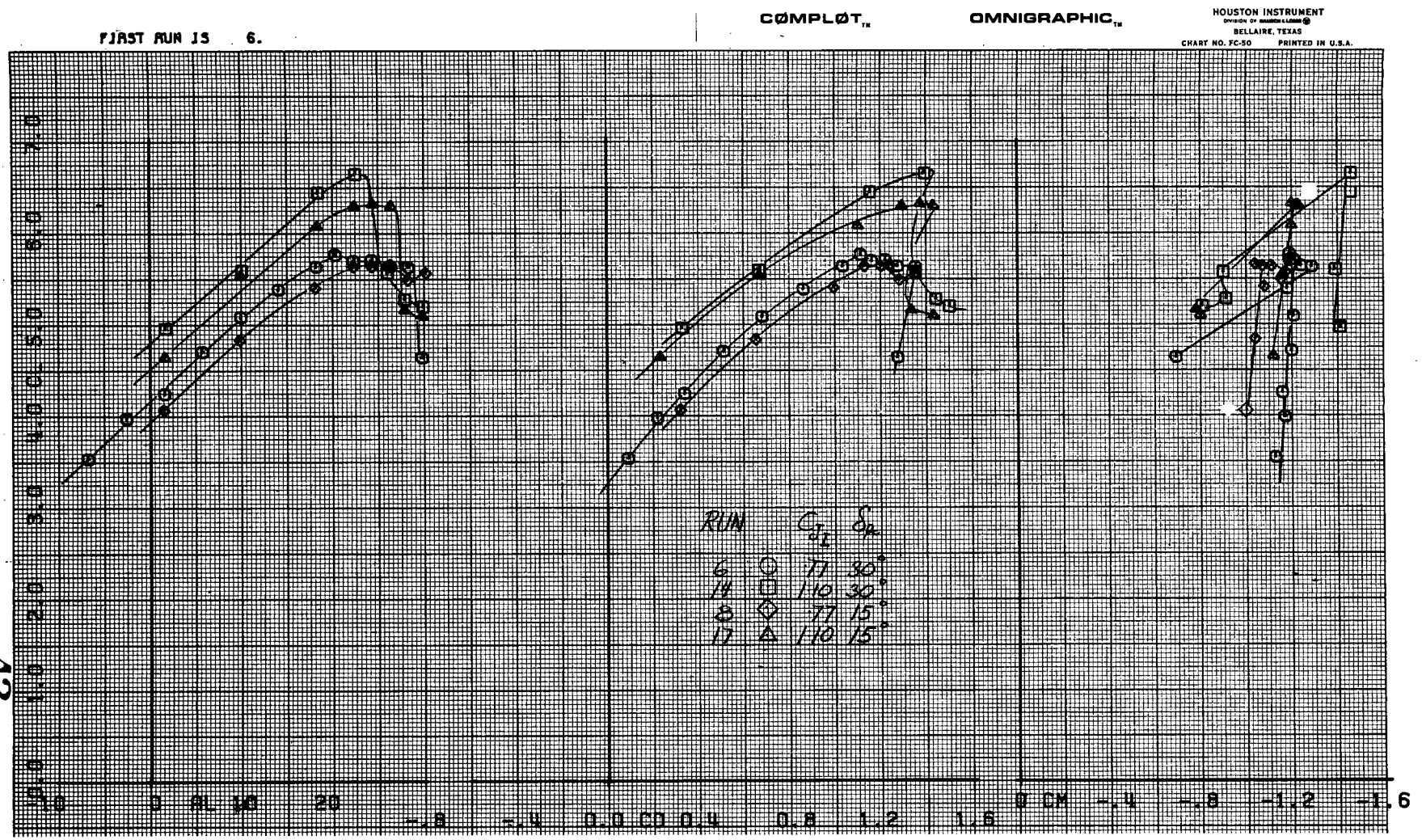

(b) $C_{J_I} = .77$ and $1.10, \delta_s = 60°$

Figure 8.- Continued.

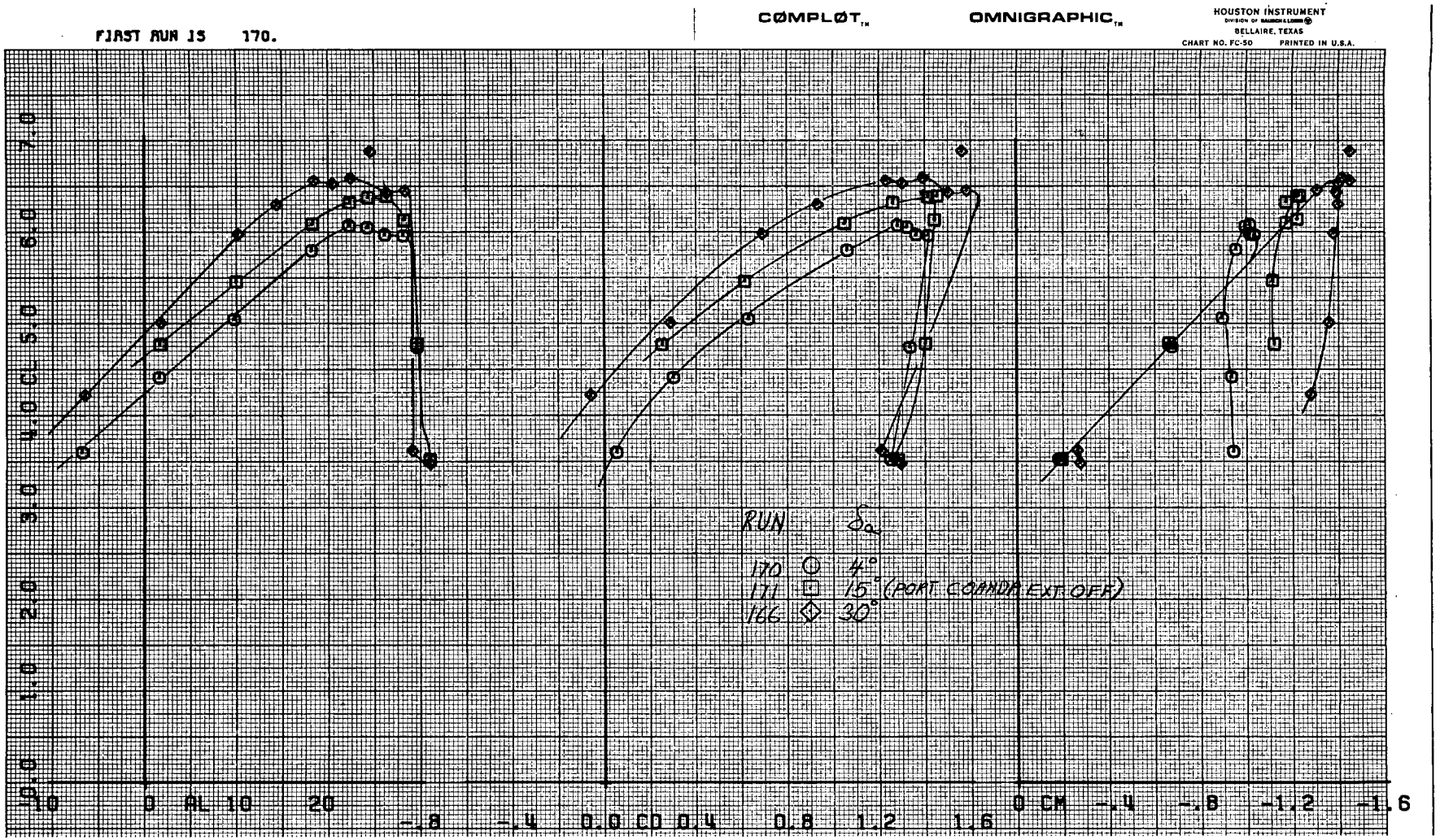

(c) $C_{J_I} = 1.10$ and $\delta_s = 50°$

Figure 8.- Concluded.

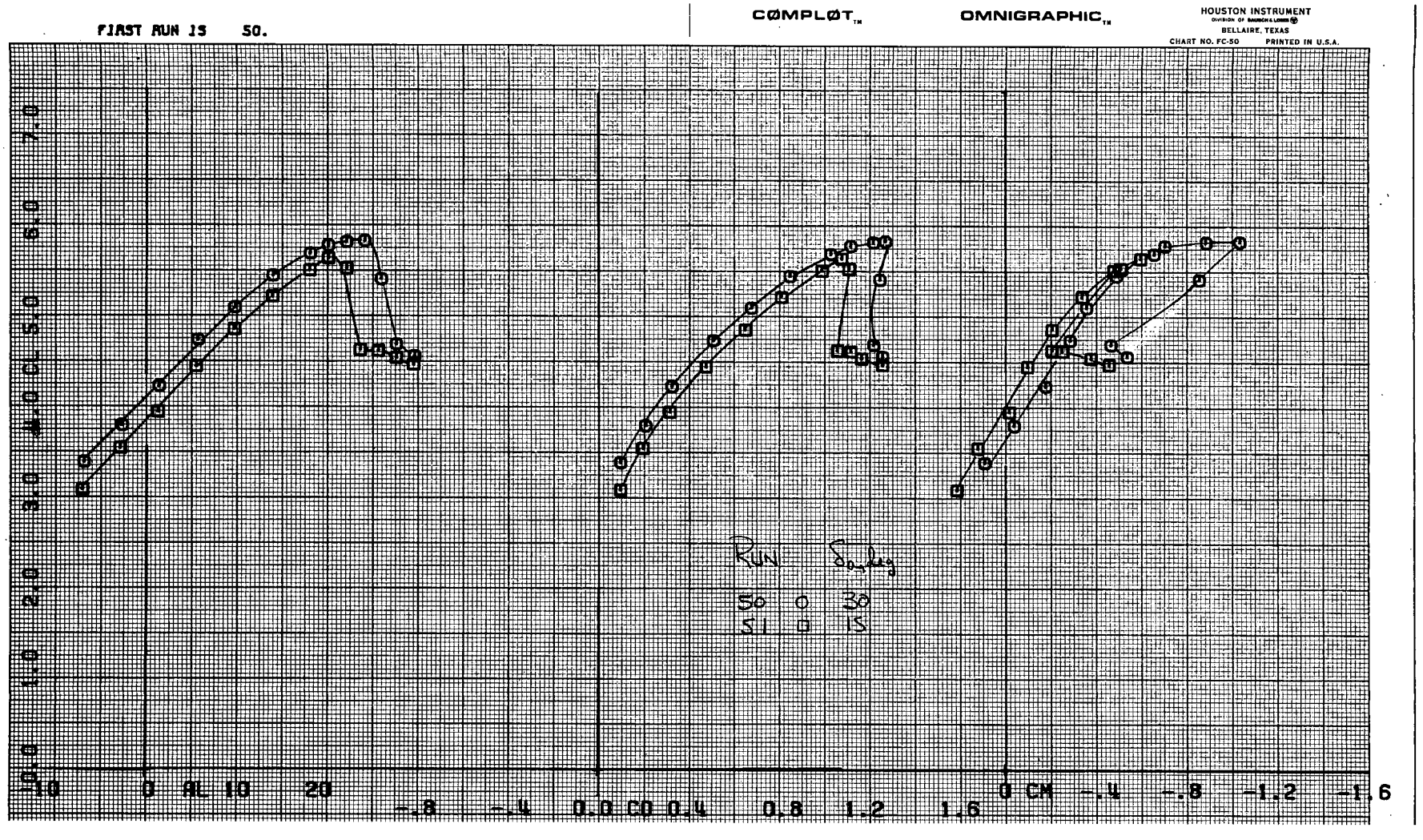

(a) $\delta_s = 60°$

Figure 9.- Effect of symmetrical aileron deflection on longitudinal aerodynamic characteristics with horizontal tail installed; $\delta_f = 70.6°$, $C_{J_I} = .77$.

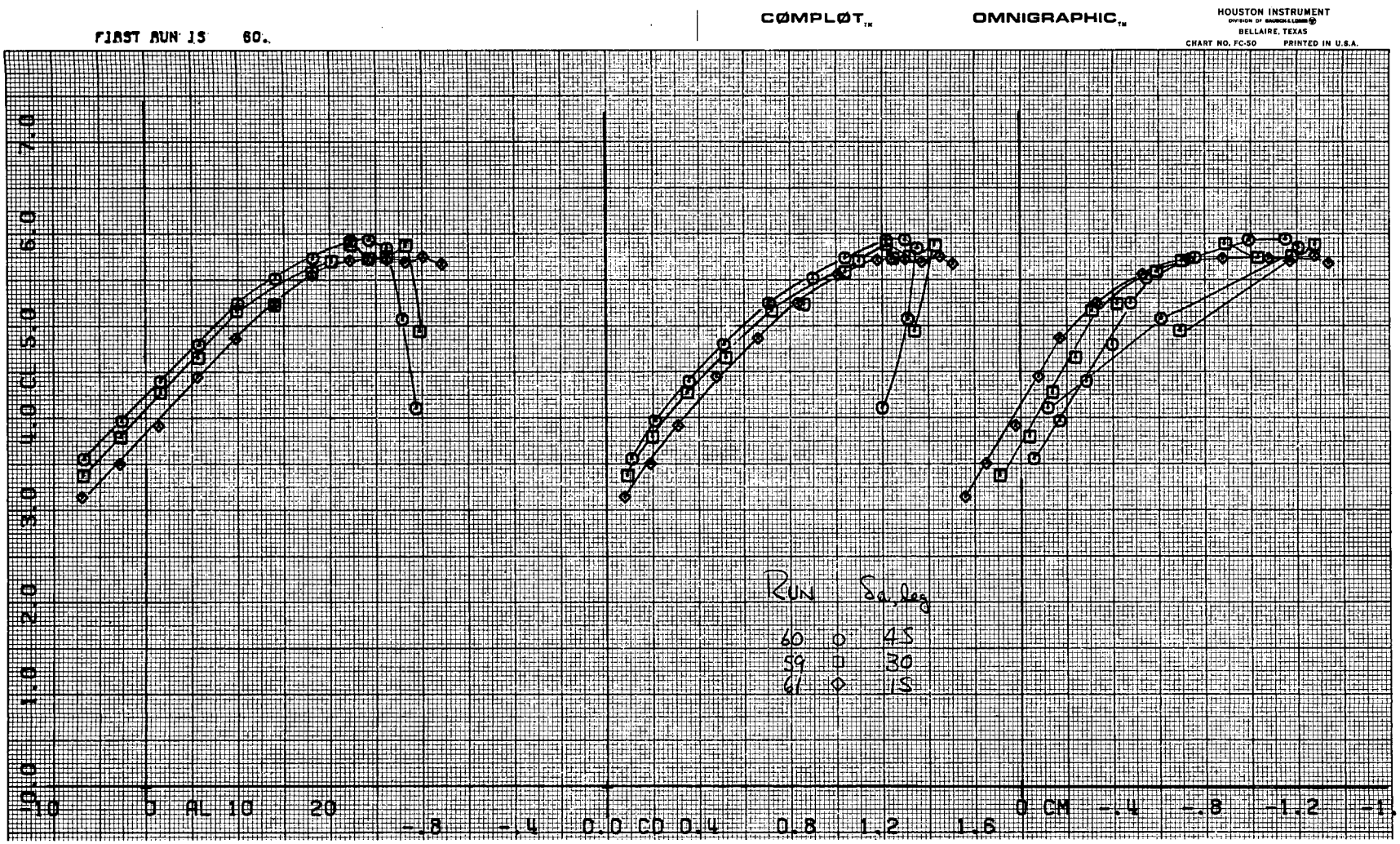

(b) $\delta_s = 60°$ (mod to stb'd)

Figure 9.- Concluded.

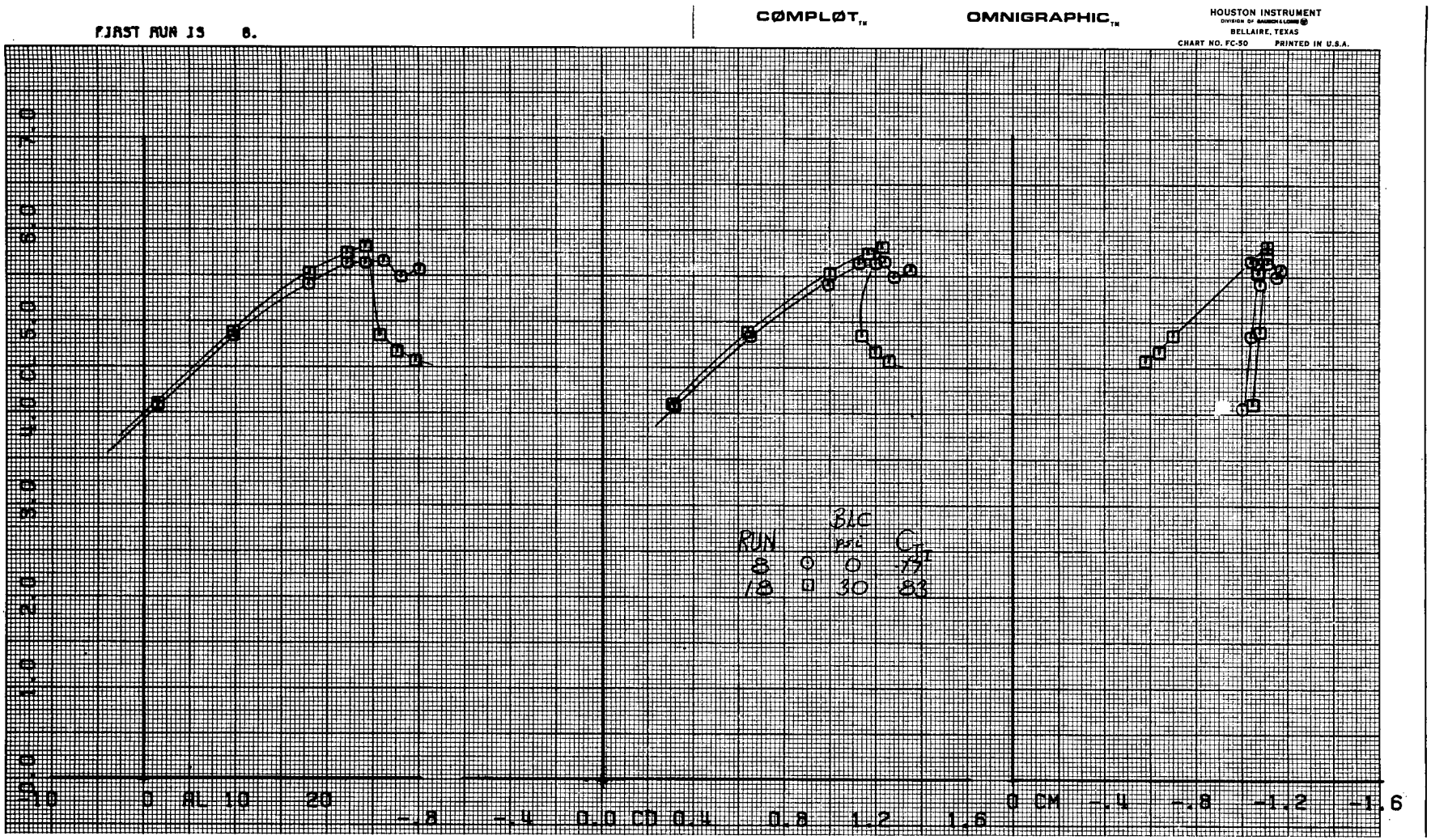

(a) $C_{J_I} = .77$

Figure 10.- Effect of fuselage BLC on longitudinal aerodynamic characteristics; $\delta_f = 70.6°$.

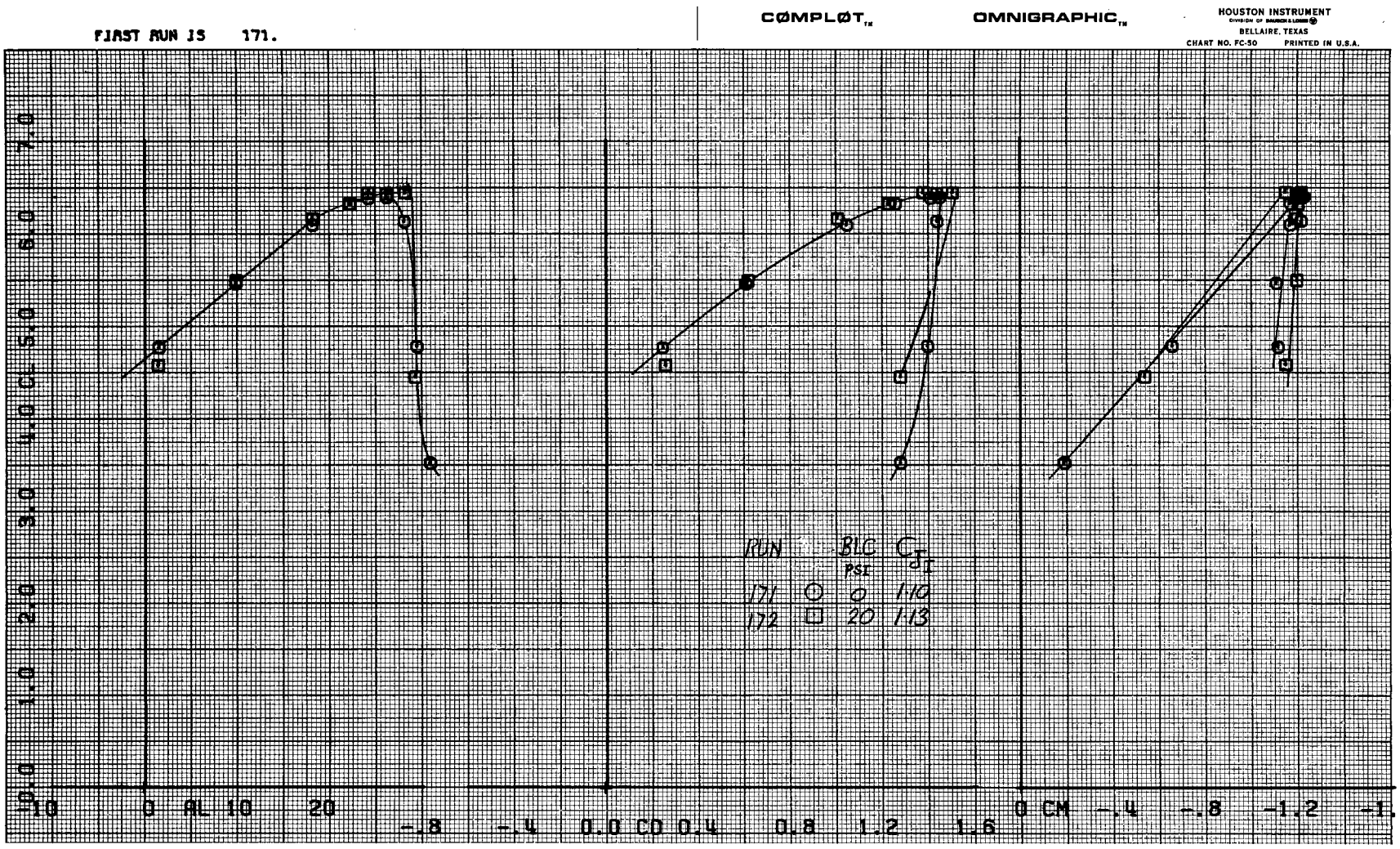

(b) $C_{J_I} = 1.10$, $\delta_s = 50°$

Figure 10.- Continued

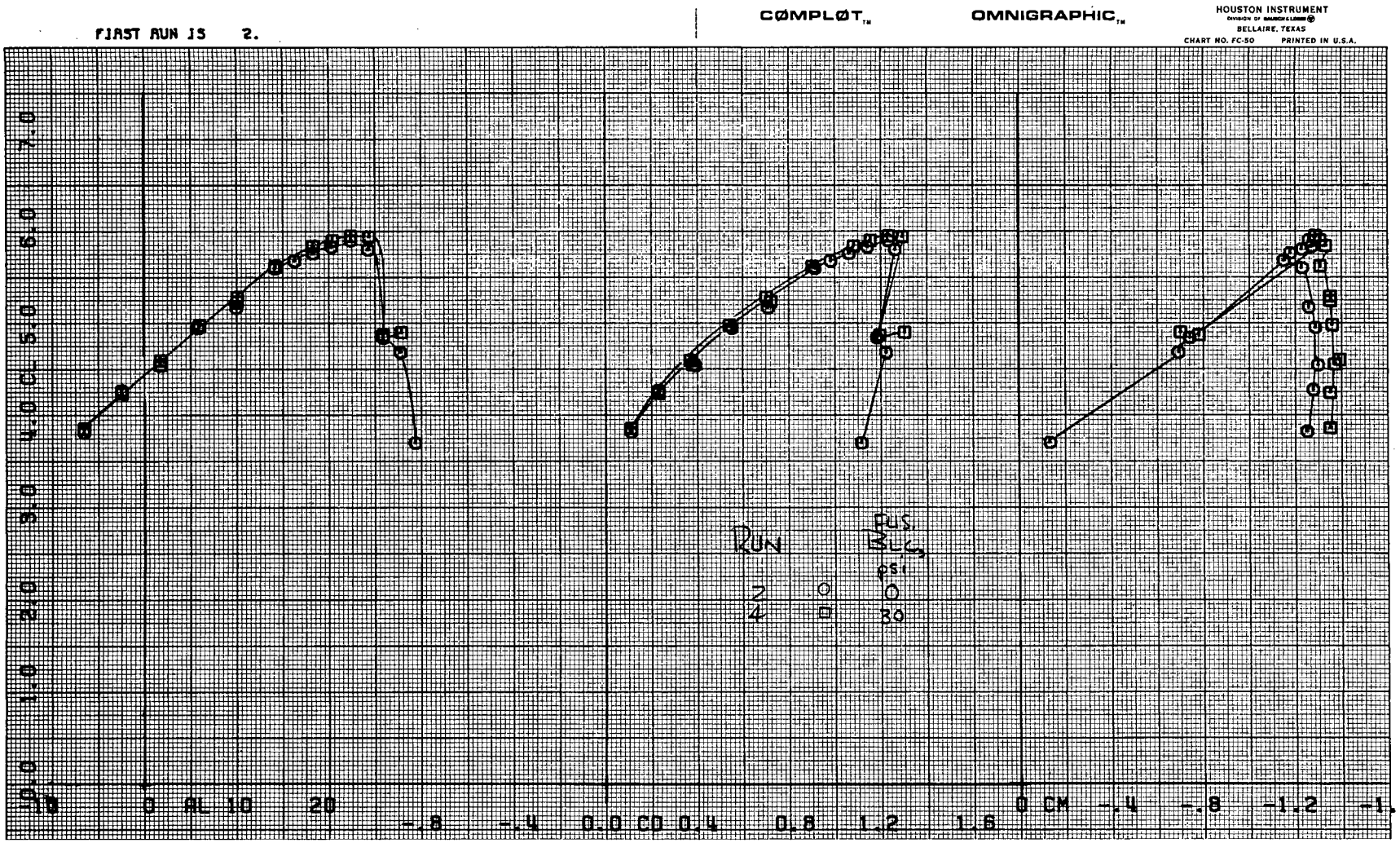

(c) $C_{J_I} = .77, \delta_s = 60°$

Figure 10.- Continued.

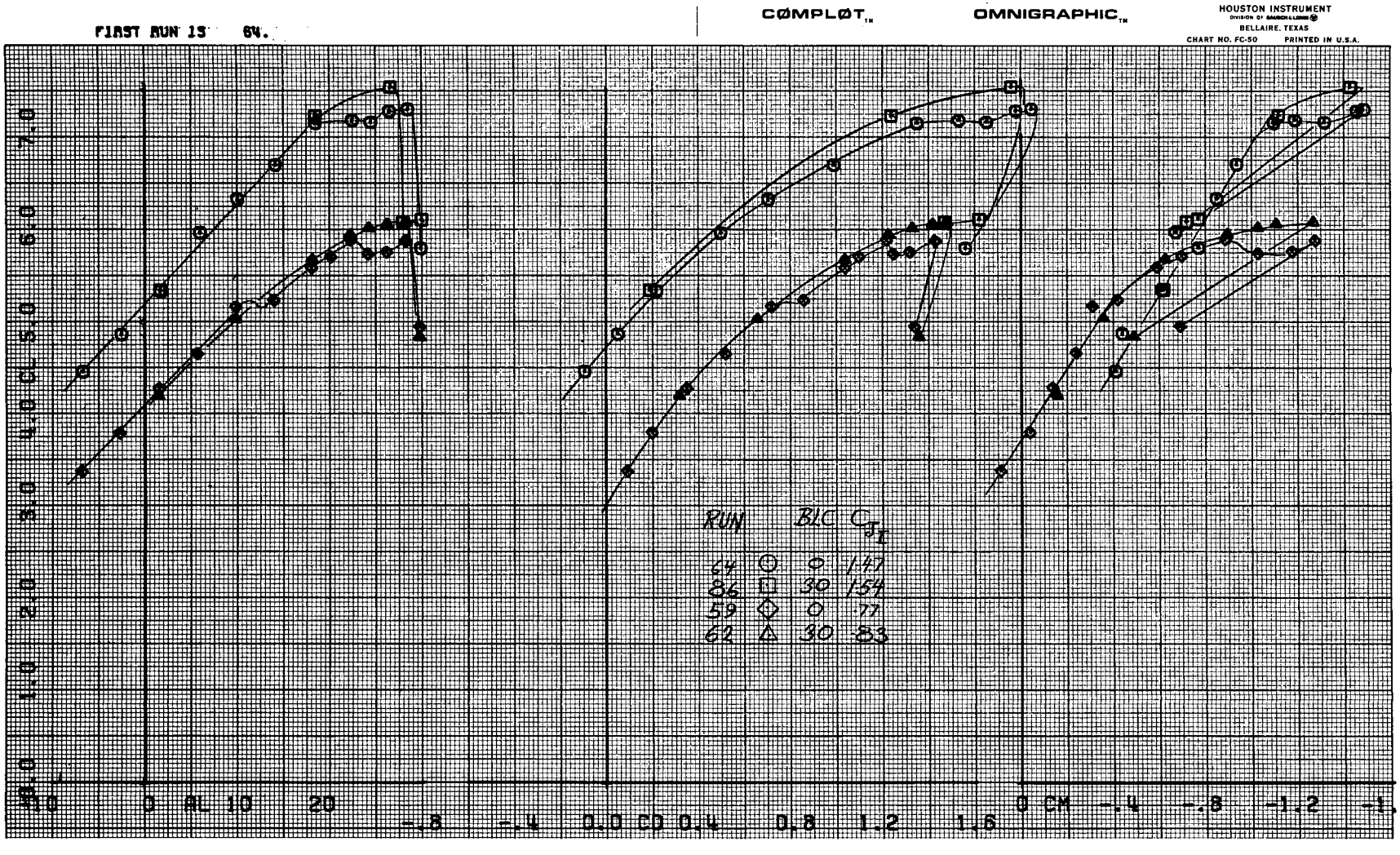

(d) $\delta_s = 60°$ (mod to stb'd), horizontal tail installed

Figure 10.- Concluded.

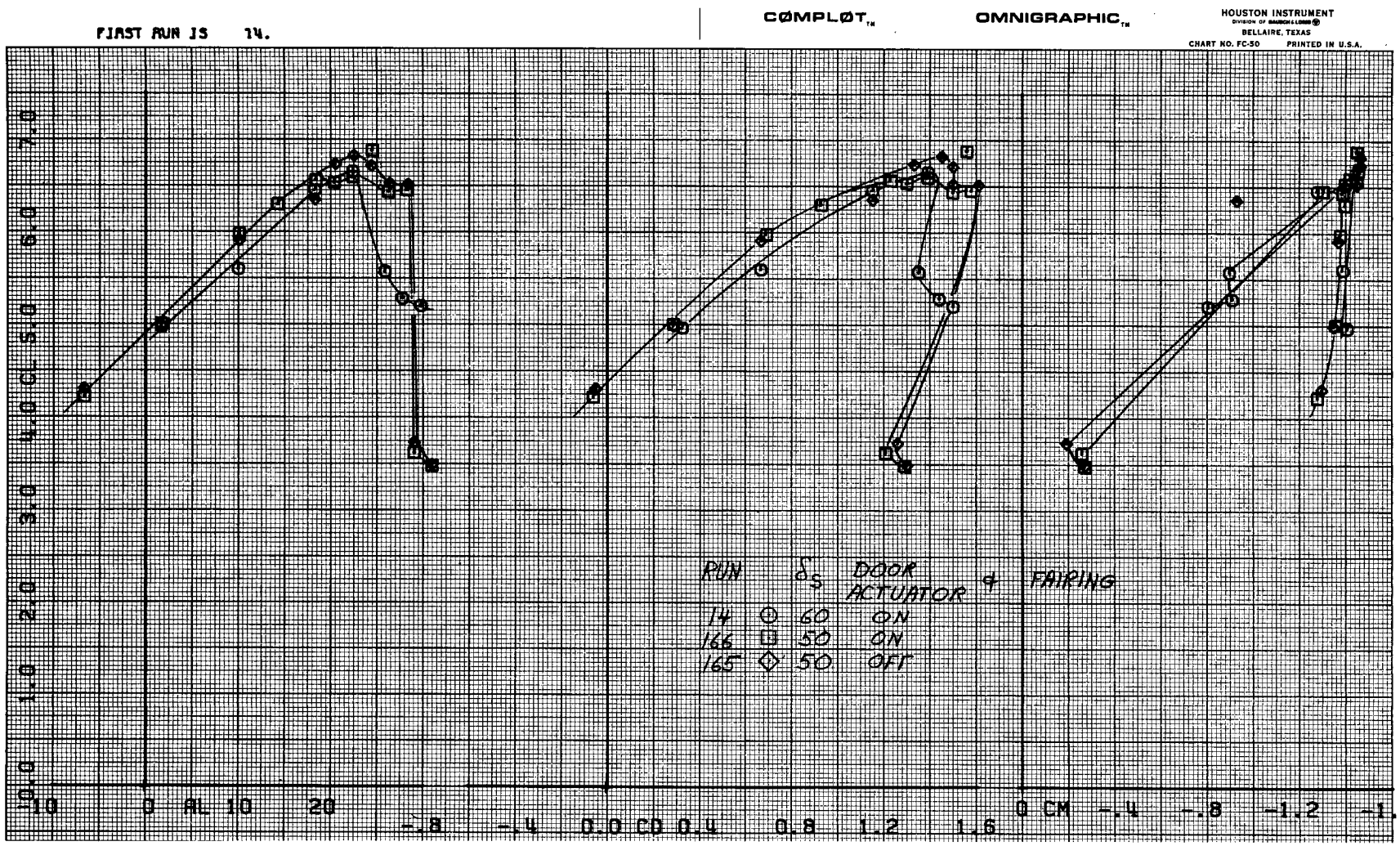

(a) δ_s = 60° and 50°

Figure 11.- The effect of intake door actuator fairing on longitudinal aerodynamic characteristics; δ_f = 70.6°.

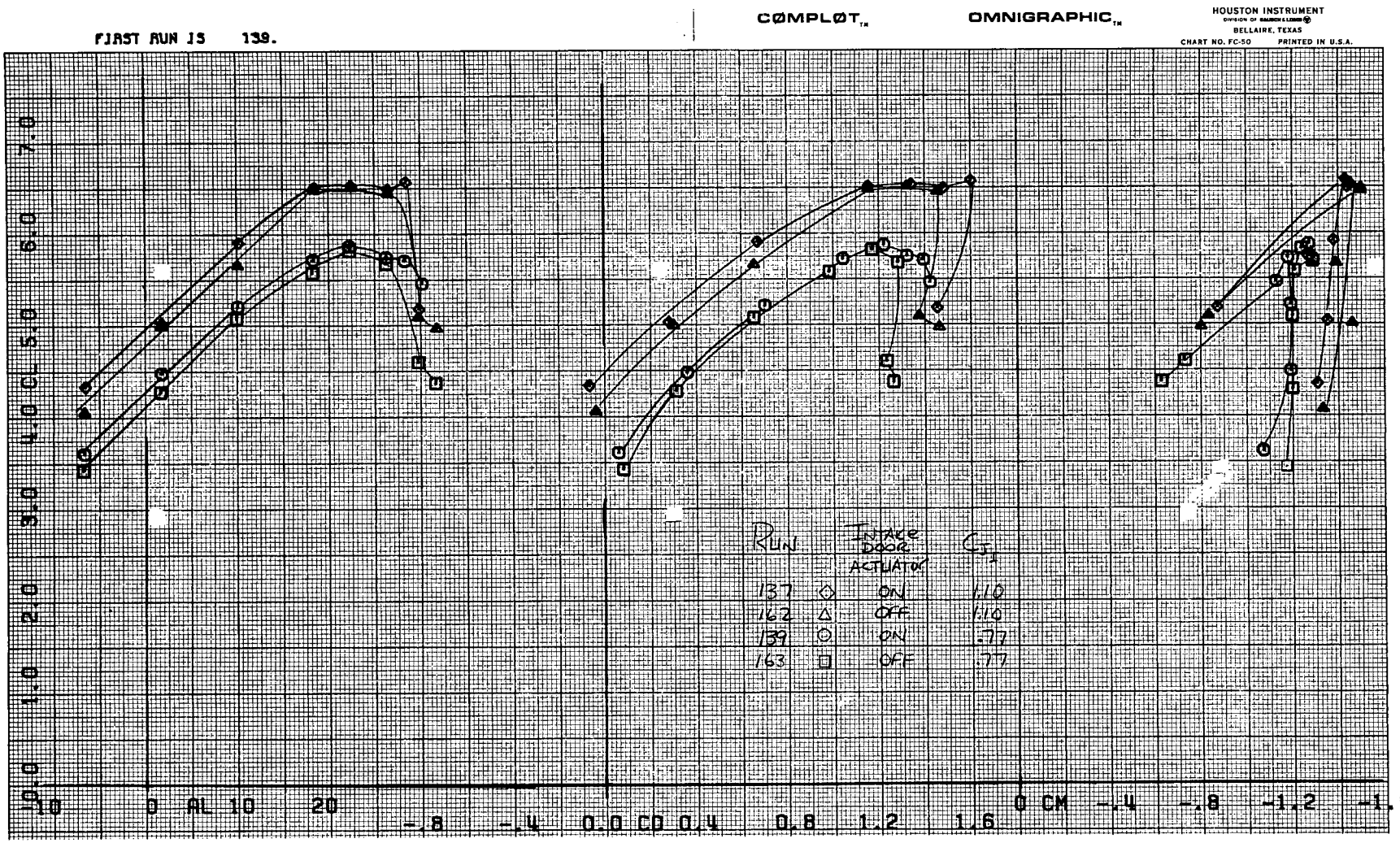

(b) $\delta_s = 60°$ (mod to stb'd)

Figure 11.- Concluded.

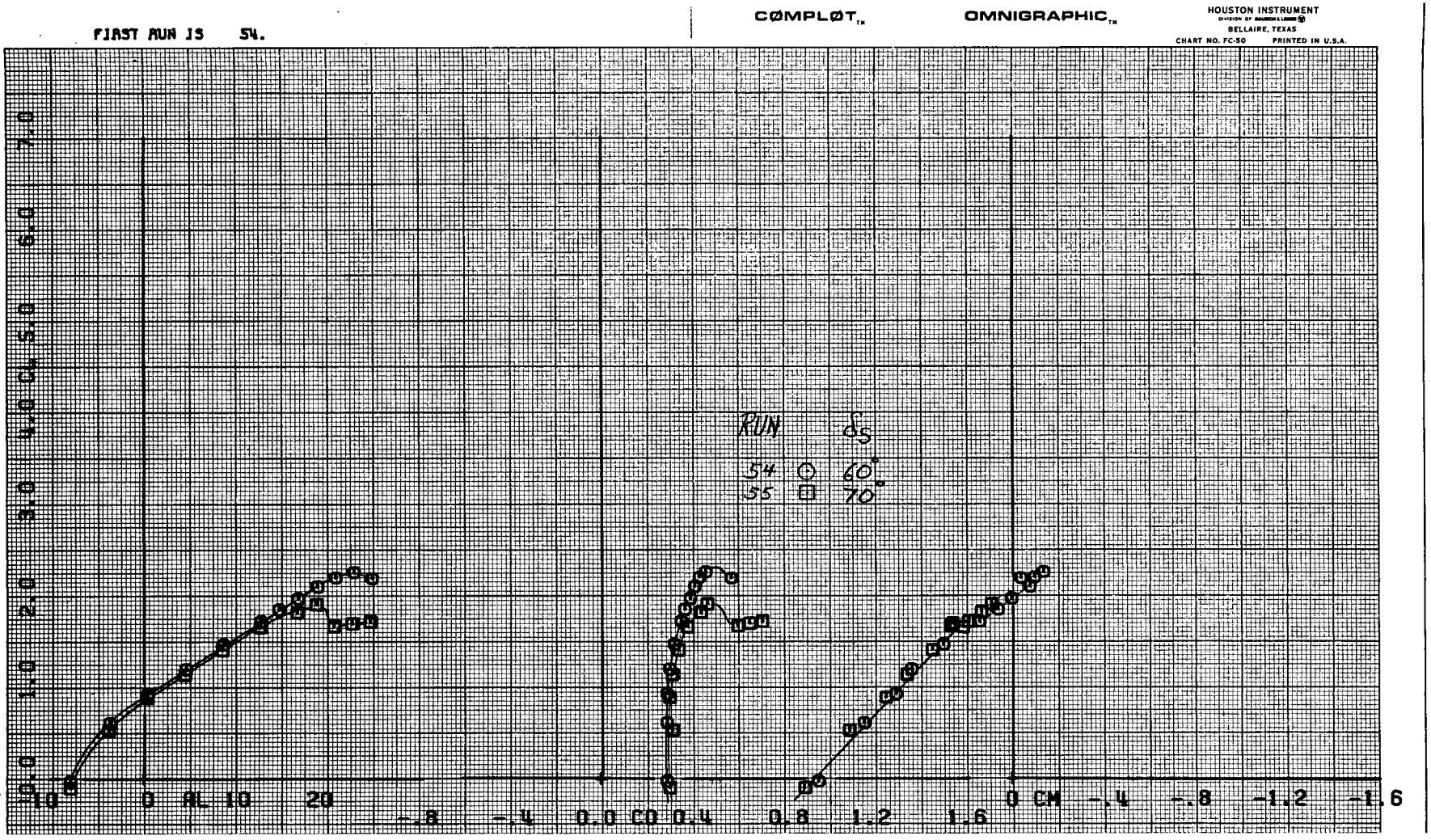

(a) $C_{J_I} = 0$

Figure 12.- Effect of slat deflection on longitudinal aerodynamic characteristics with horizontal tail installed; $\delta_f = 70.6°$.

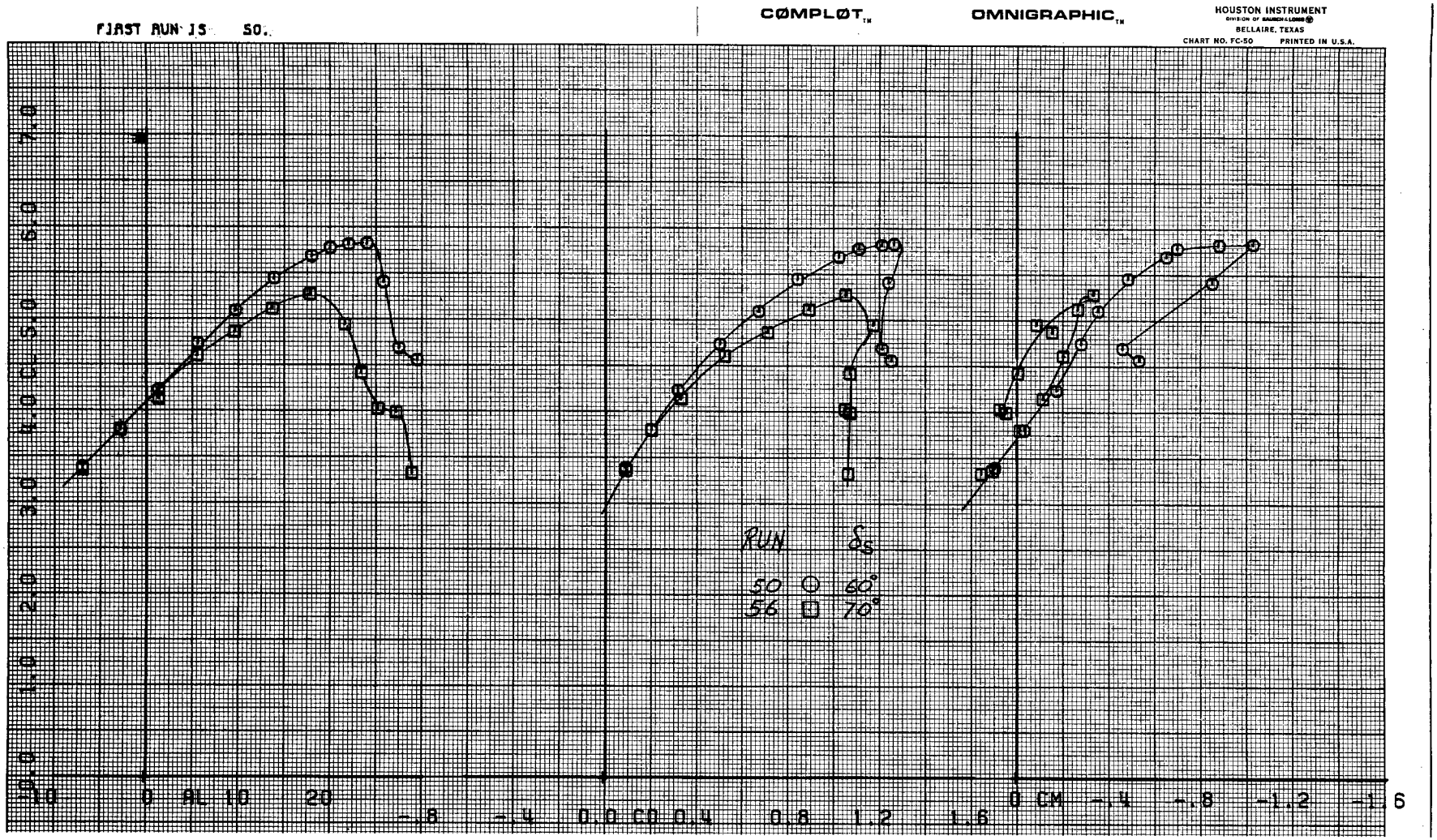

(b) $C_{J_I} = .77$

Figure 12.- Concluded.

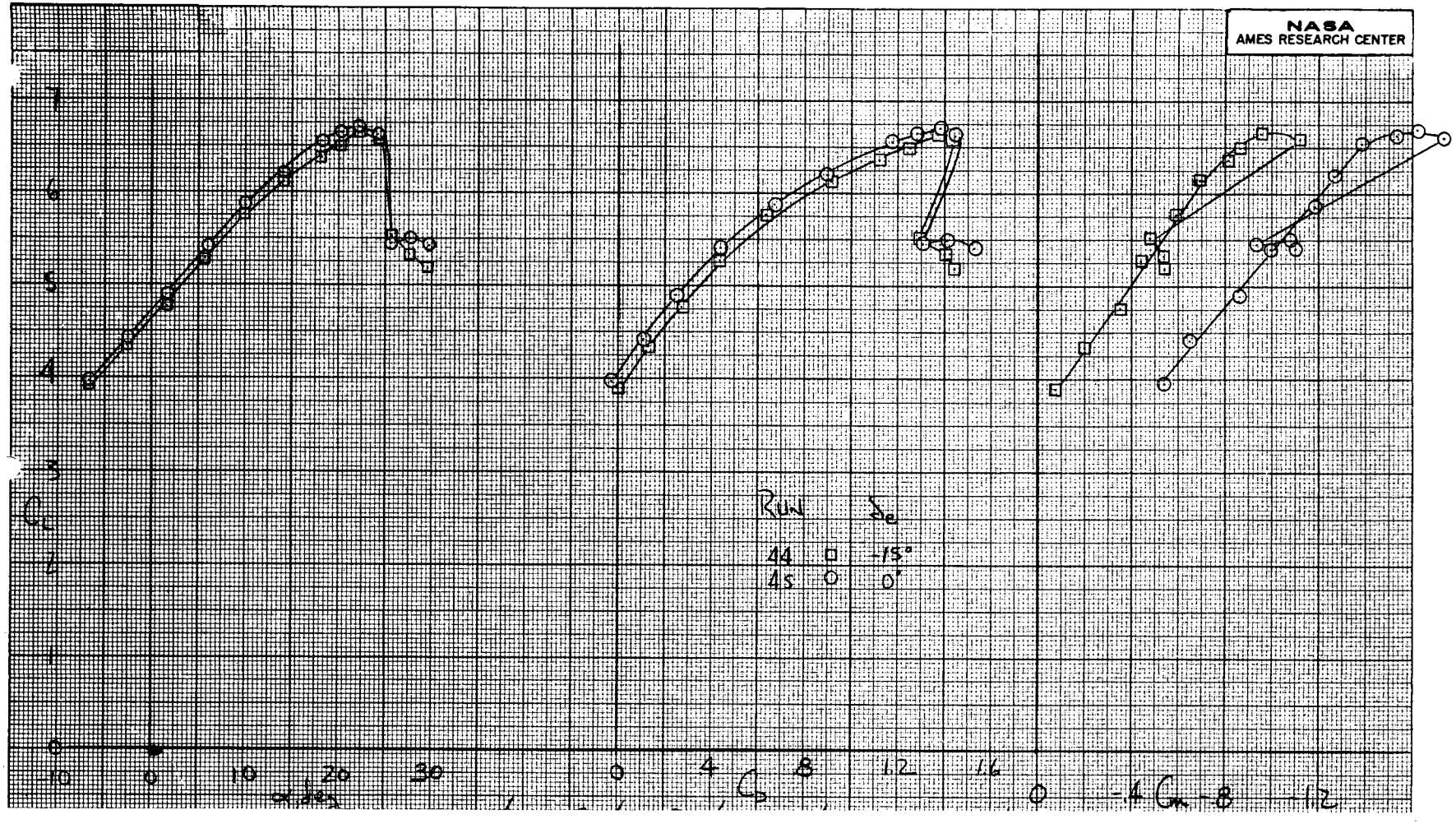

(a) $C_{J_I} = 1.10$, $i_t = -1°$

Figure 13. - Effect of elevator deflection on longitudinal aerodynamic characteristics; $\delta_f = 70.6$.

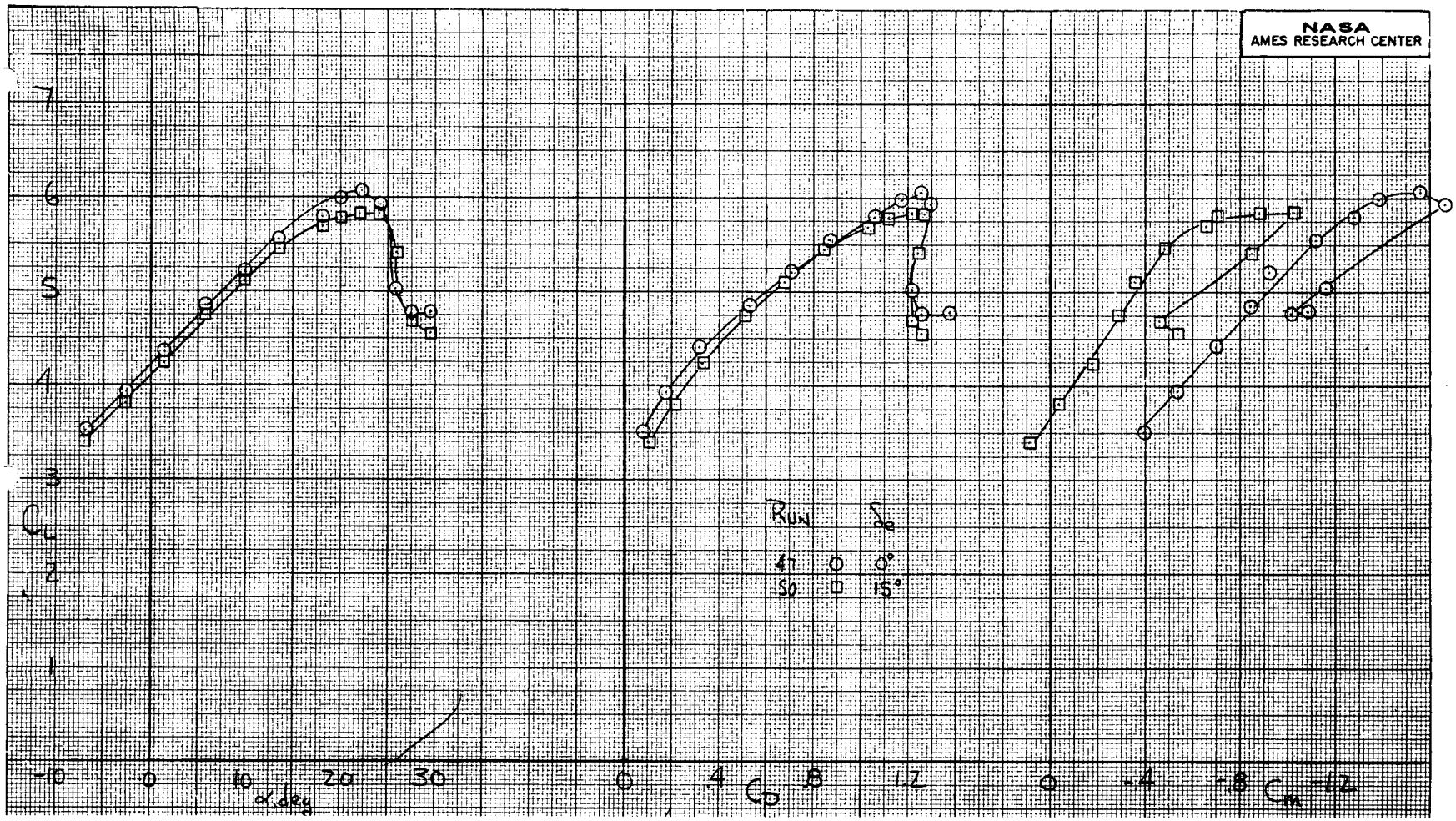

(b) $C_{J_I} = .77$, $i_t = -1$

Figure 13.- Continued.

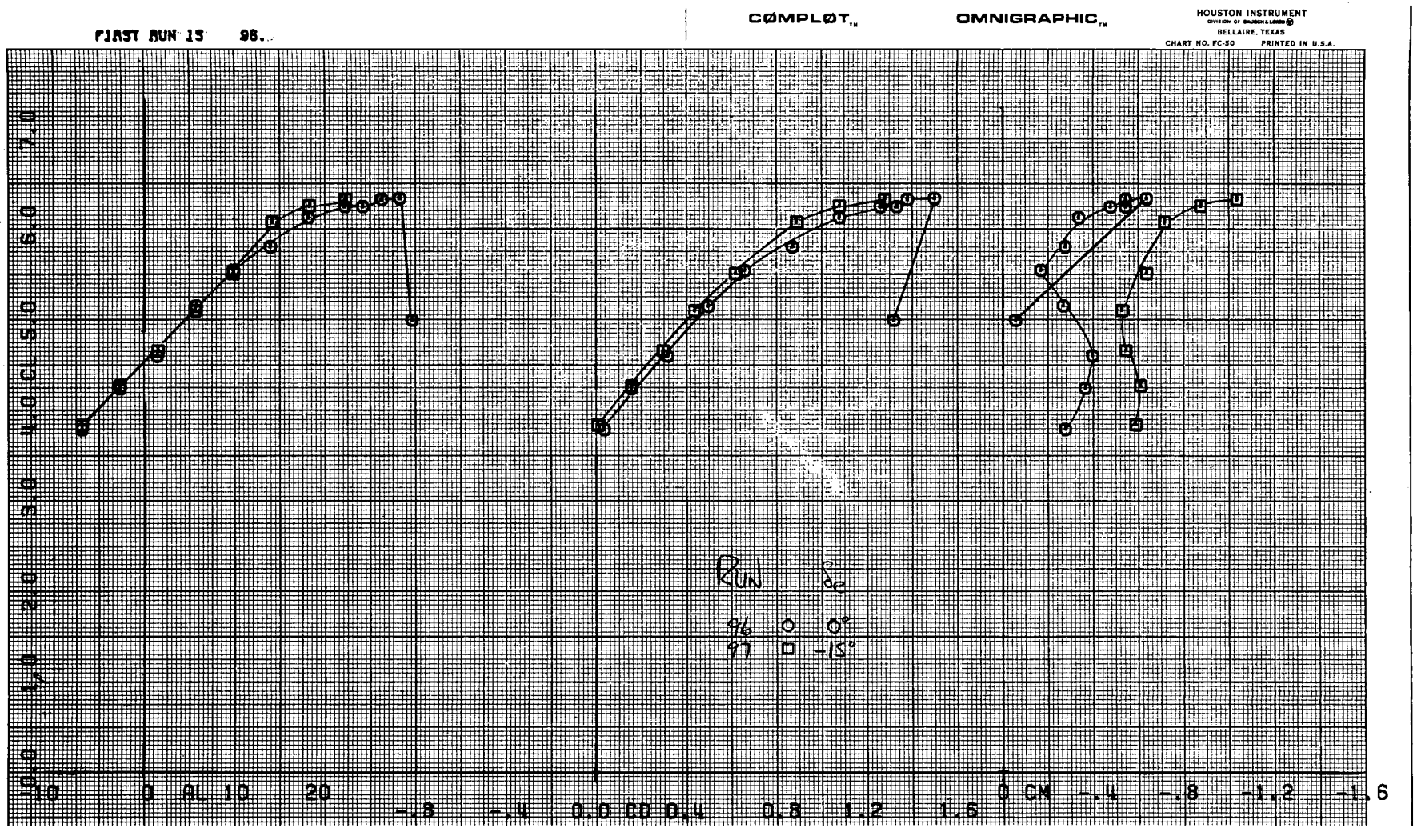

(c) $C_{J_I} = 1.10$, $i_t = -10.1°$

Figure 13.- Continued.

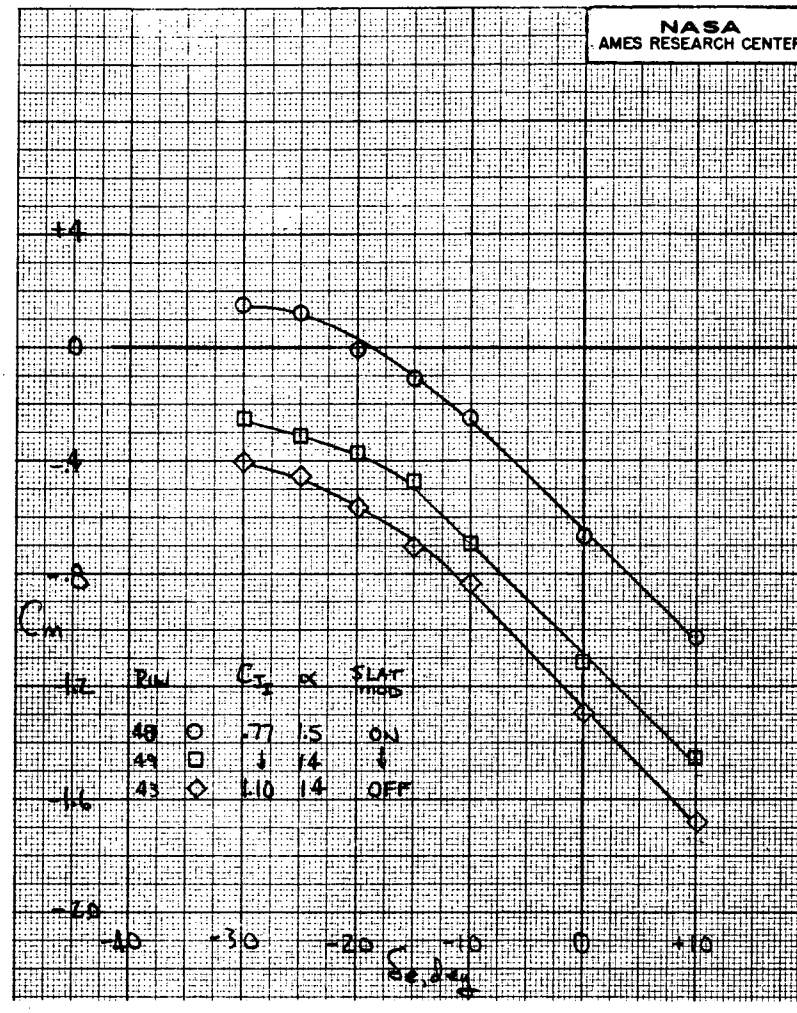

(d) C_m vs. δ_e

Figure 13.- Concluded.

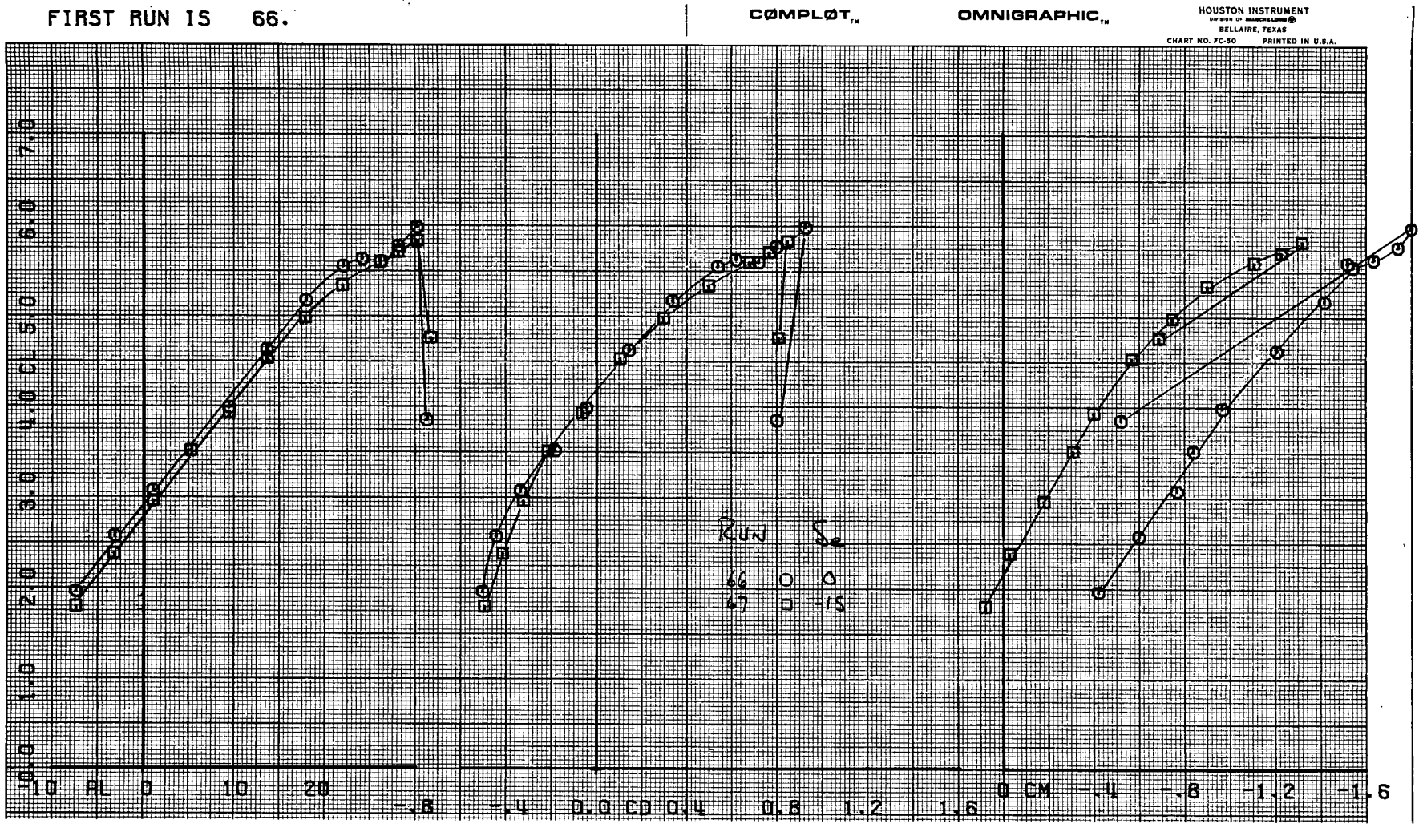

Figure 14.- Effect of elevator deflection on longitudinal aerodynamic characteristics; $\delta_f = 41.1°$, $C_{J_I} = .77$, $i_t = -1°$.

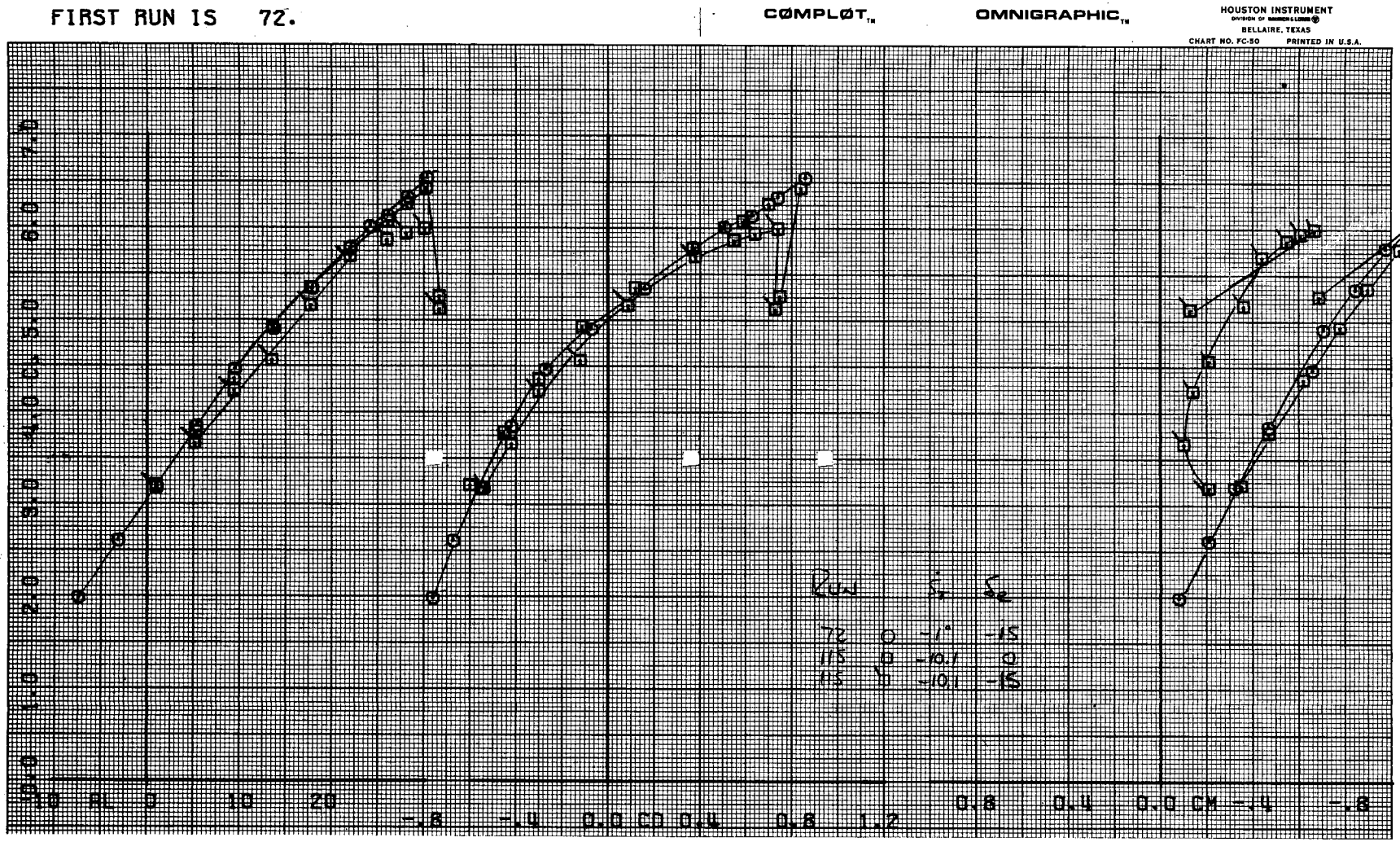

Figure 15.- Effect of tail incidence on longitudinal aerodynamic characteristics; $\delta_f = 41.1$, $C_{J_I} = 1.10$.

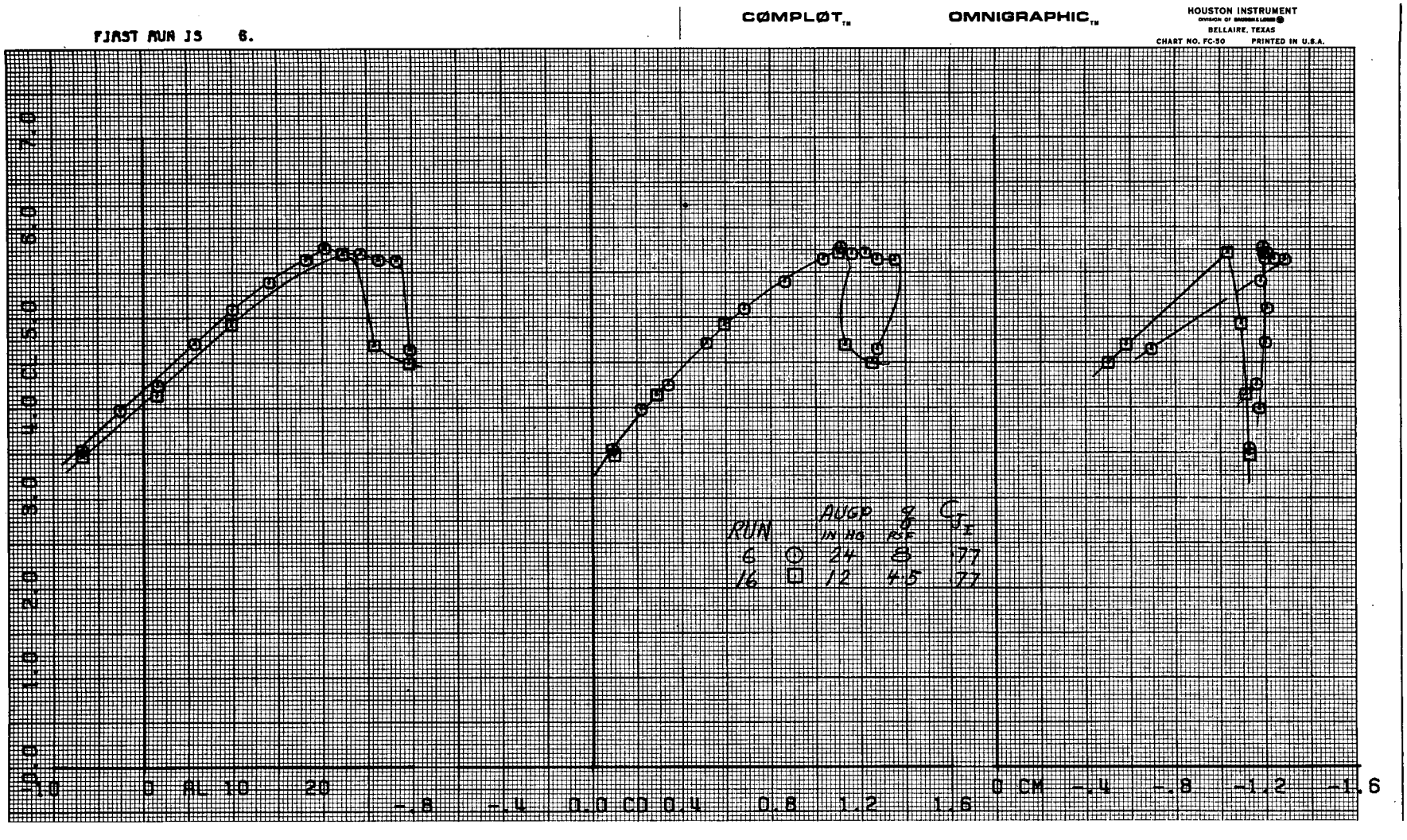

Figure 16.- Correlation of C_{J_I}; $\delta_f = 70.6°$, $C_{J_I} = .77$.

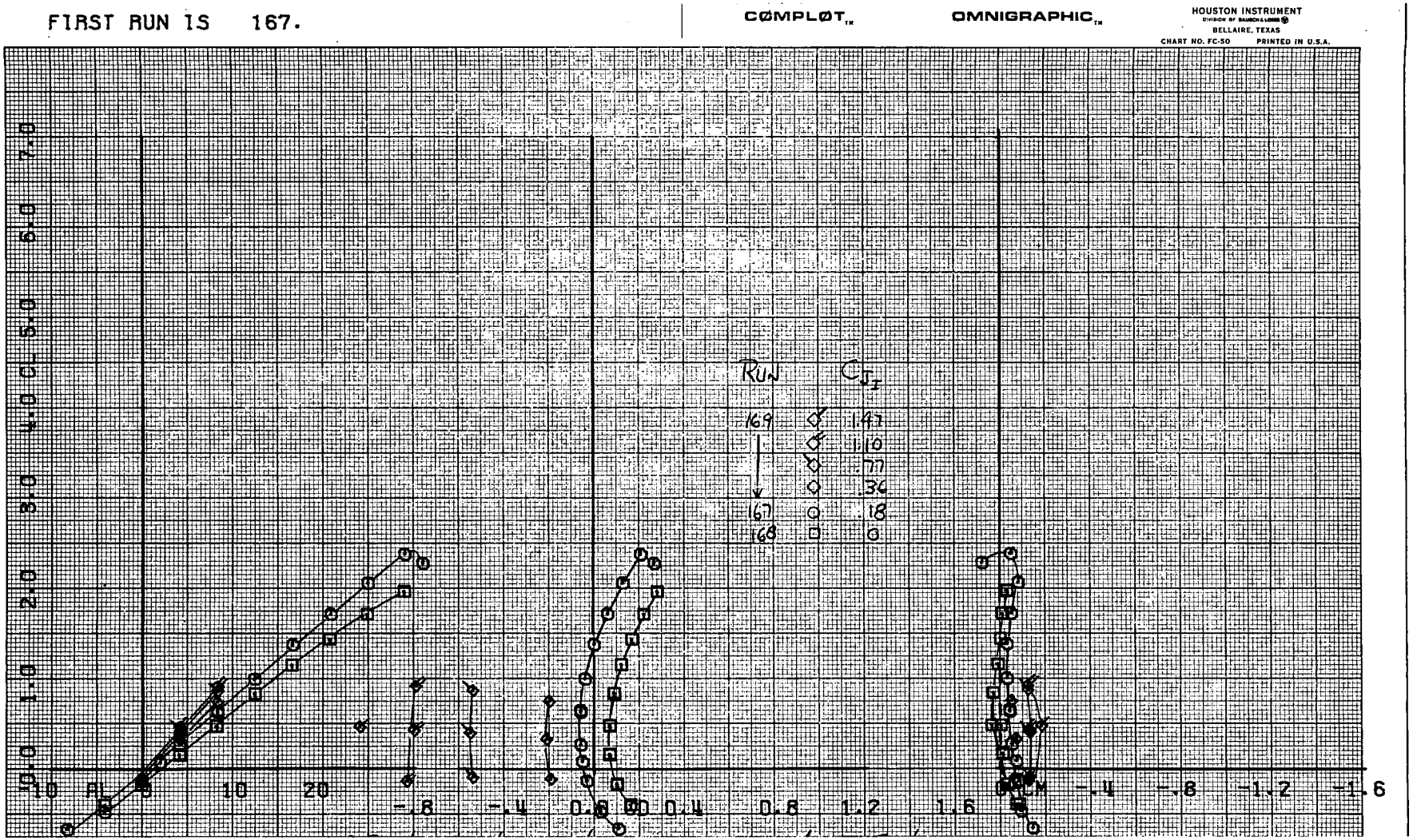

Figure 17.- Effect of C_{J_I} on the longitudinal aerodynamic characteristics with horizontal tail removed; $\delta_f = 0°$ and $\delta_s = 50°$.

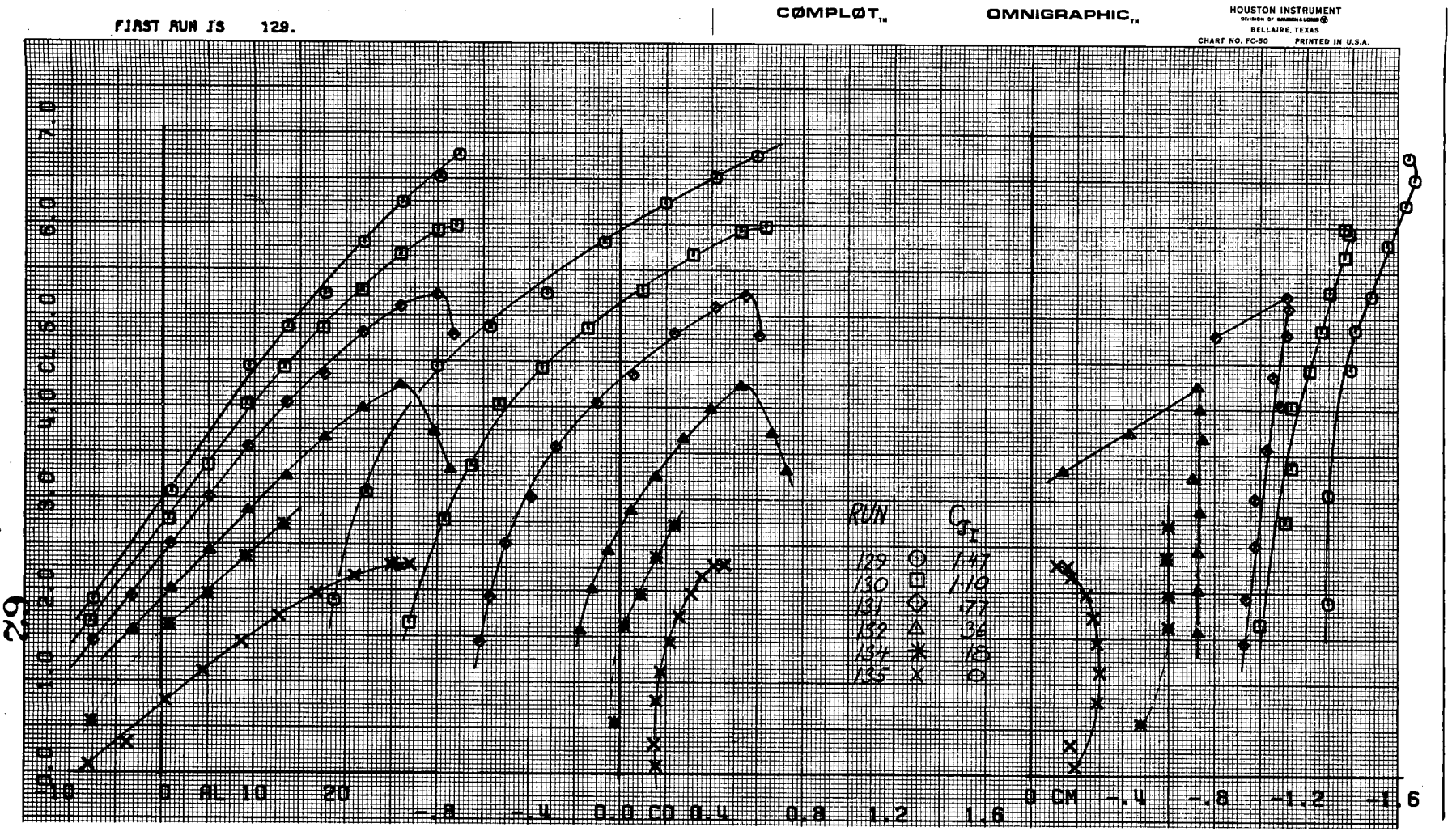

Figure 18.- Effect of C_{J_I} ON Longitudinal aerodynamic characteristics with horizontal tail removed; δ_f = 31.8° and δ_s = 60° (mod to stb'd).

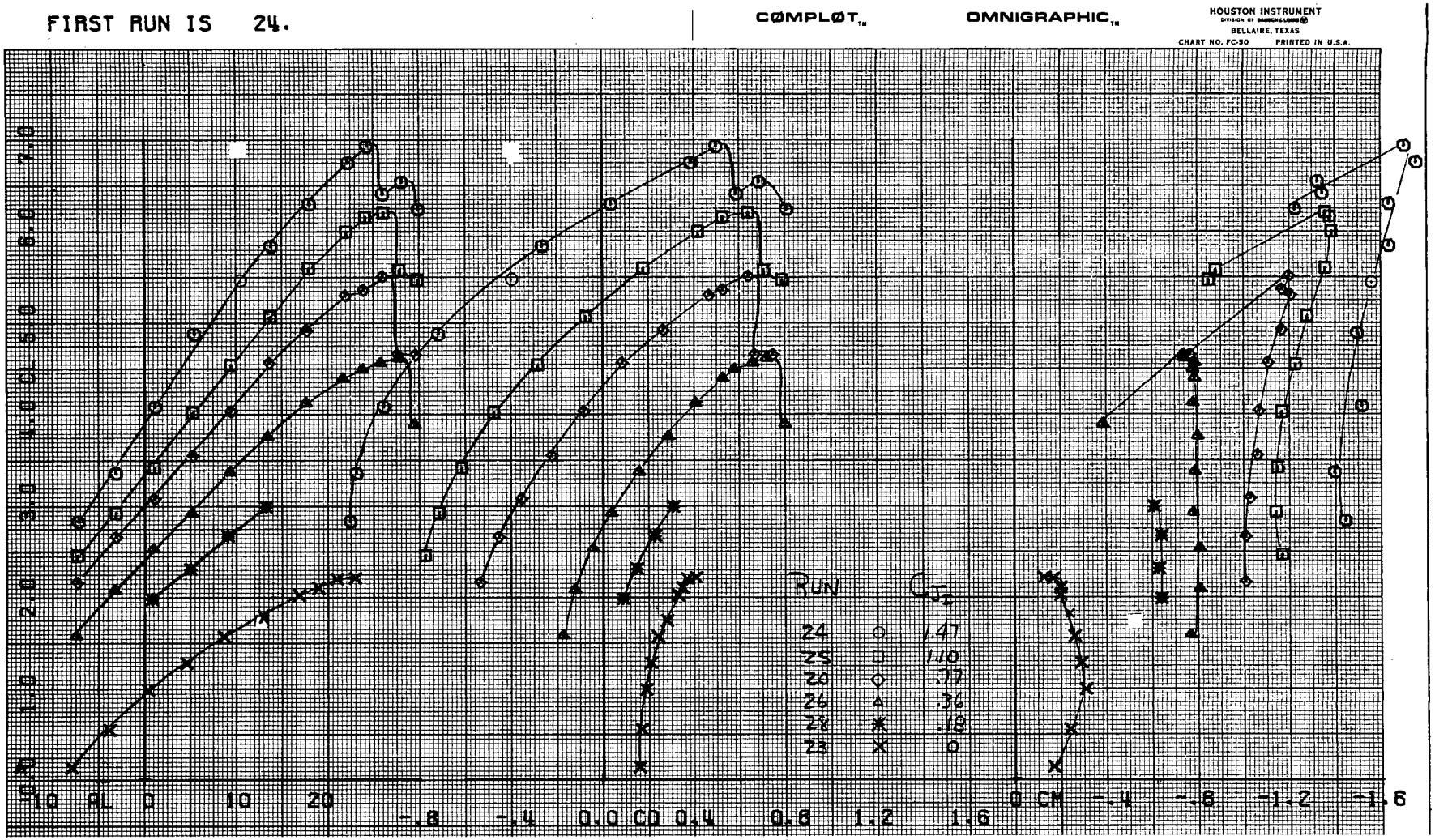

(a) Effect of C_{J_I}

Figure 19.- Longitudinal aerodynamic characteristics with horizontal tail removed; δ_f = 41.1° and δ_s = 60°.

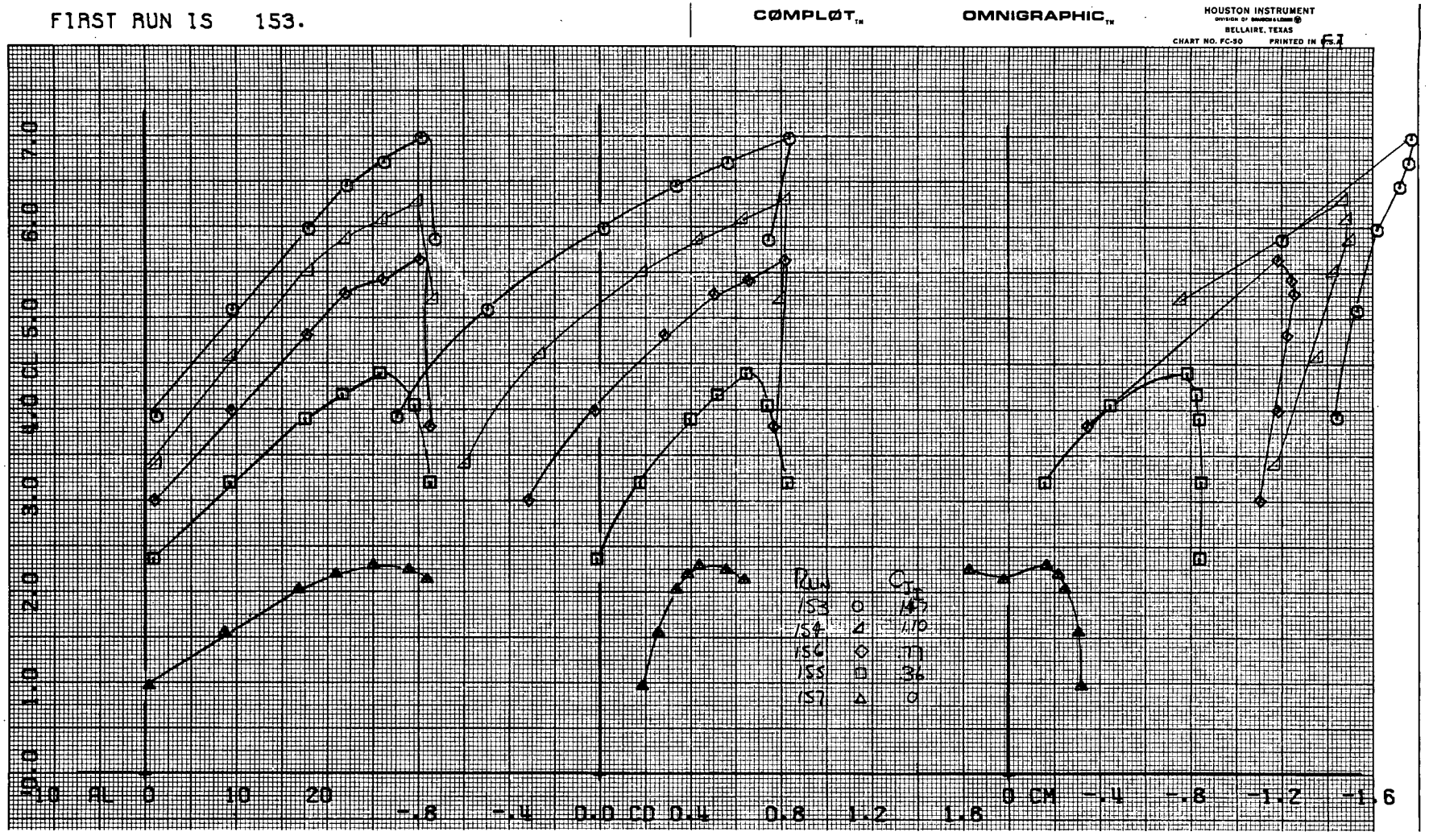

(b) Effect of C_{J_T}; $\delta_s = 60°$ (mod. to stb'd)
Figure 19.- Concluded.

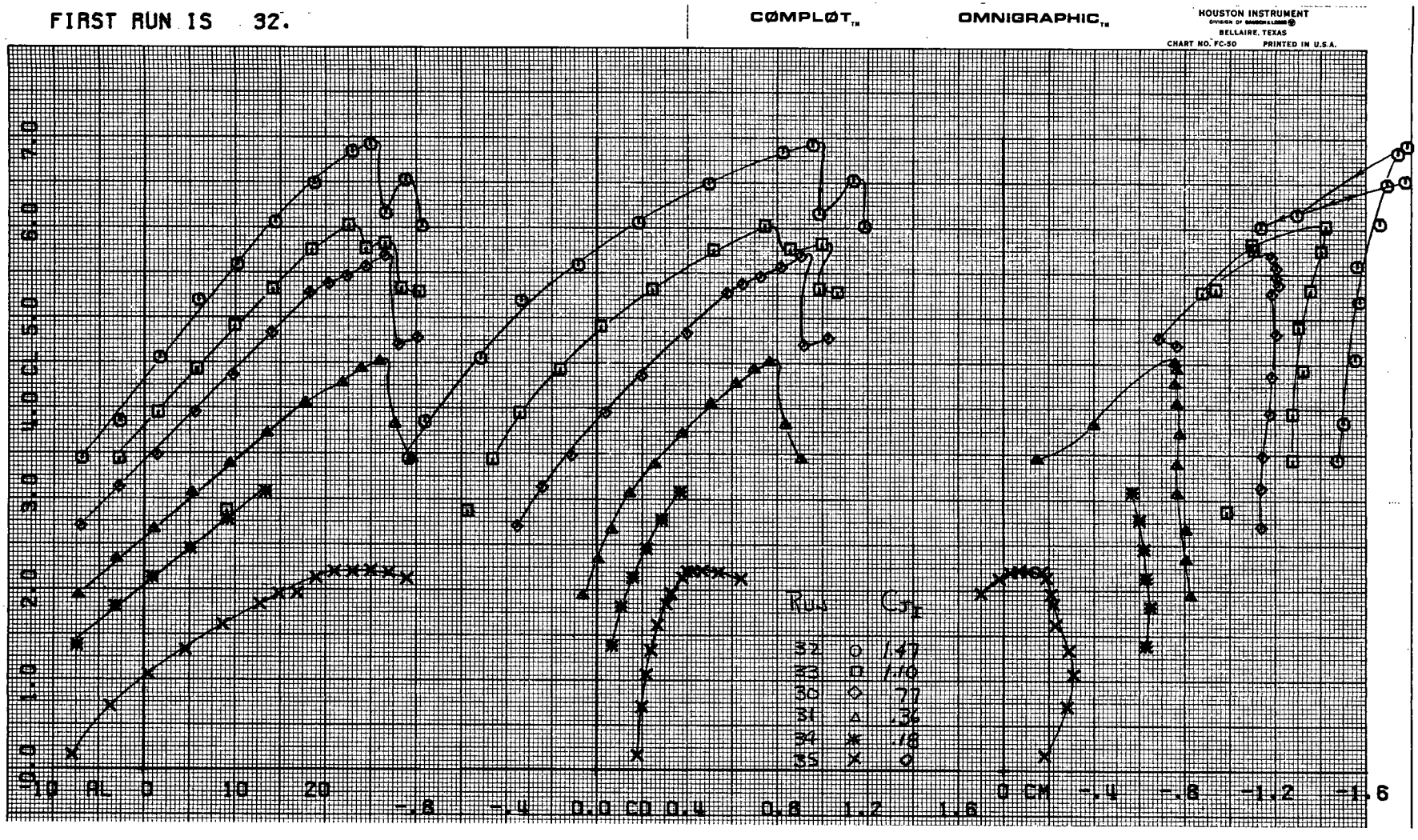

Figure 20.- Effect of C_{J_I} on the longitudinal aerodynamic characteristics with horizontal tail removed; $\delta_f = 51.1°$ and $\delta_s = 60°$.

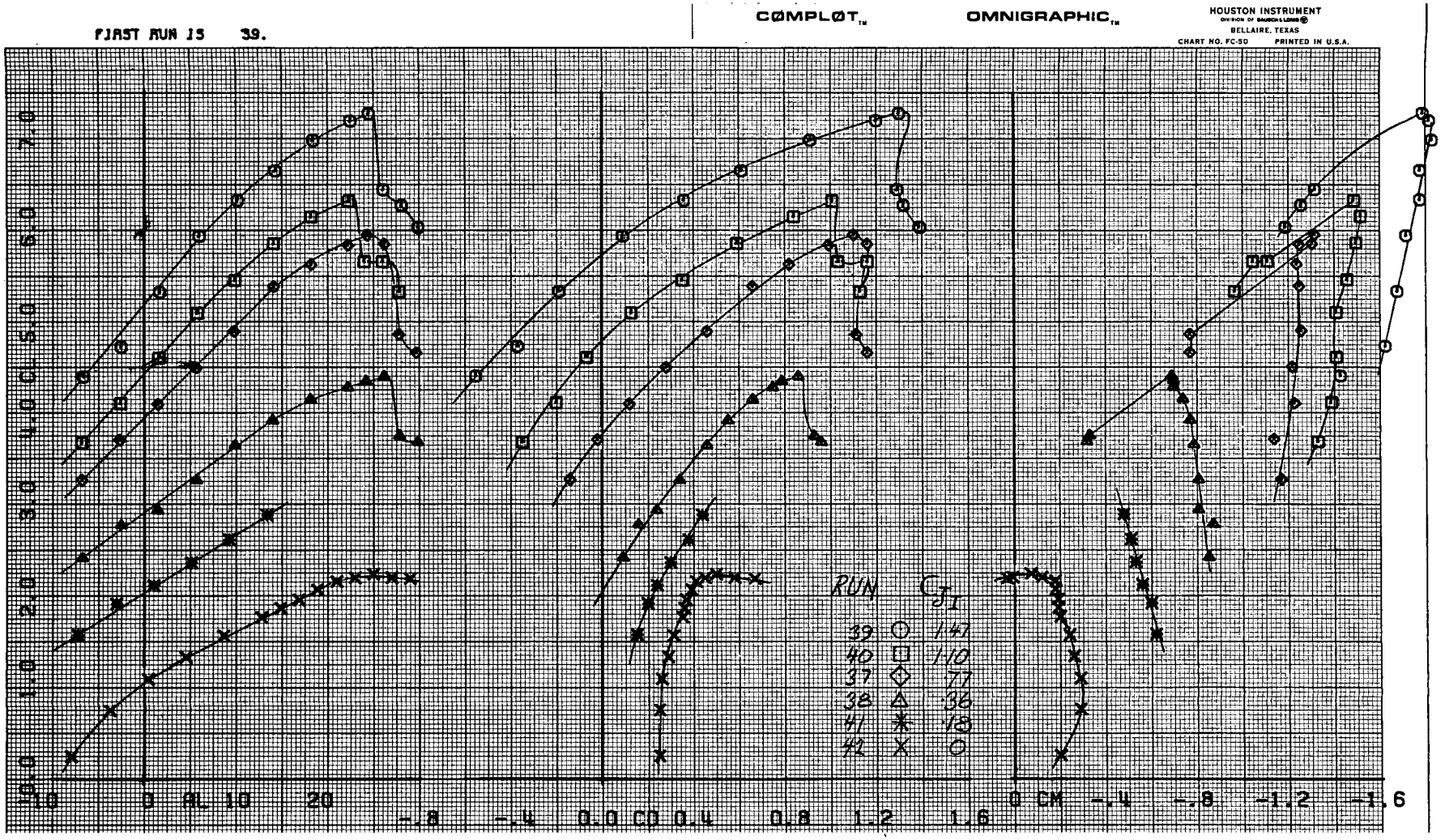

Figure 21.- Effect of C_{J_I} on the longitudinal aerodynamic characteristics with horizontal tail removed; $\delta_f = 61.2°$ and $\delta_s = 60°$

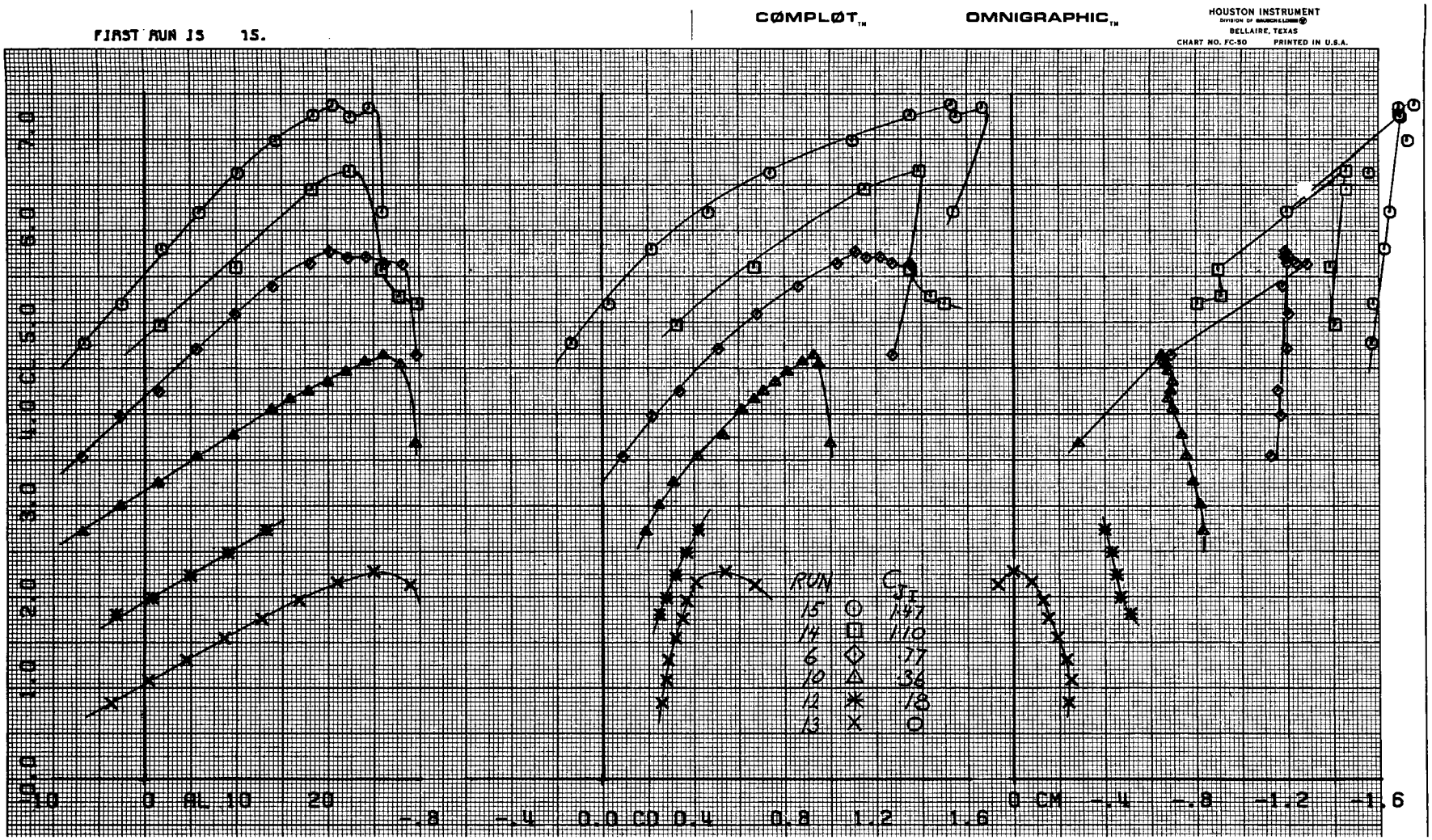

(a) Effect of C_{J_I}

Figure 22.- Longitudinal aerodynamic characteristics with horizontal tail removed; δ_f = 70.6° and δ_s = 60°.

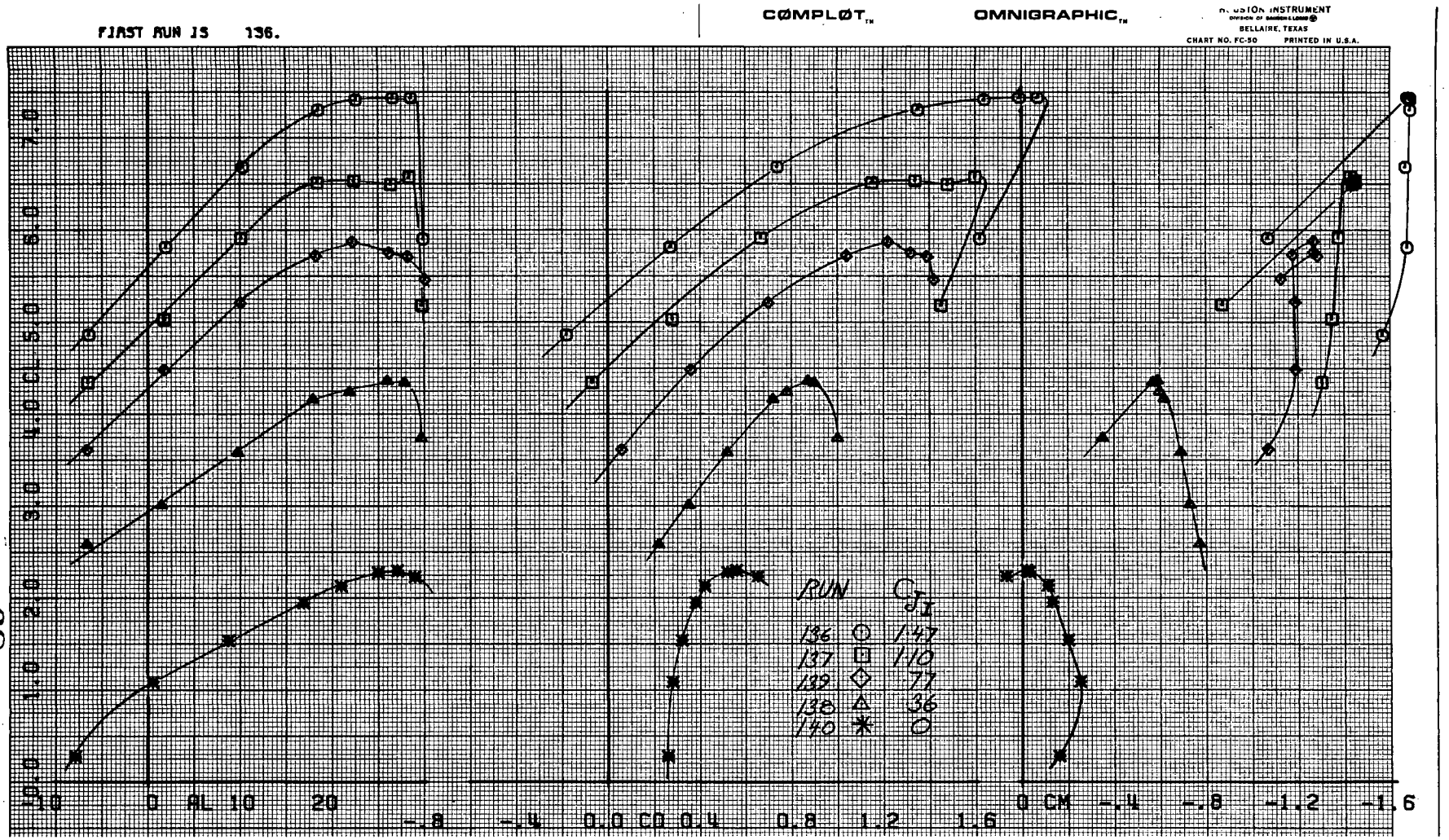

(b) Effect of C_{J_I}; $\delta_s = 60°$ (mod. to stb'd)

Figure 22.- Concluded.

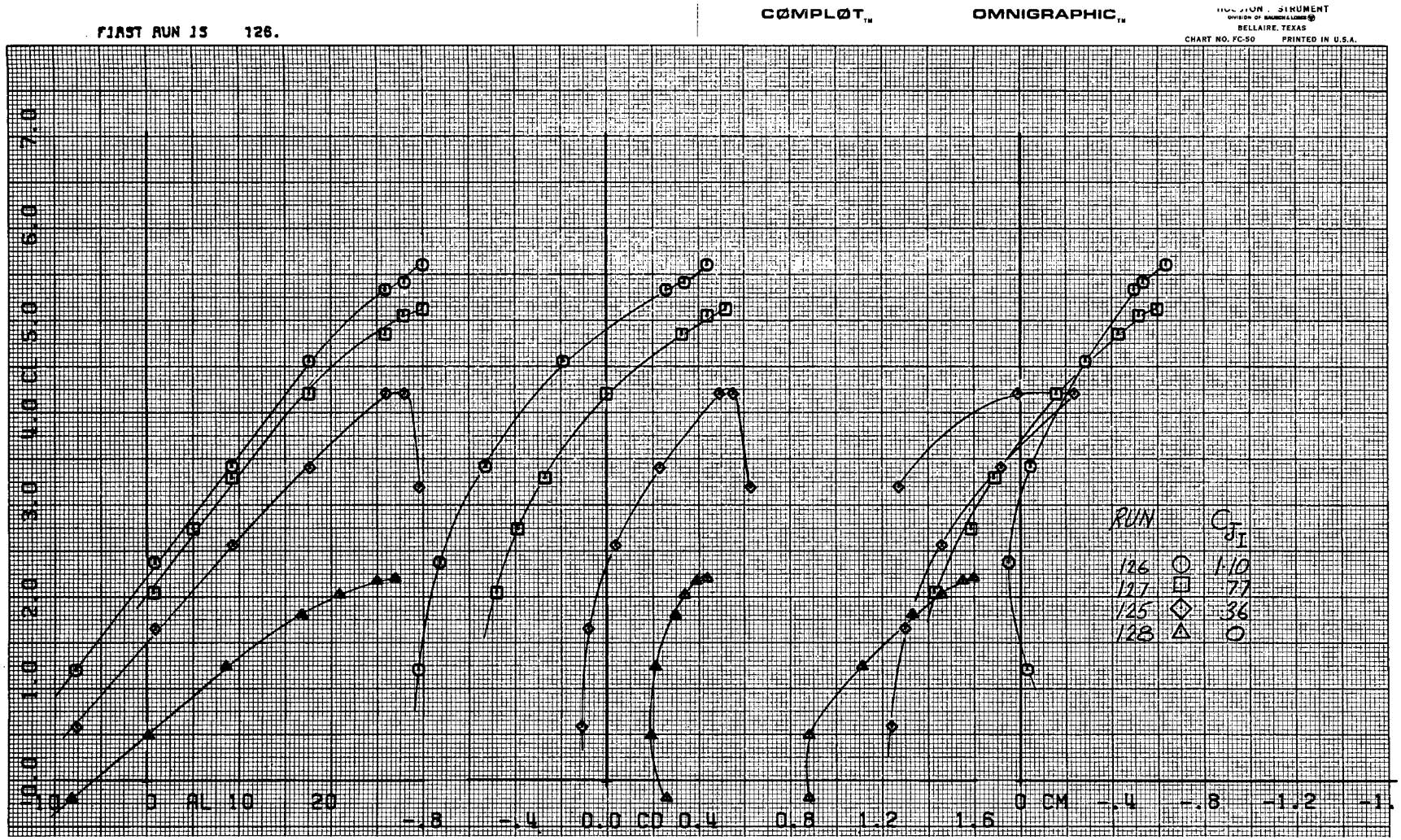

Figure 23.- Effect of C_{J_I} on longitudinal aerodynamic characteristics with horizontal tail installed; $\delta_f = 31.8°$, $\delta_s = 60°$ (mod to stb'd), and $i_t = -10.1°$.

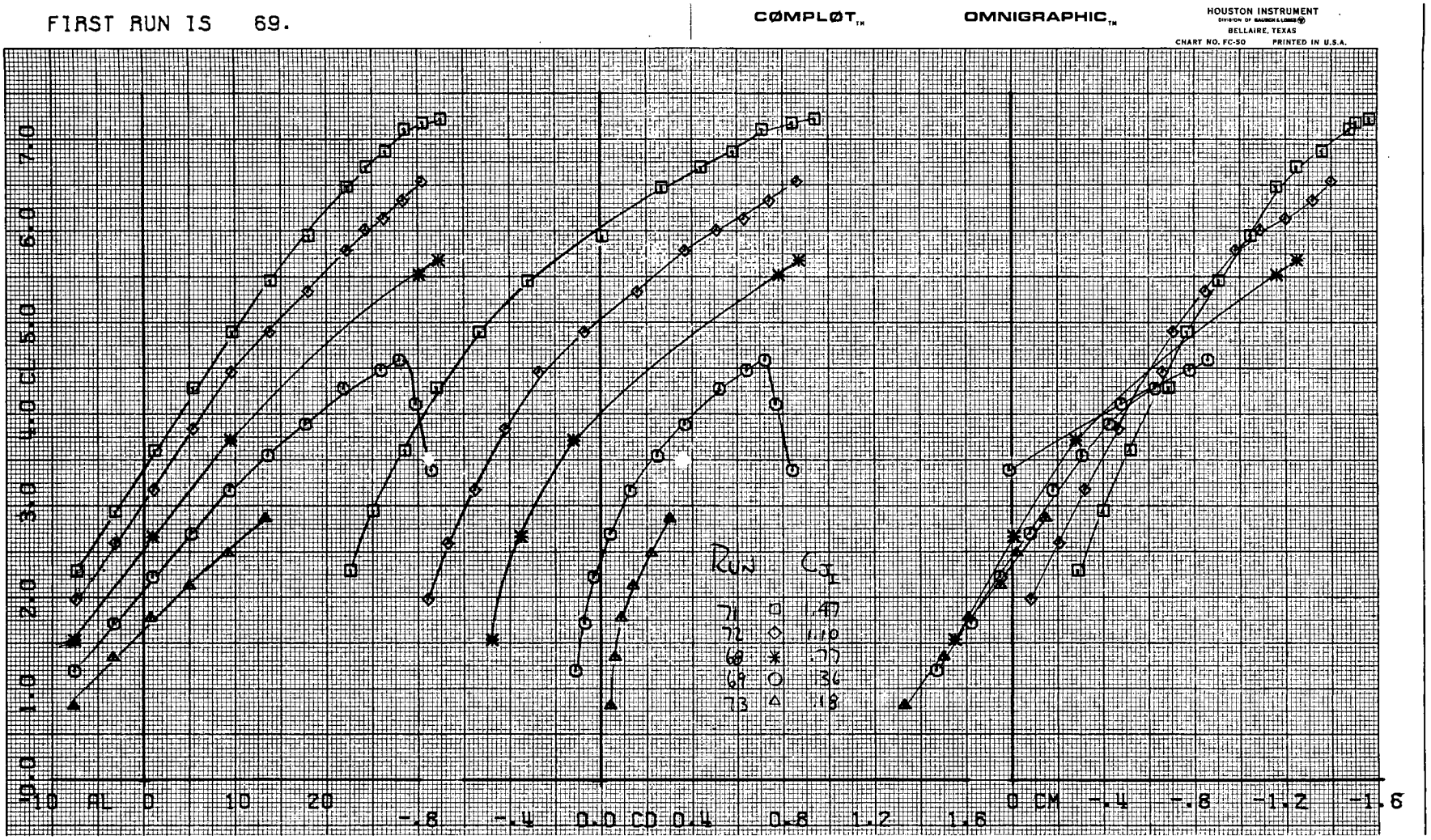

Figure 24.- Longitudinal aerodynamic characteristics with horizontal tail installed; δ_f = 41.1, δ_s = 60° (mod to stb'd), and i_t = -10.1°.

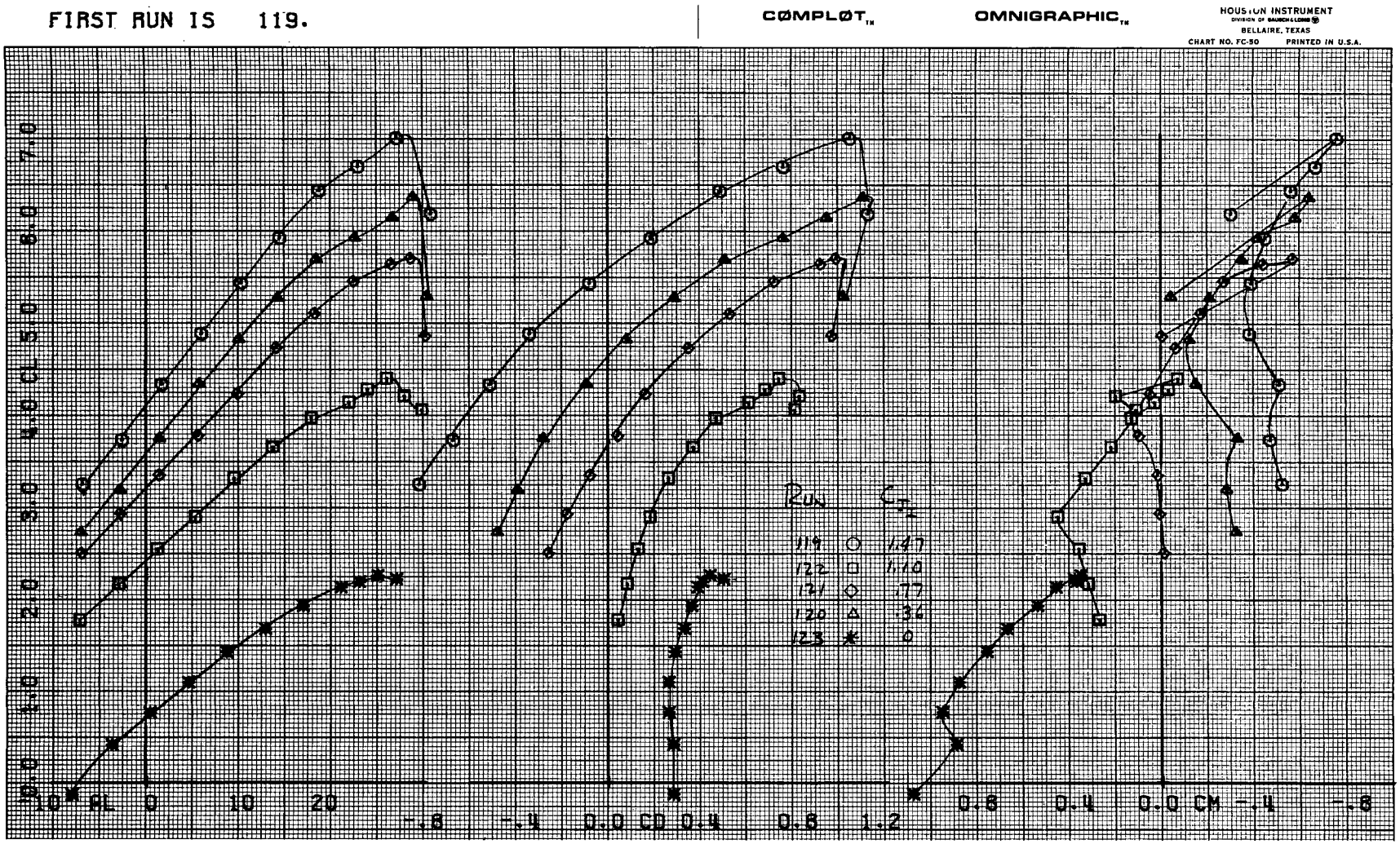

Figure 25.- Effect of C_{J_I} on longitudinal aerodynamic characteristics with horizontal tail installed; δ_f = 51.1, δ_s = 60° (mod to stb'd), and i_t = -10.1°.

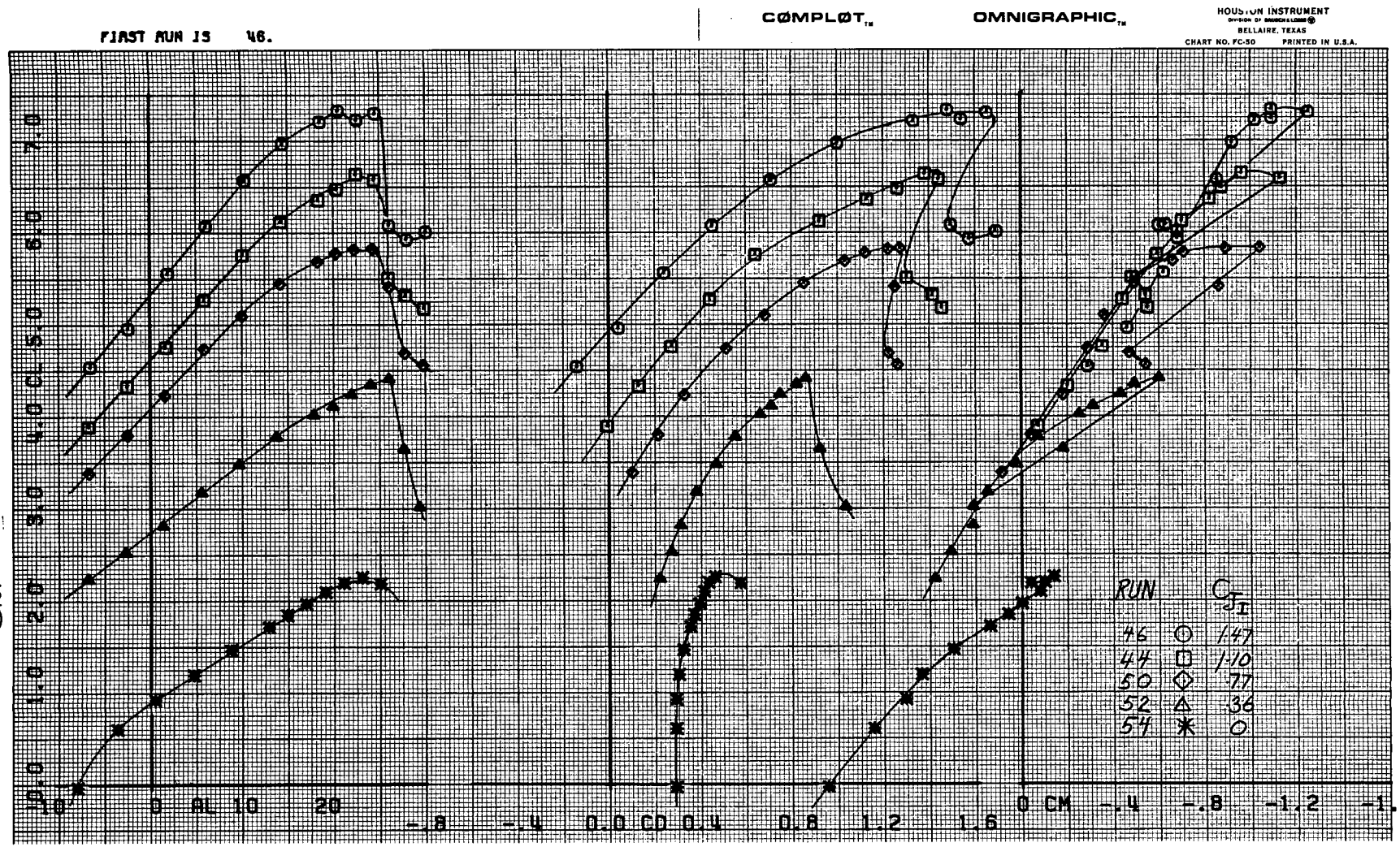

(a) Effect of C_{J_I}; $\delta_e = -15°$

Figure 26.- Longitudinal aerodynamic characteristics with horizontal tail installed; $\delta_f = 70.6°$, = 60°, and $i_t = -1°$.

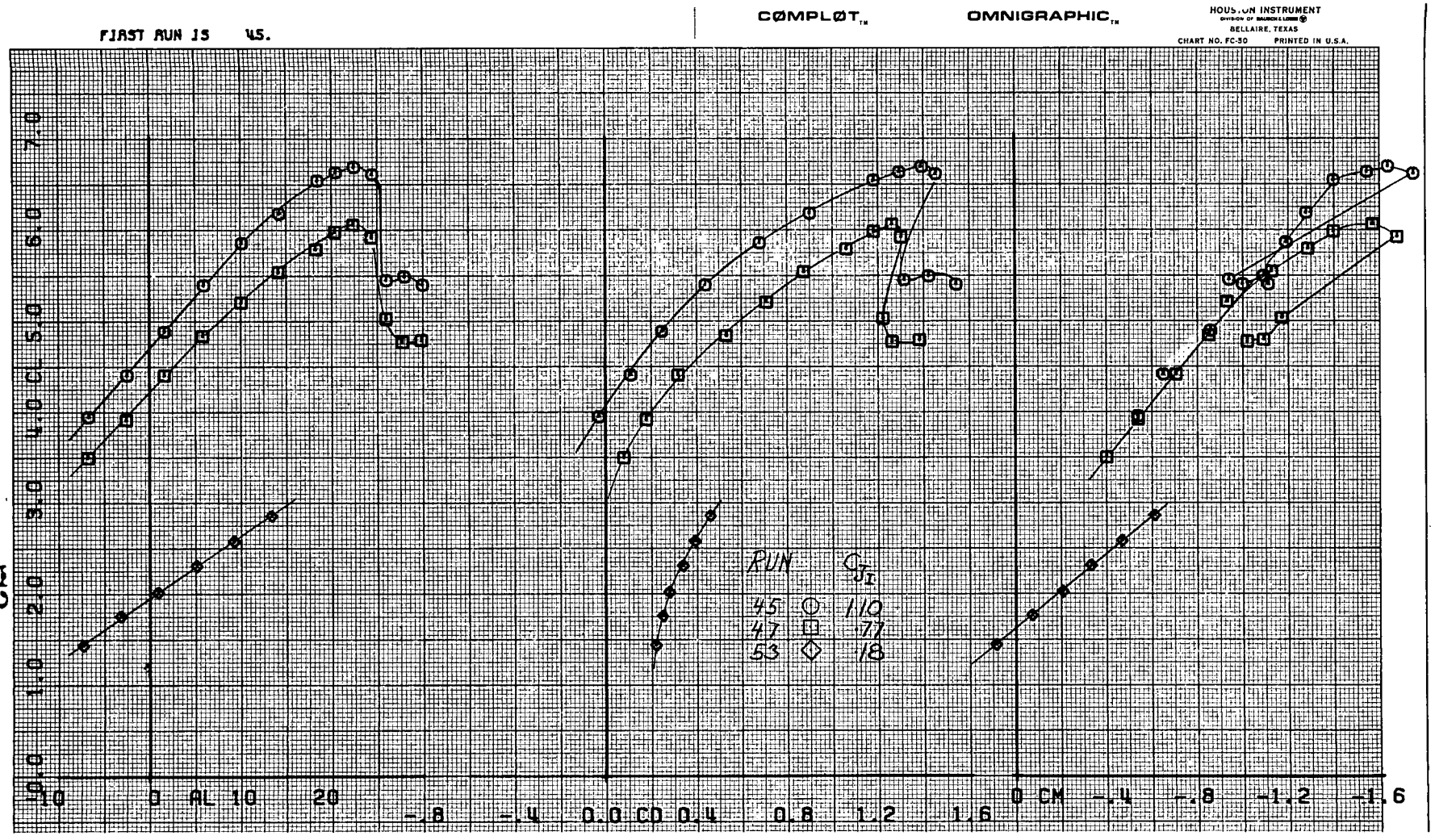

(b) Effect of C_{J_I}; $\delta_e = 0°$

Figure 26.- Continued.

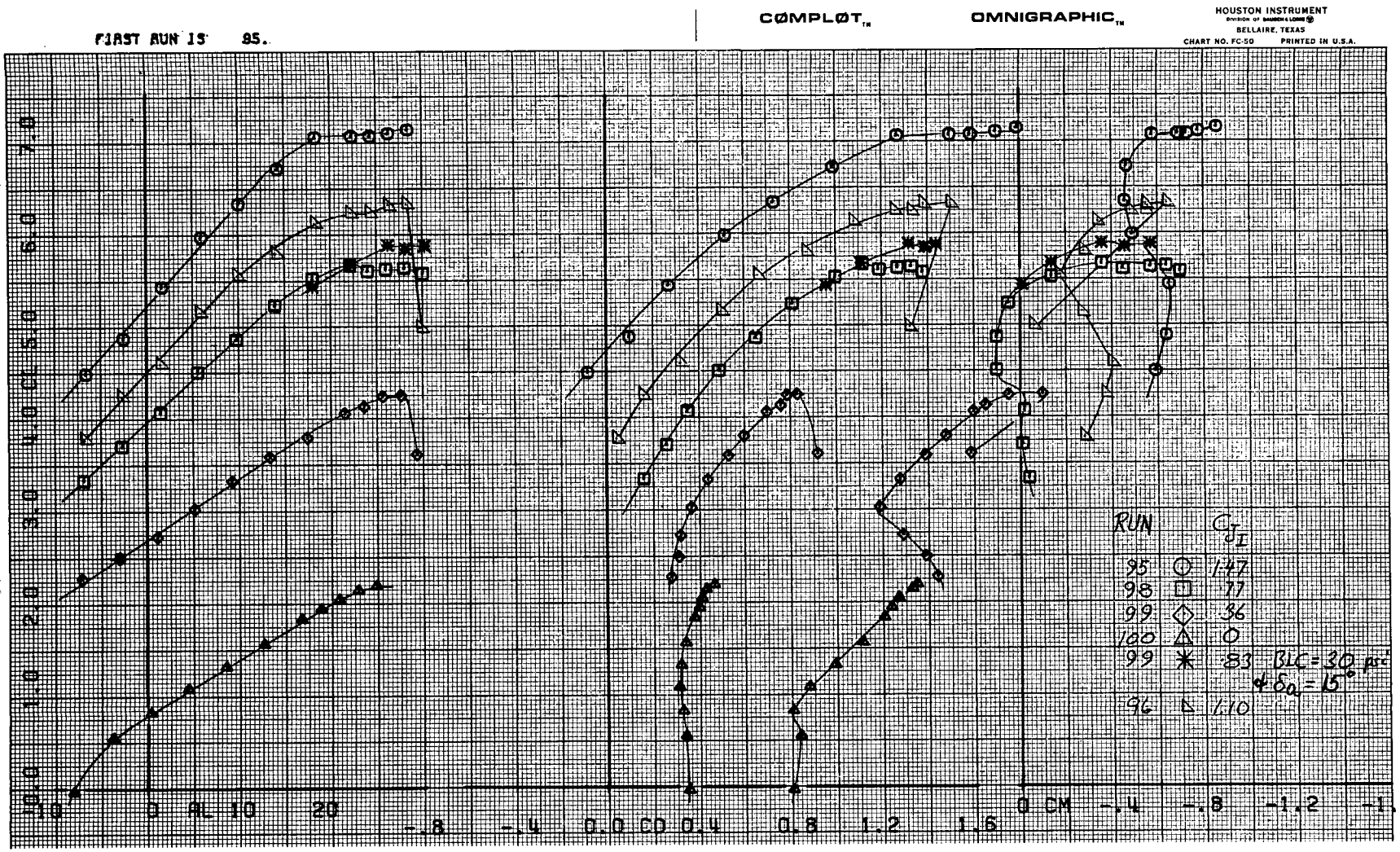

(c) Effect of C_{J_I}; $\delta_s = 60°$ (mod. to stb'd), and $i_t = -10.1°$

Figure 26. Continued.

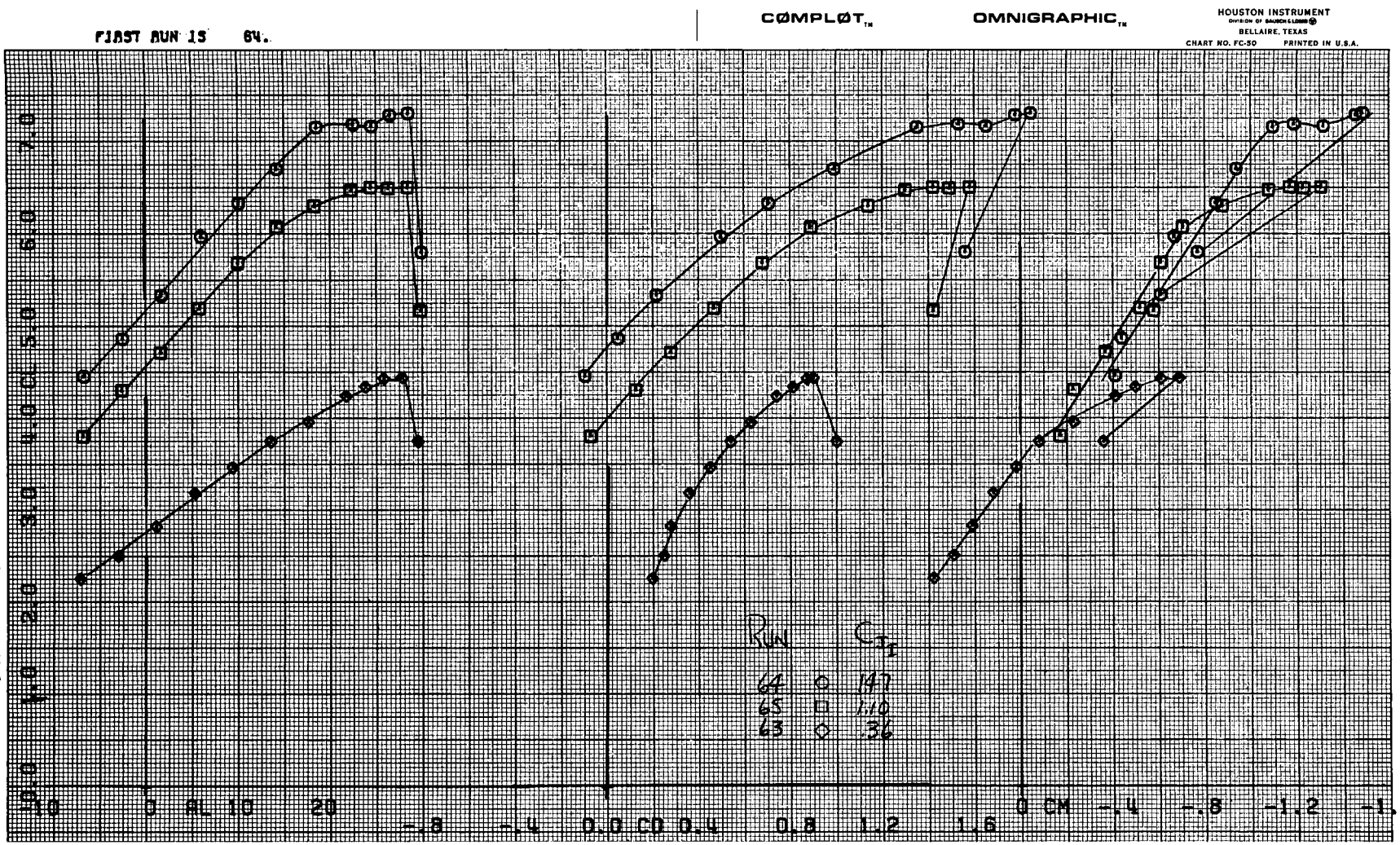

(d) Effect of C_{J_I}; δ_s = 60° (mod. to stb'd), i_t = -1°

Figure 26.- Concluded.

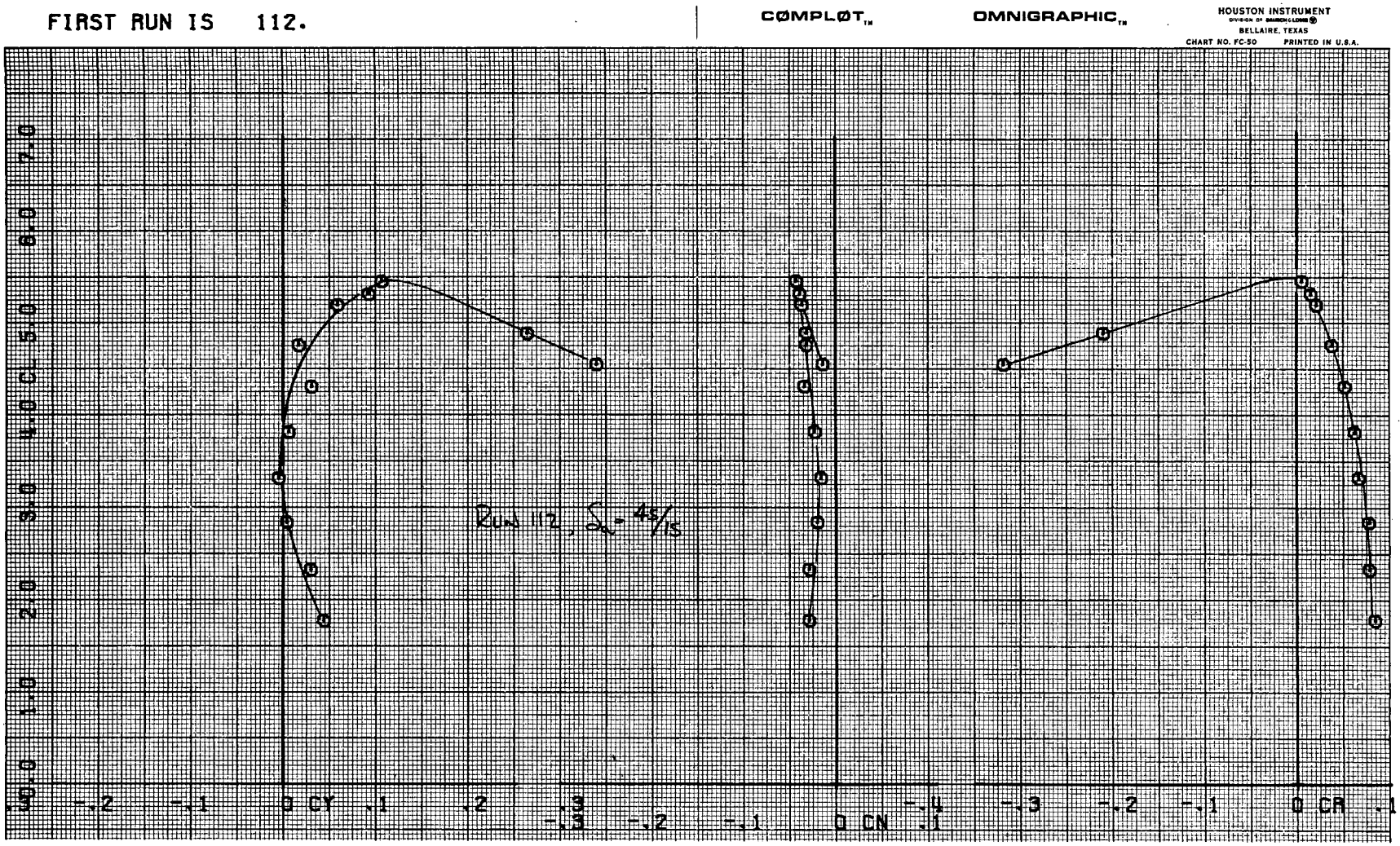

(a) δ_a = 45/15°

Figure 27.- Effect of differential aileron deflection on lateral-direction characteristics; δ_f = 41.1°.

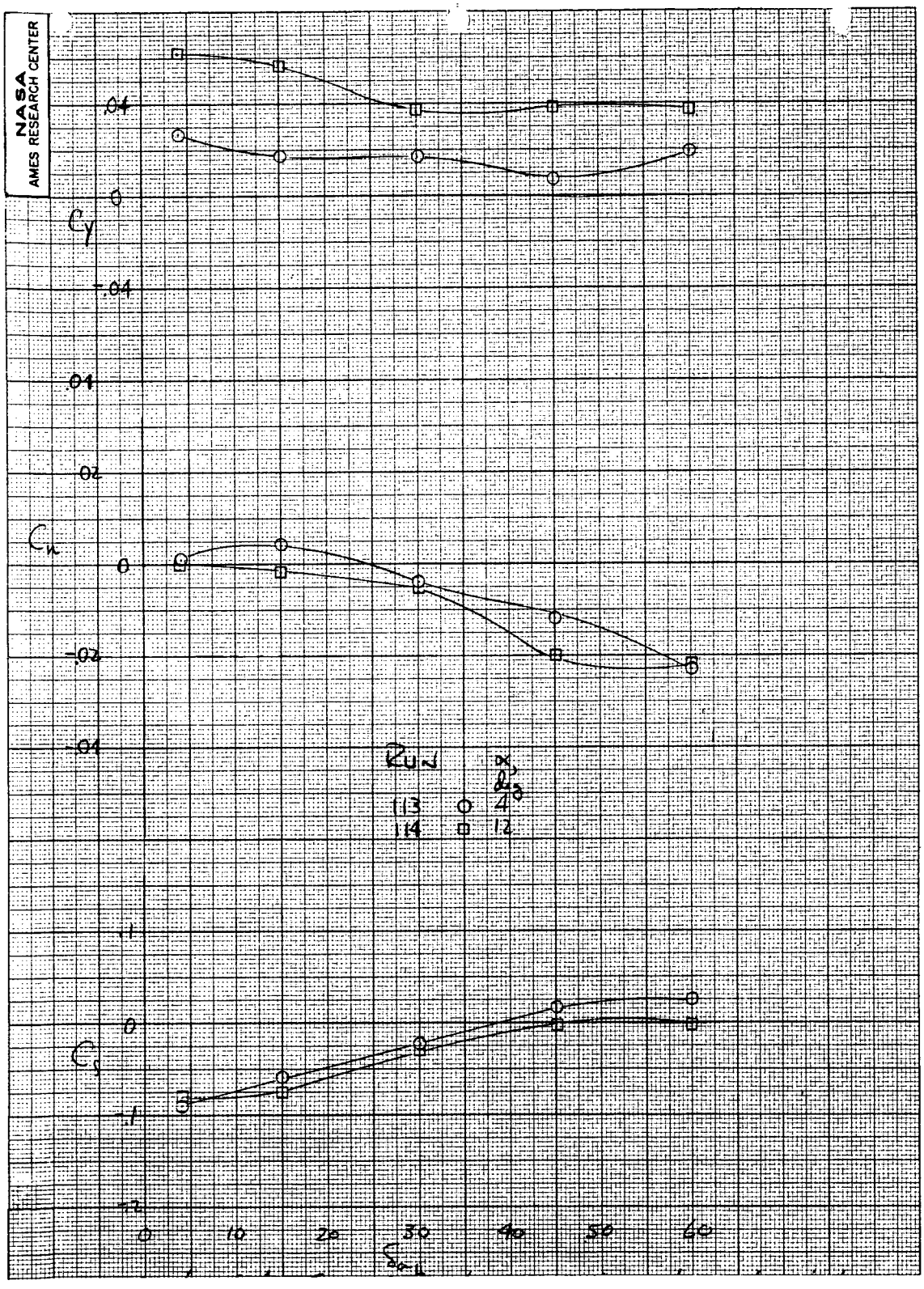

(b) $\delta_a = n/30°$

Figure 27.- Concluded.

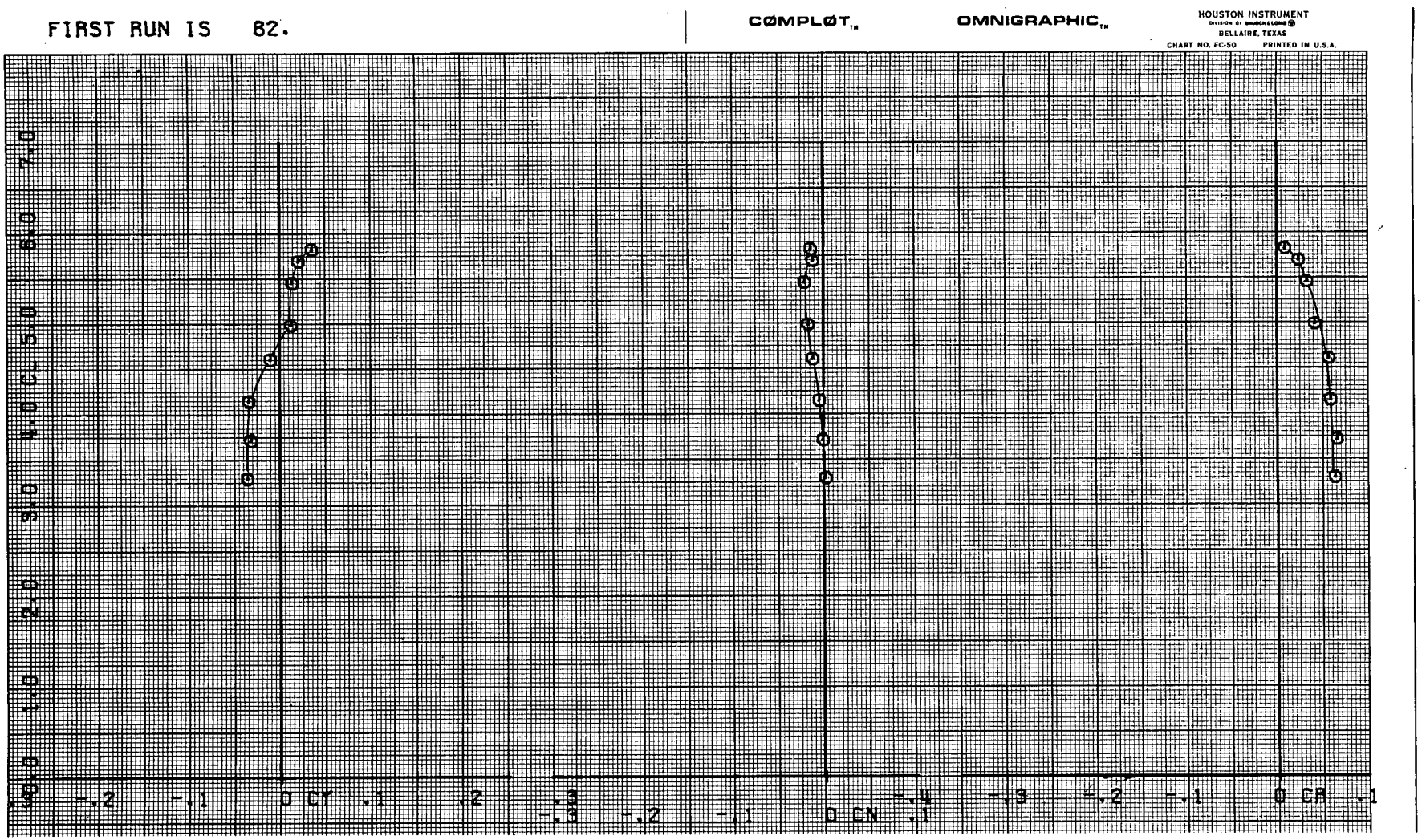

(a) $\delta_a = 45/15°$

Figure 28.- Effect of differential aileron deflection lateral-directional characteristics; $\delta_f = 70.6°$.

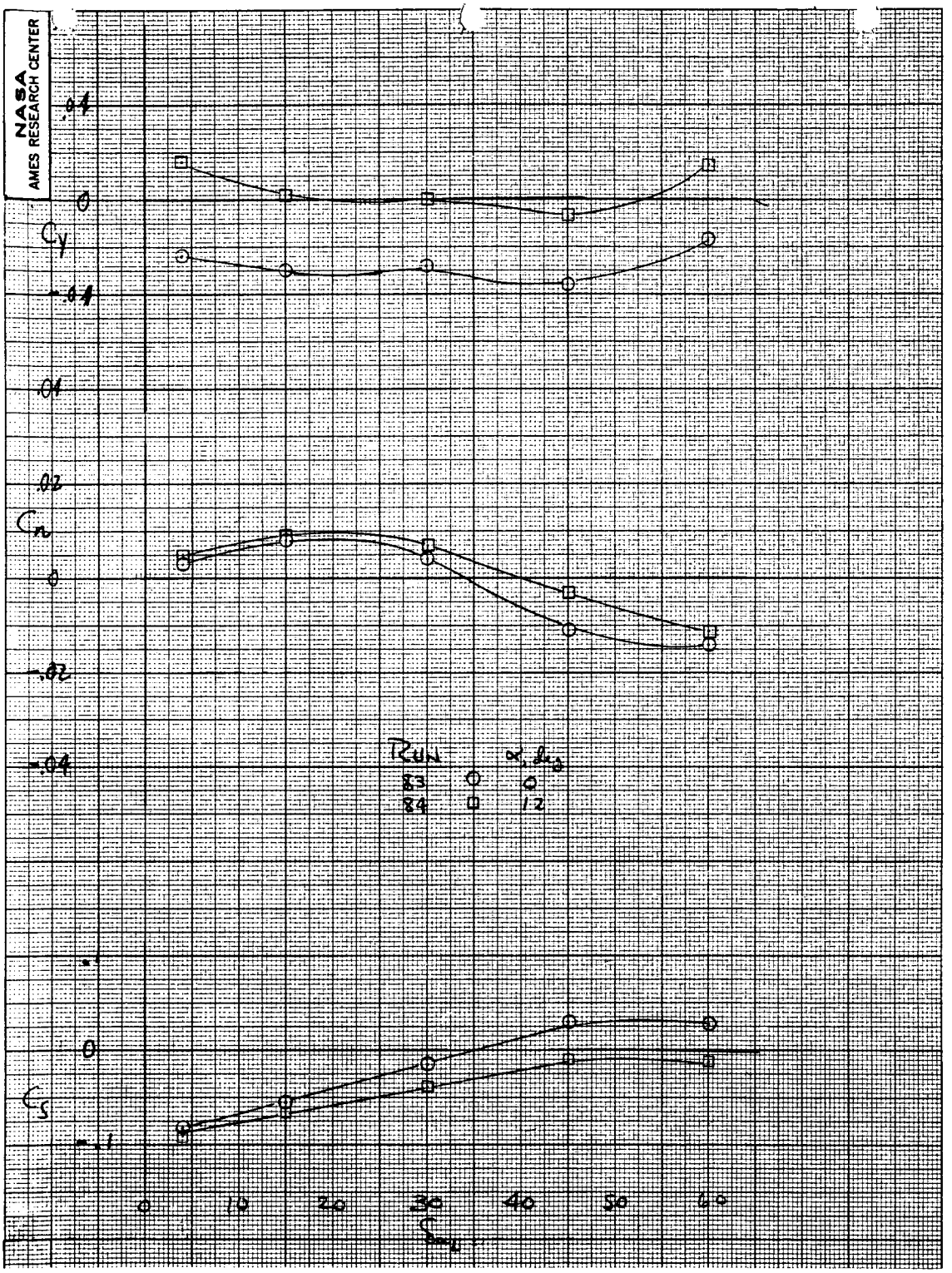

(b) Effect of variable port aileron; $\delta_a = n/30$, $\alpha = 0°$ and $12°$
Figure 28.- Continued.

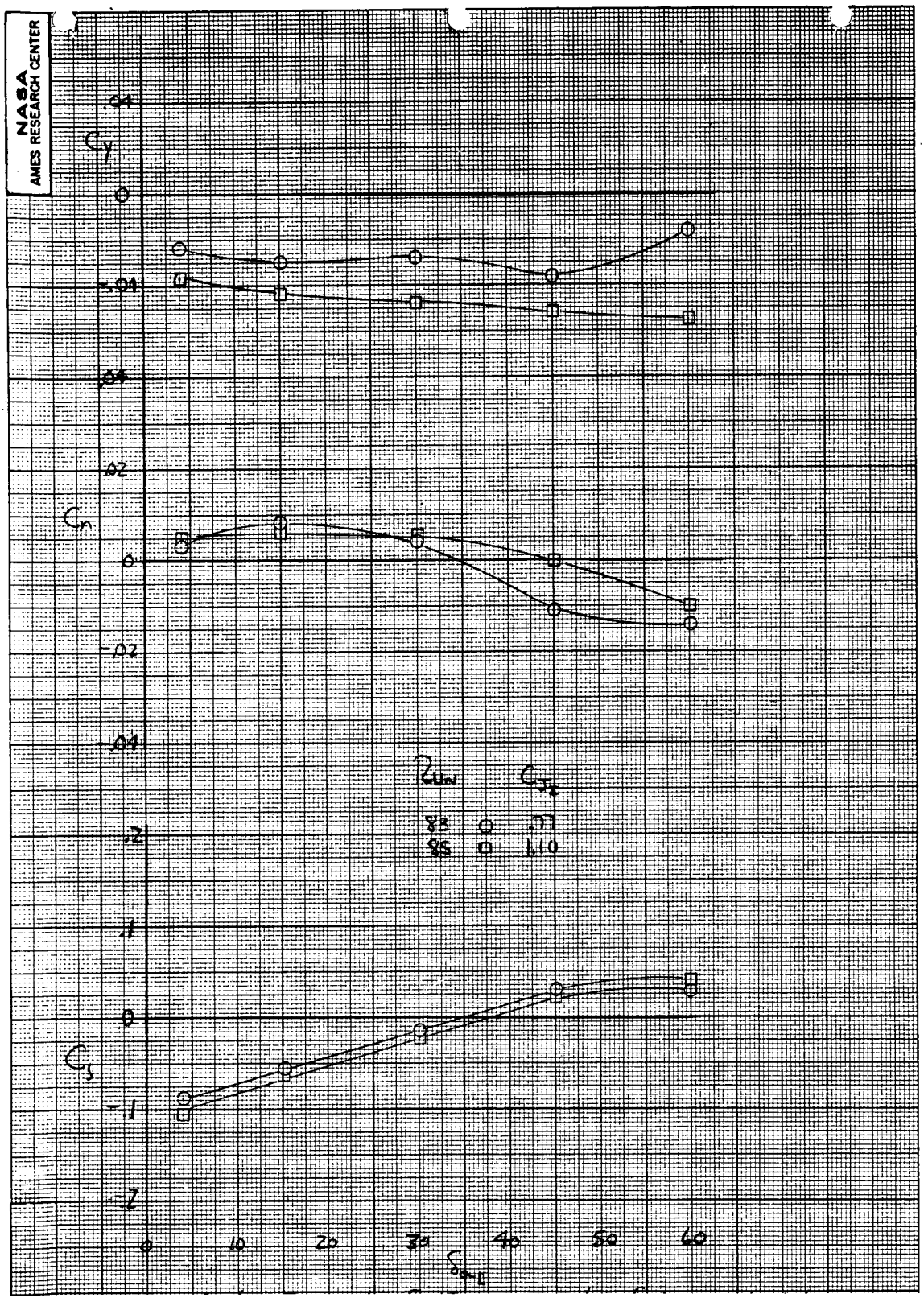

(c) Effect of variable port aileron; $\delta_a = n/30°$ and $C_{J_I} = .77$ and 1.10
Figure 28.- Concluded.

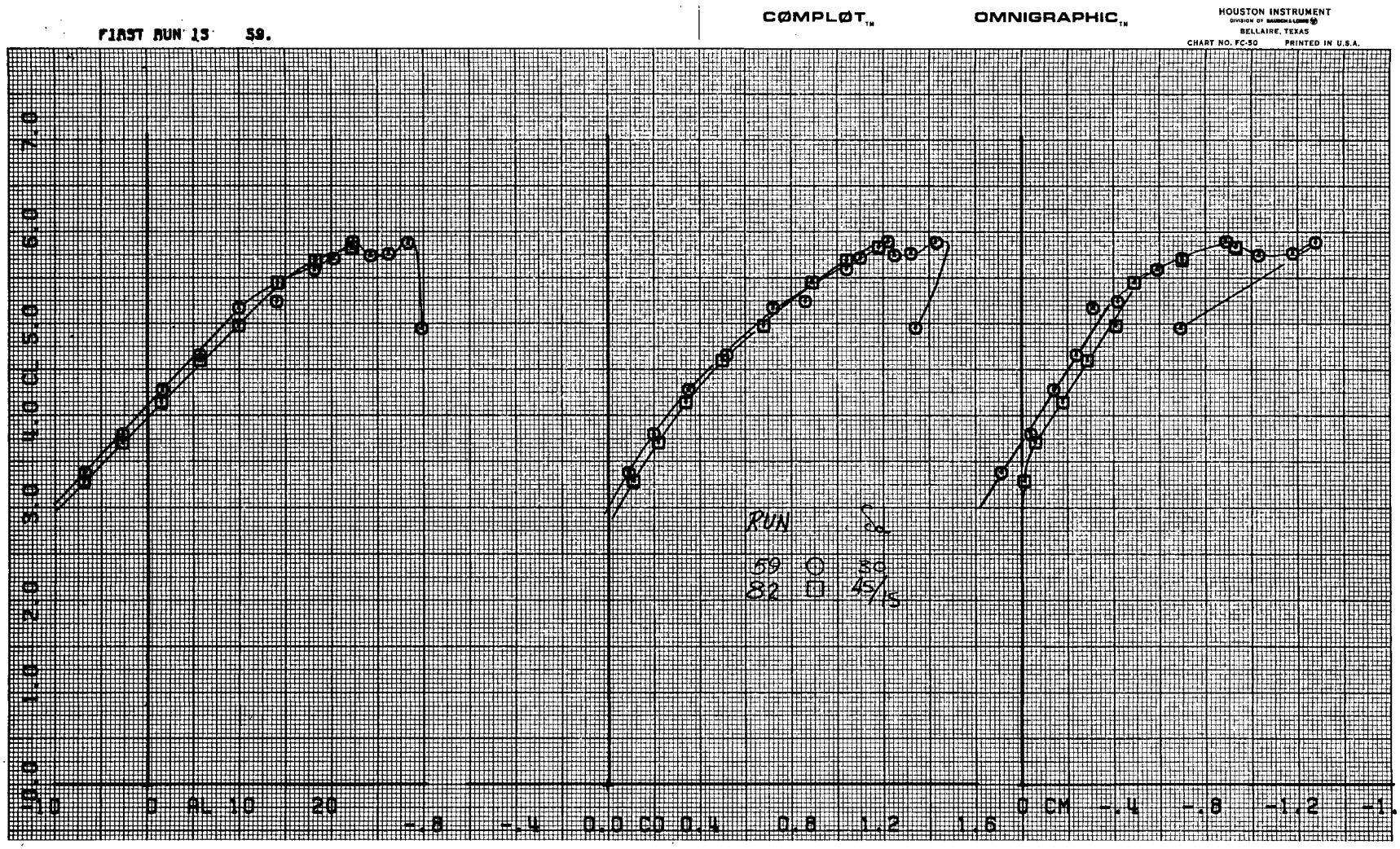

Figure 29.- Effect of differential aileron deflection on longitudinal aerodynamic characteristics with horizontal tail installed; δ_f = 70.6, δ_s = 60° (mod to stb'd) δ_a = 30° and 45/15° and i_t = -1°

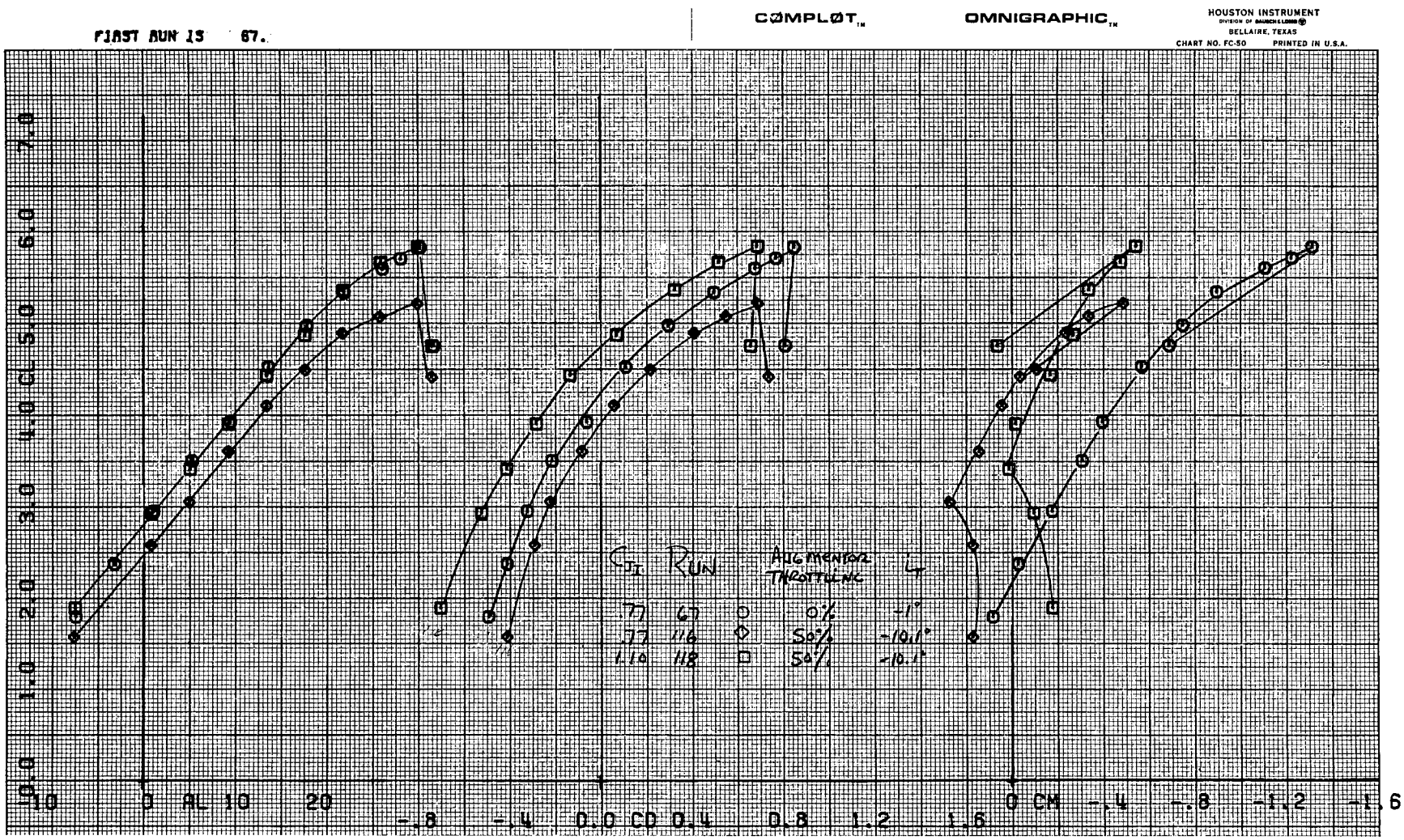

Figure 30.- Effect of augmentor throttling on longitudinal aerodynamic characteristics with horizontal tail installed; δ_f = 41.1, δ_s = 60° (mod to stb'd).

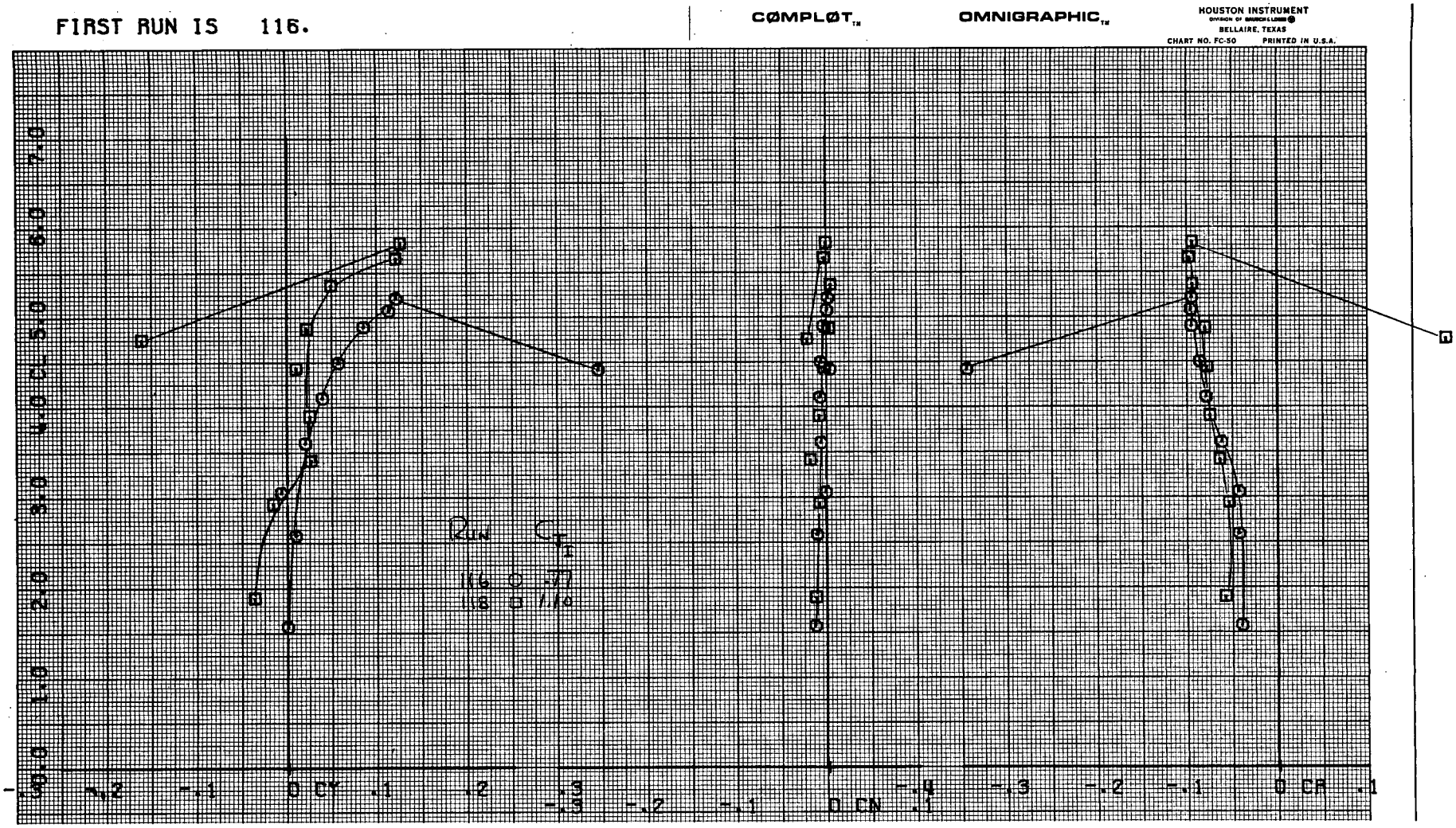

(a) C_{J_I} = .77 and 1.10

Figure 31.- Effect of augmentor throttling on lateral-directional characteristics; δ_f = 41.1 and Δd = 50%.

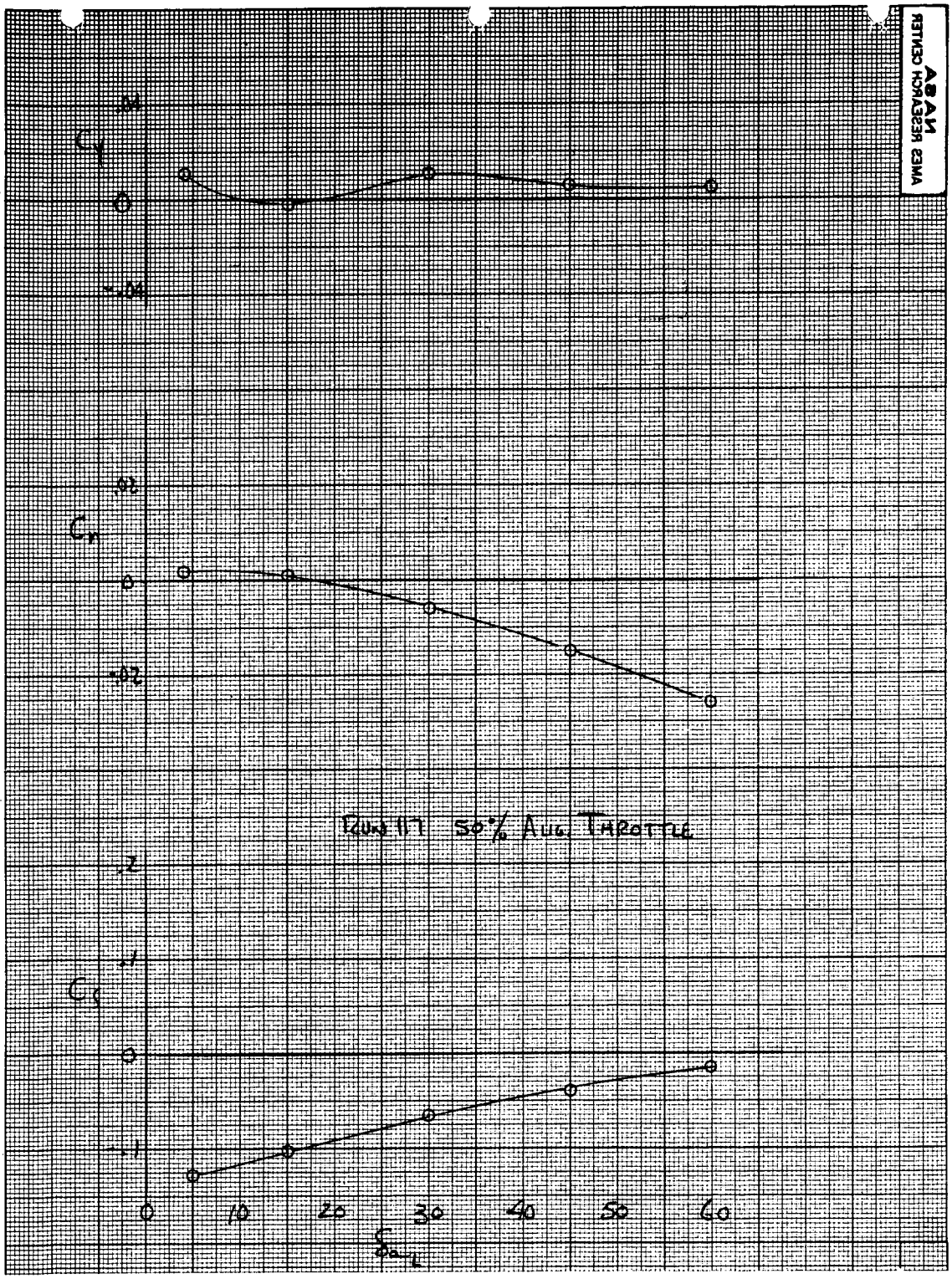

(b) $\delta_a = n/30°$

Figure 31.- Concluded.

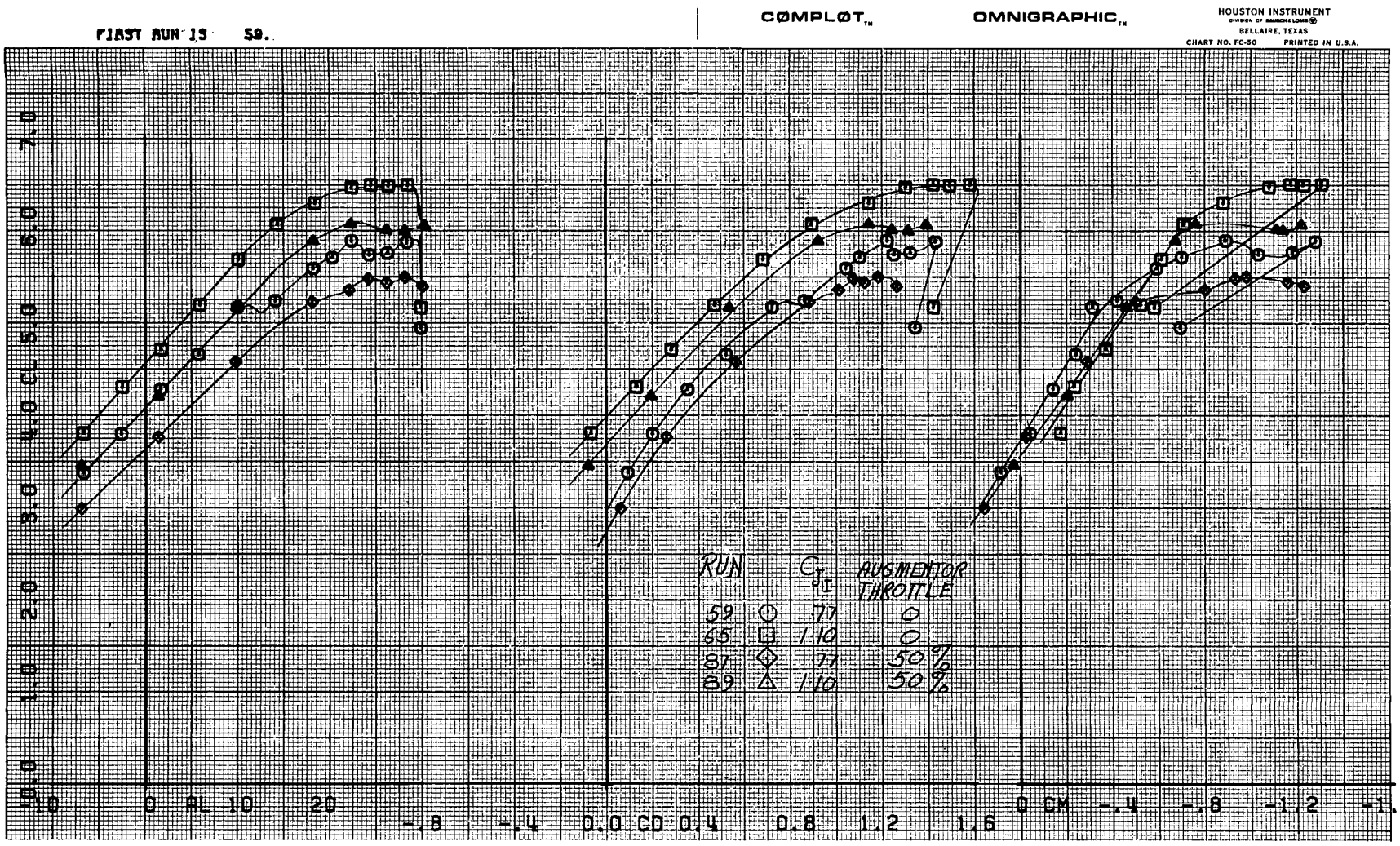

Figure 32.- Effect of augmentor throttling on longitudinal aerodynamic characteristics with horizontal tail installed; δ_f = 70.6°, δ_s = 60° (mod on stb'd), i_t = -1° and Δd = 0 and 50%.

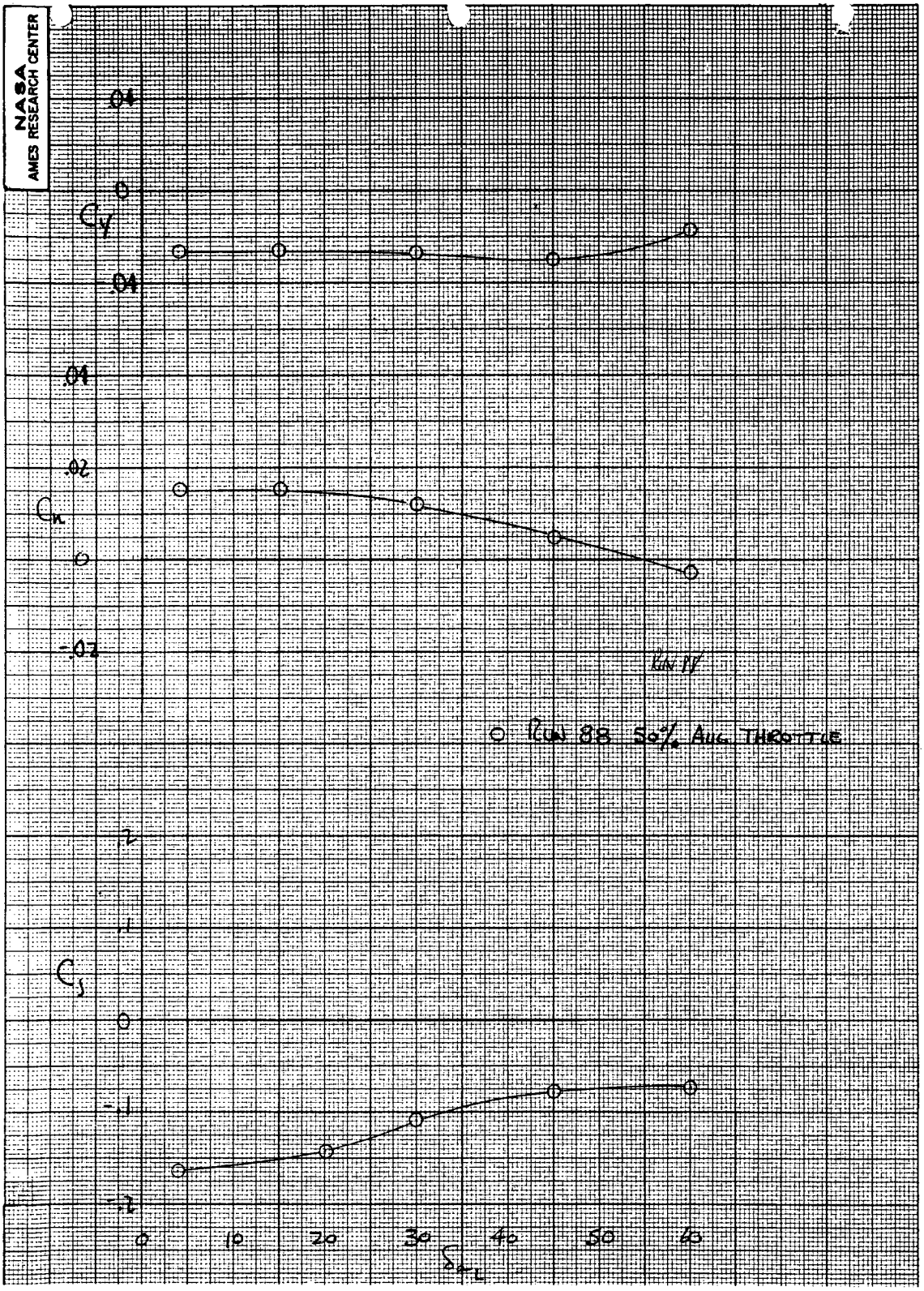

(a) $\delta_a = n/30°$

Figure 33.- Effect of augmentor throttling on lateral-directional characteristics; $\delta_f = 70.6$, $\Delta d = 50\%$.

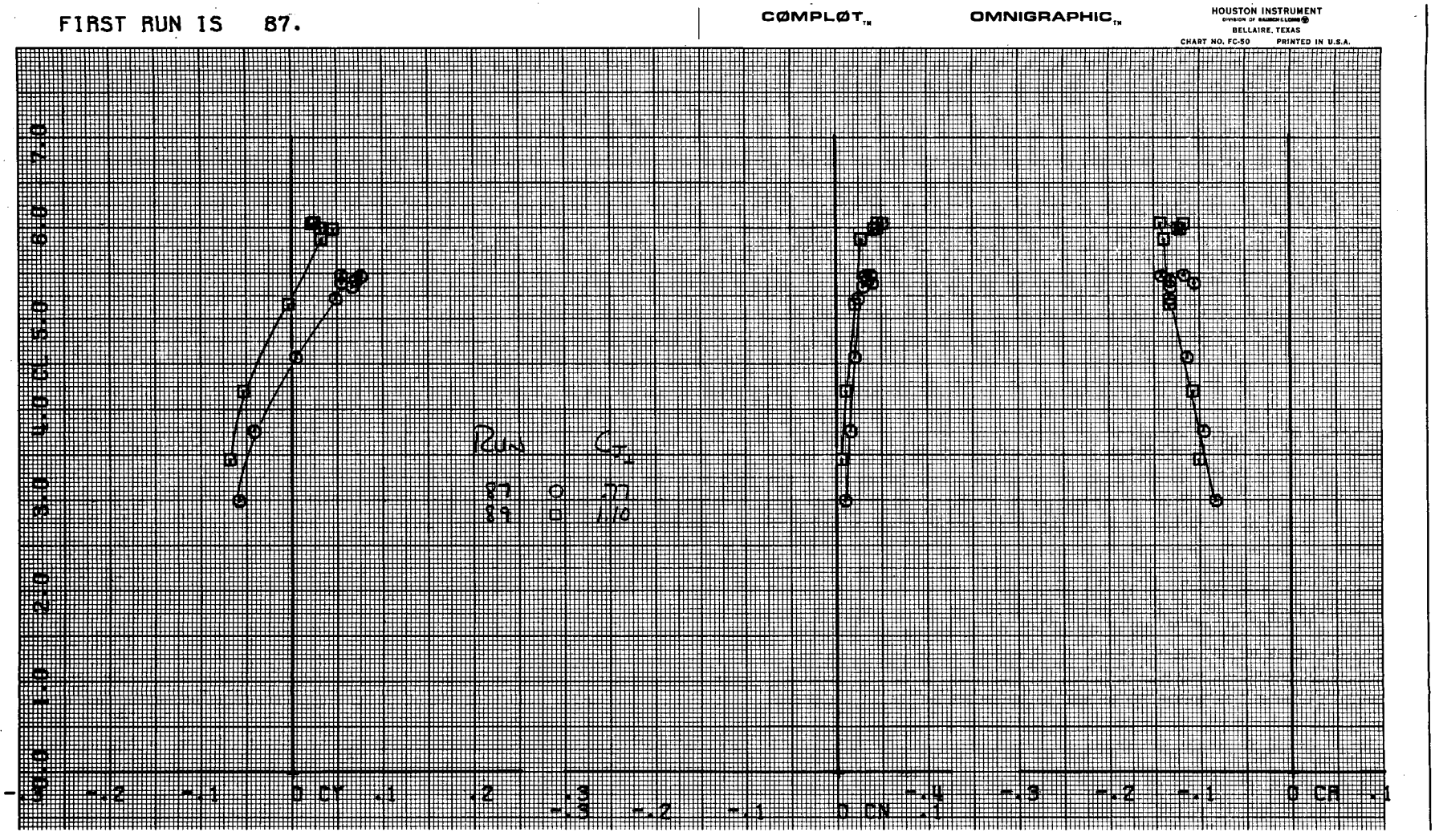

(b) C_{J_I} = .77 and 1.10

Figure 33.- Concluded.

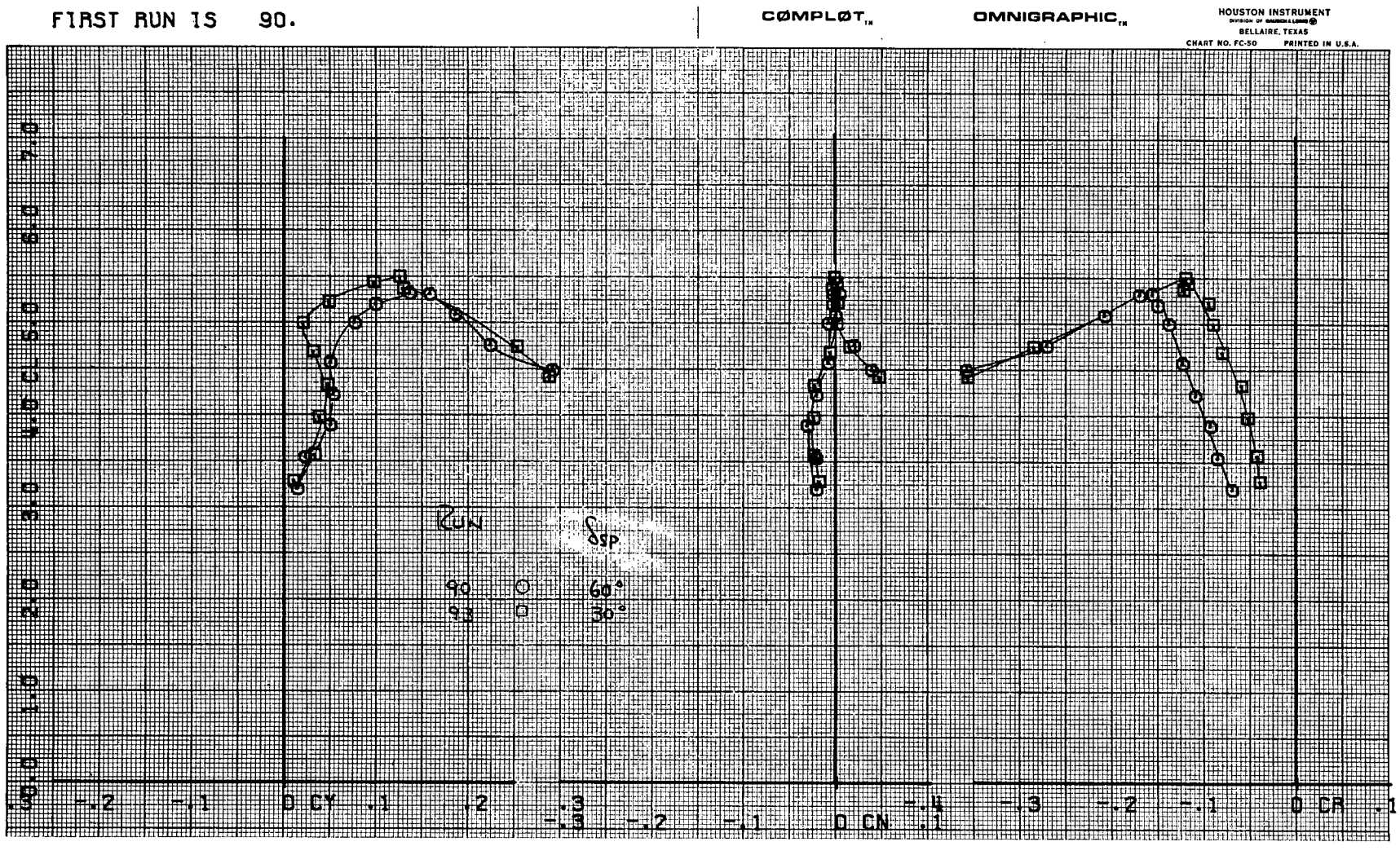

(a) δ_{sp} = 30 and 60°

Figure 34.- Effect of spoilers on lateral-directional characteristics; δ_f = 70.6°.

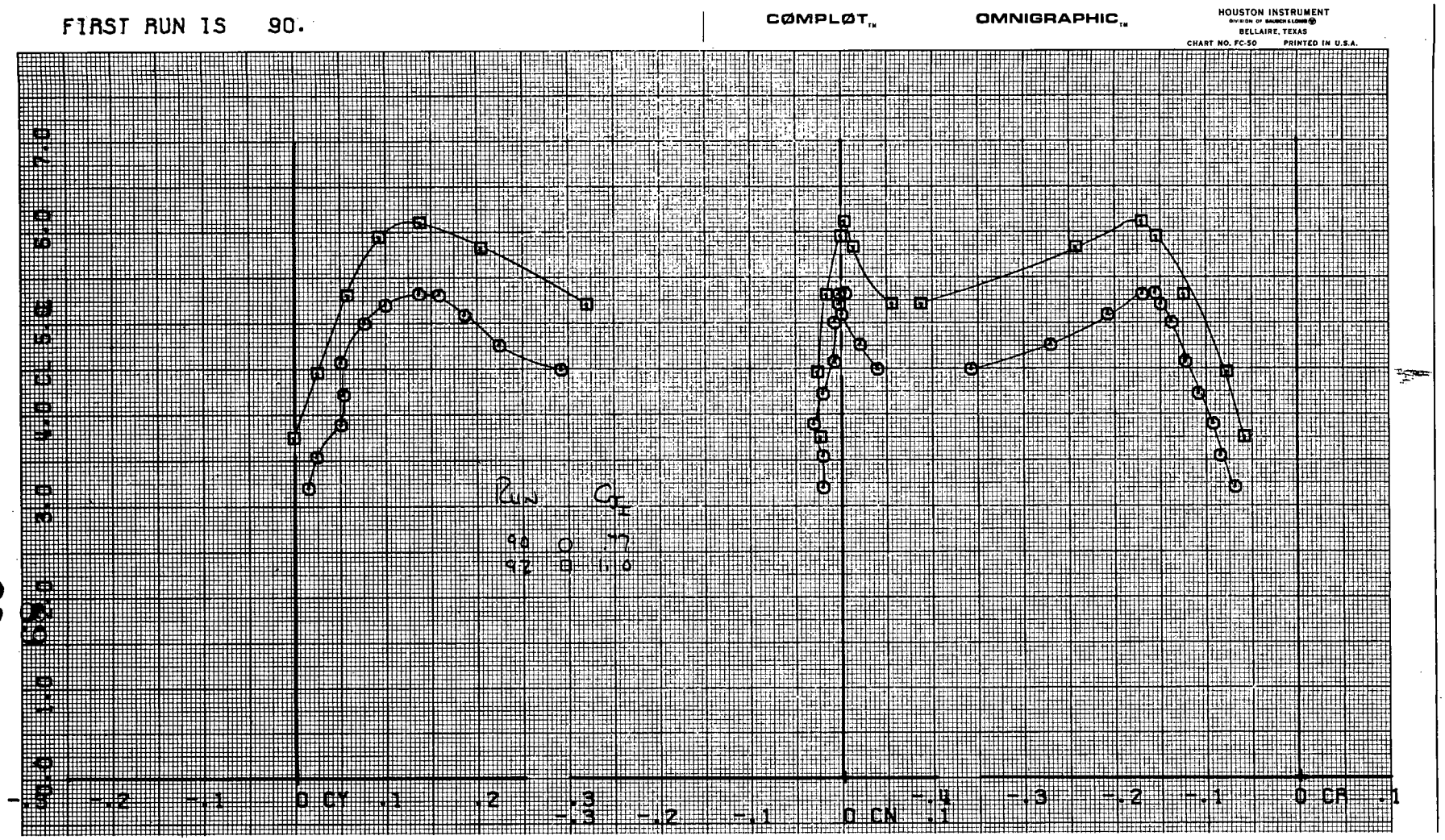

(b) δ_{sp} = 60° and C_{J_I} = .77 and 1.10

Figure 31.- Continued.

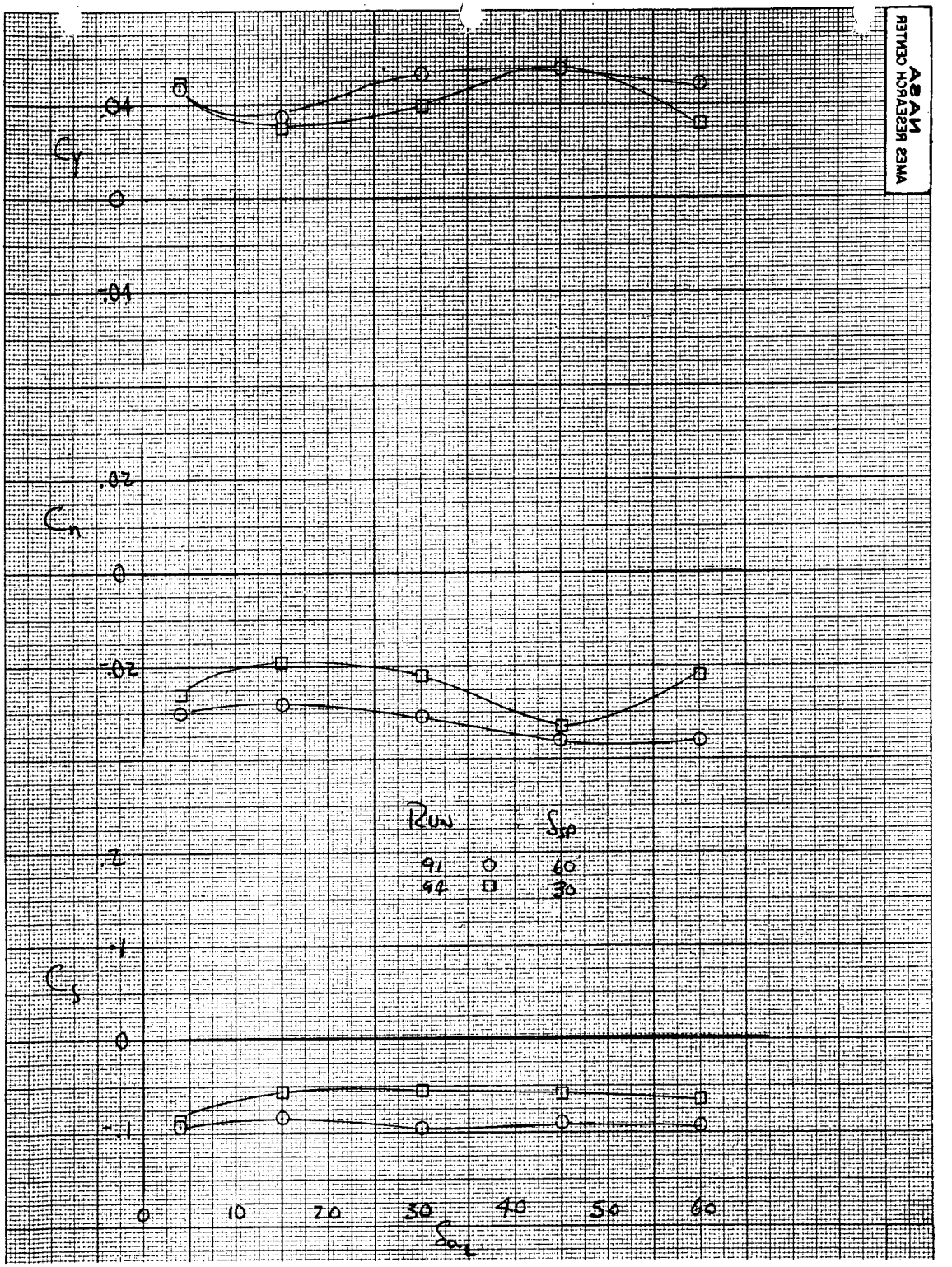

(c) δ_{sp} = 30 and 60° and δ_a = n/30°

Figure 34.- Concluded.

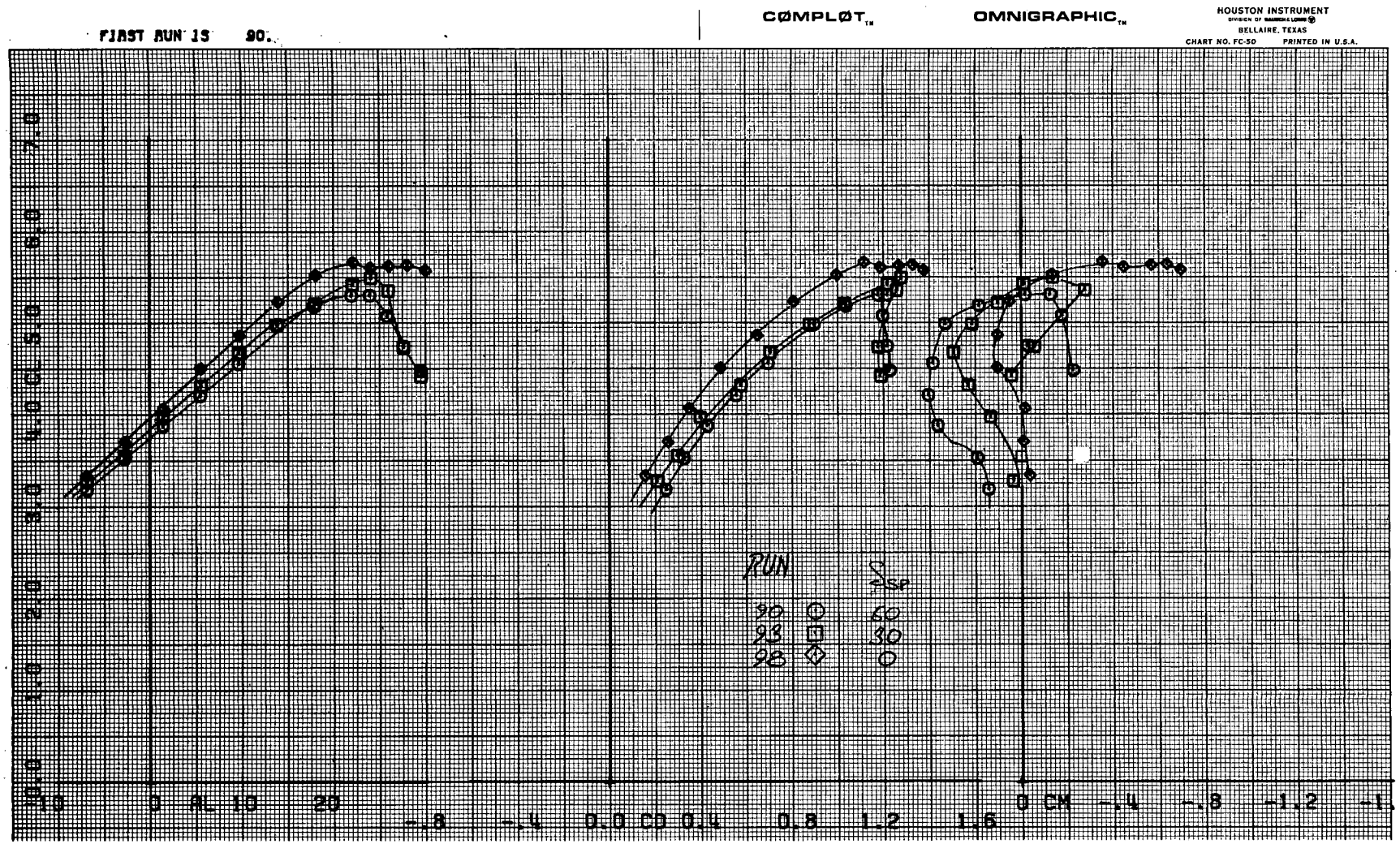

(a) $C_{J_I} = .77$

Figure 35.- Effect of spoilers on longitudinal aerodynamic characteristics with horizontal tail installed; $\delta_f = 70.6°$, $\delta_s = 60°$ (mod to stb'd), $i_t = -10.1°$.

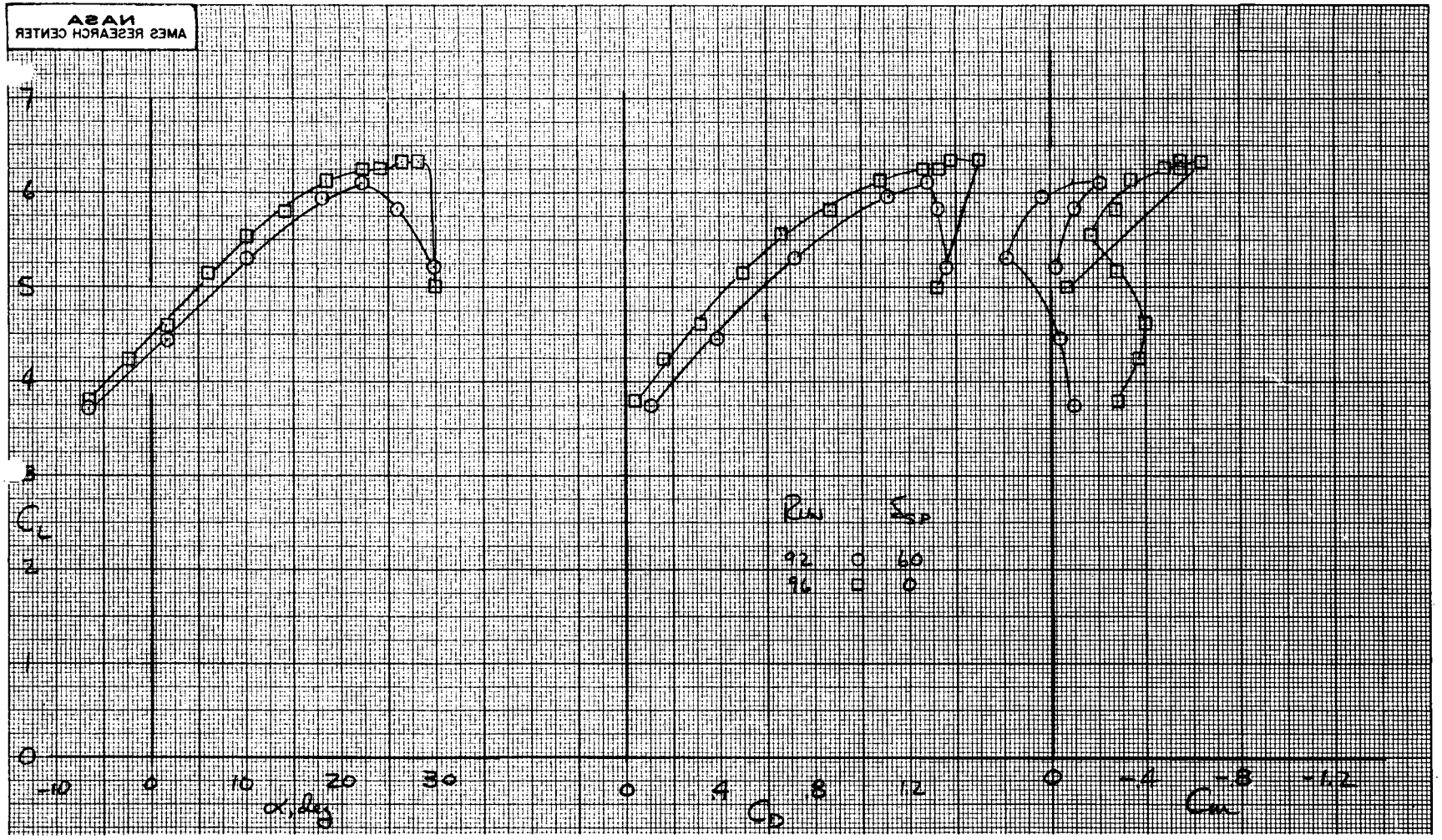

(b) $C_{J_I} = 1.10$

Figure 35.- Concluded.

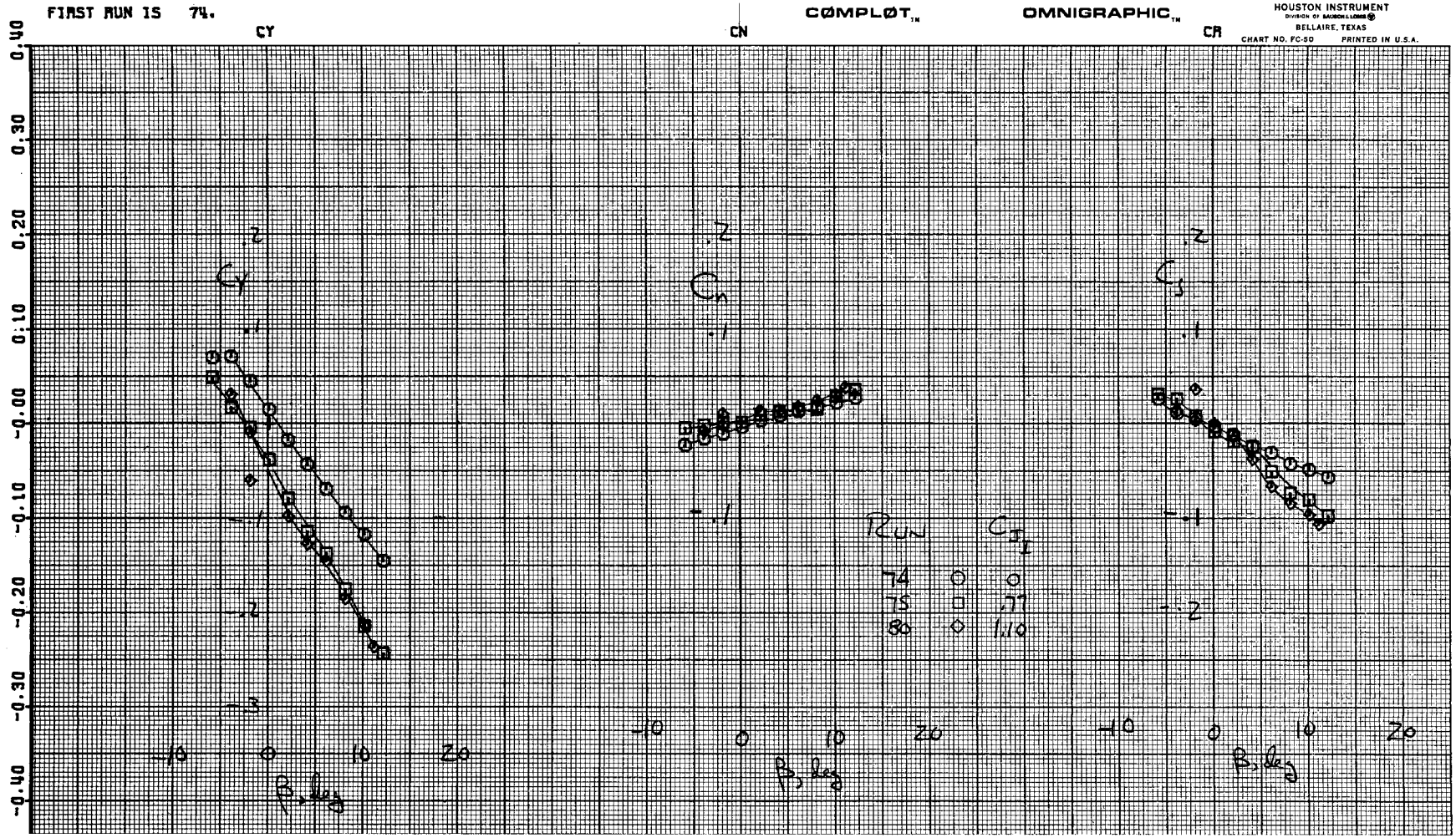

(a) Effect of C_{J_I}; $\alpha = 0°$

Figure 36.- Lateral-directional characteristics; $\delta_f = 70.6°$.

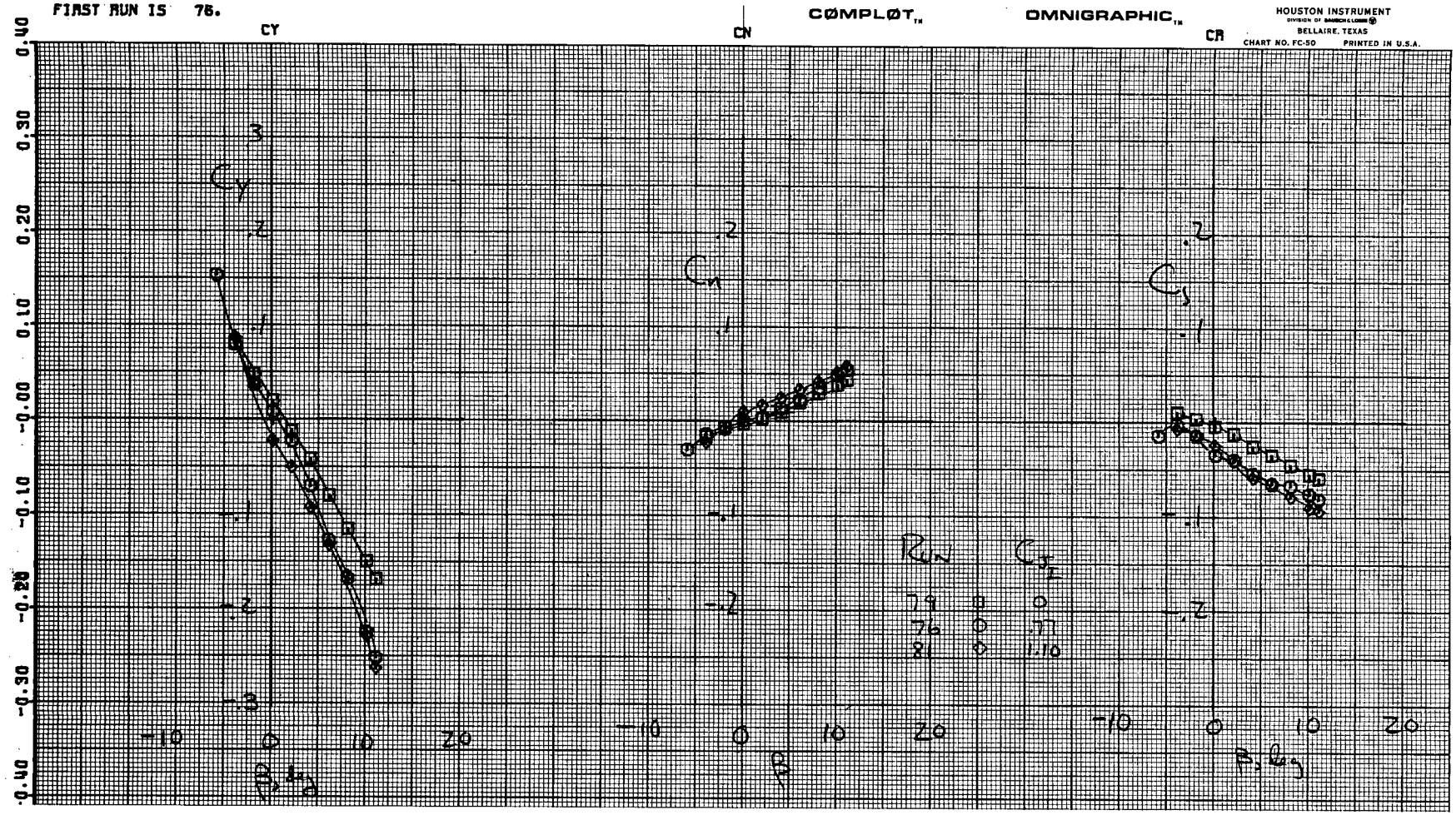

(b) Effect of C_{J_I}; $\alpha = 12°$

Figure 36.- Continued.

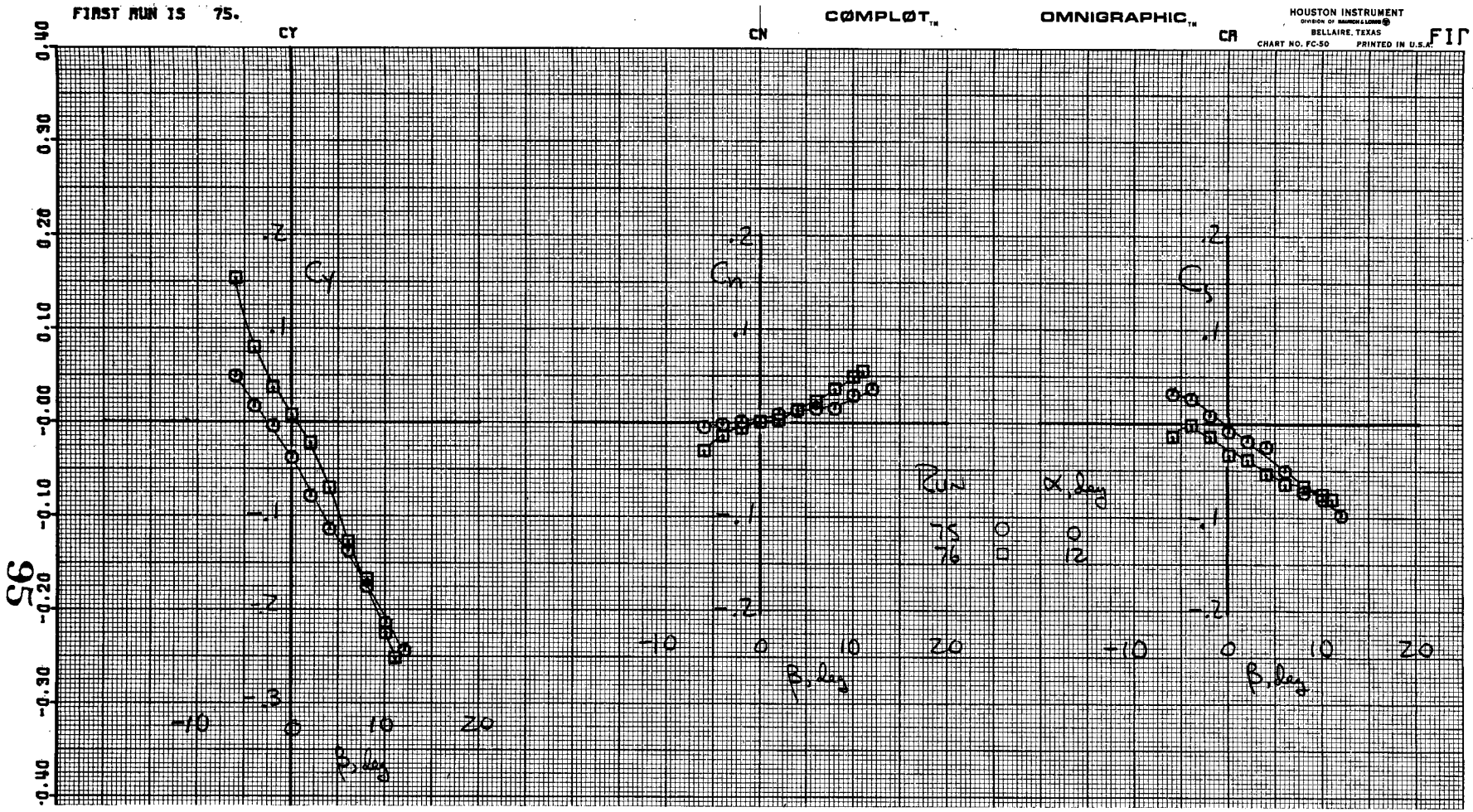

(c) Effect of α; $C_{J_I} = .77$

Figure 36.- Continued.

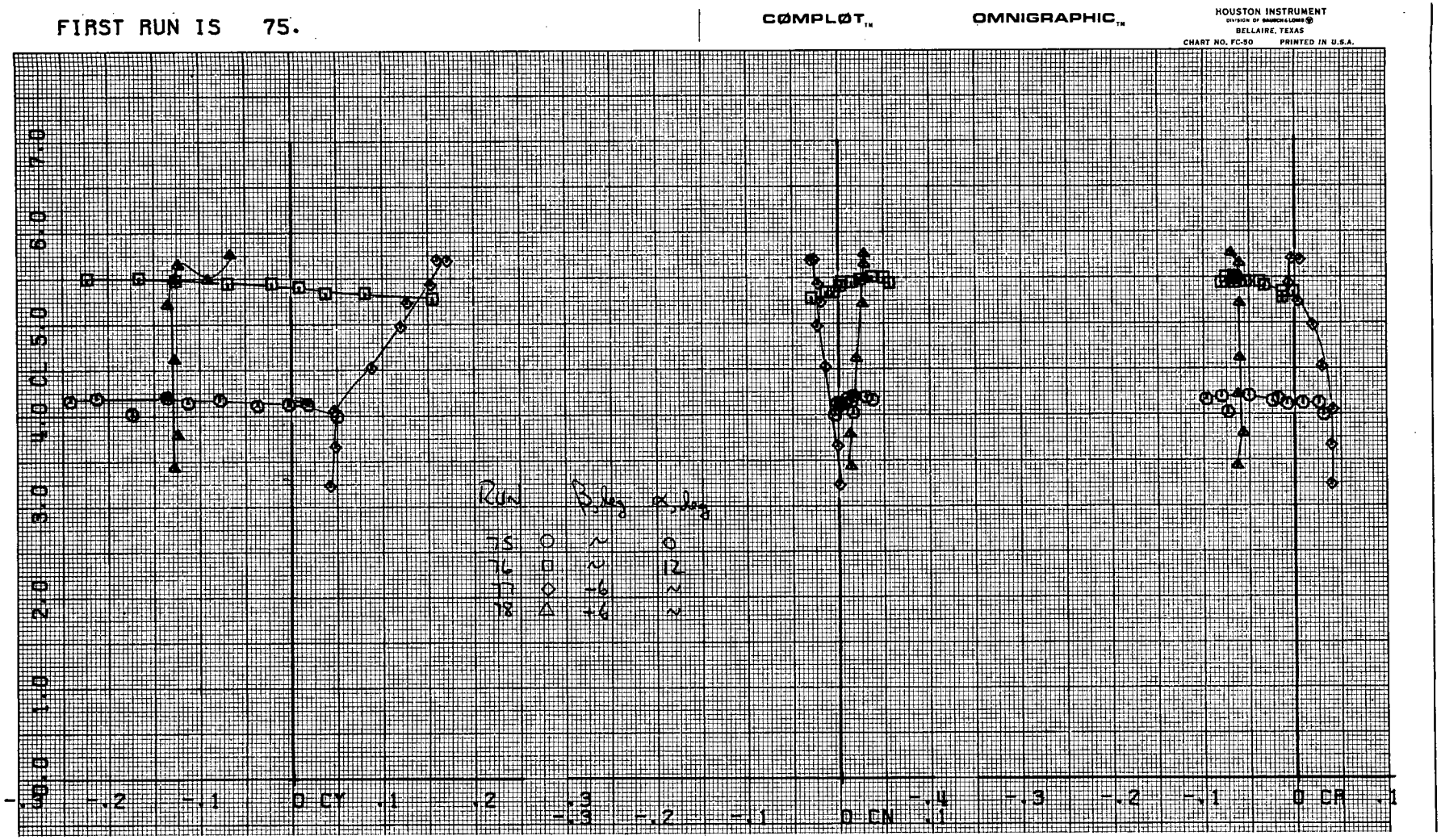

(d) Effect of α and β; $C_{J_I} = .77$

Figure 36.- Continued.

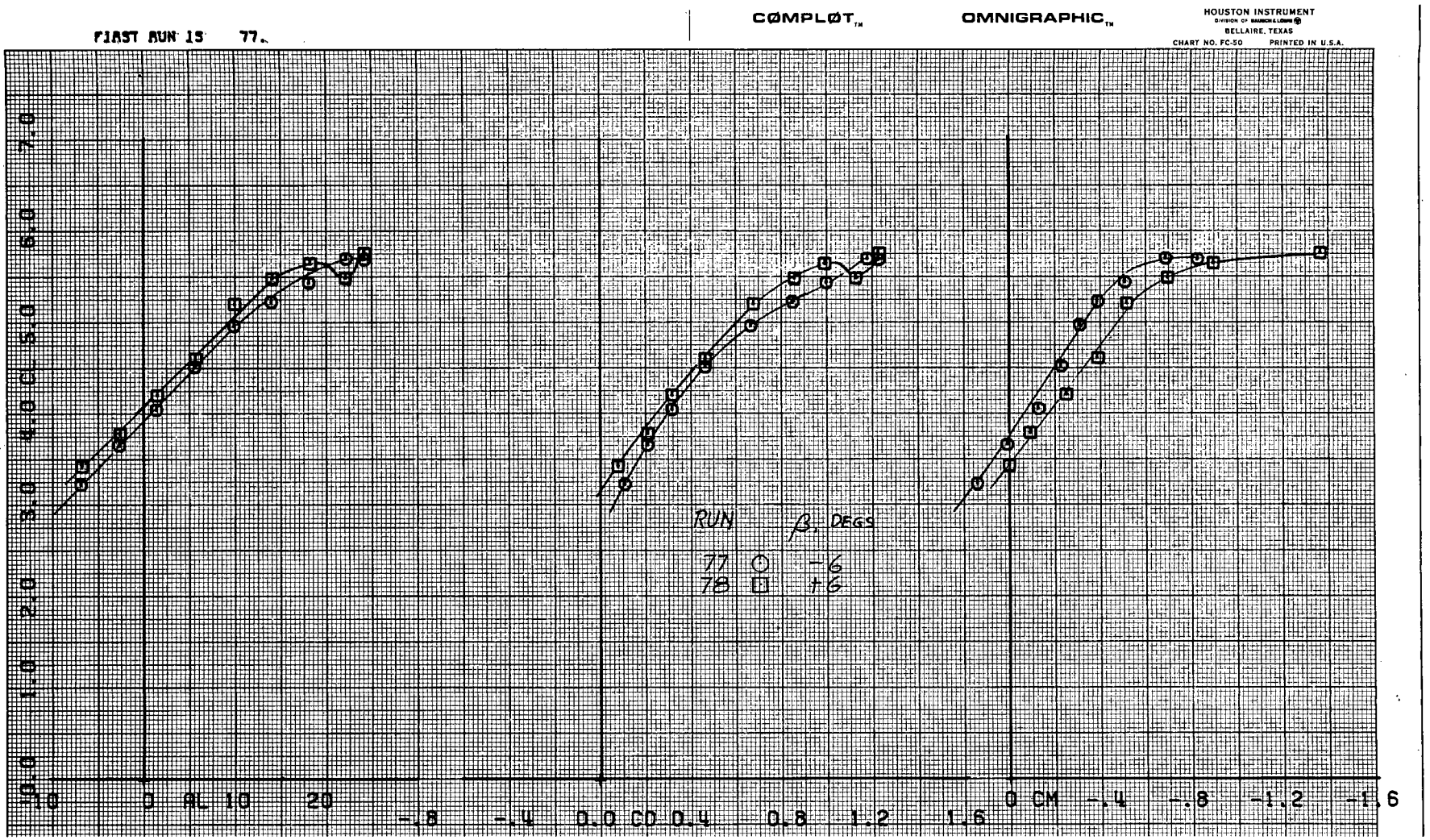

(e) Effect of β on longitudinal characteristics
Figure 36.- Concluded.

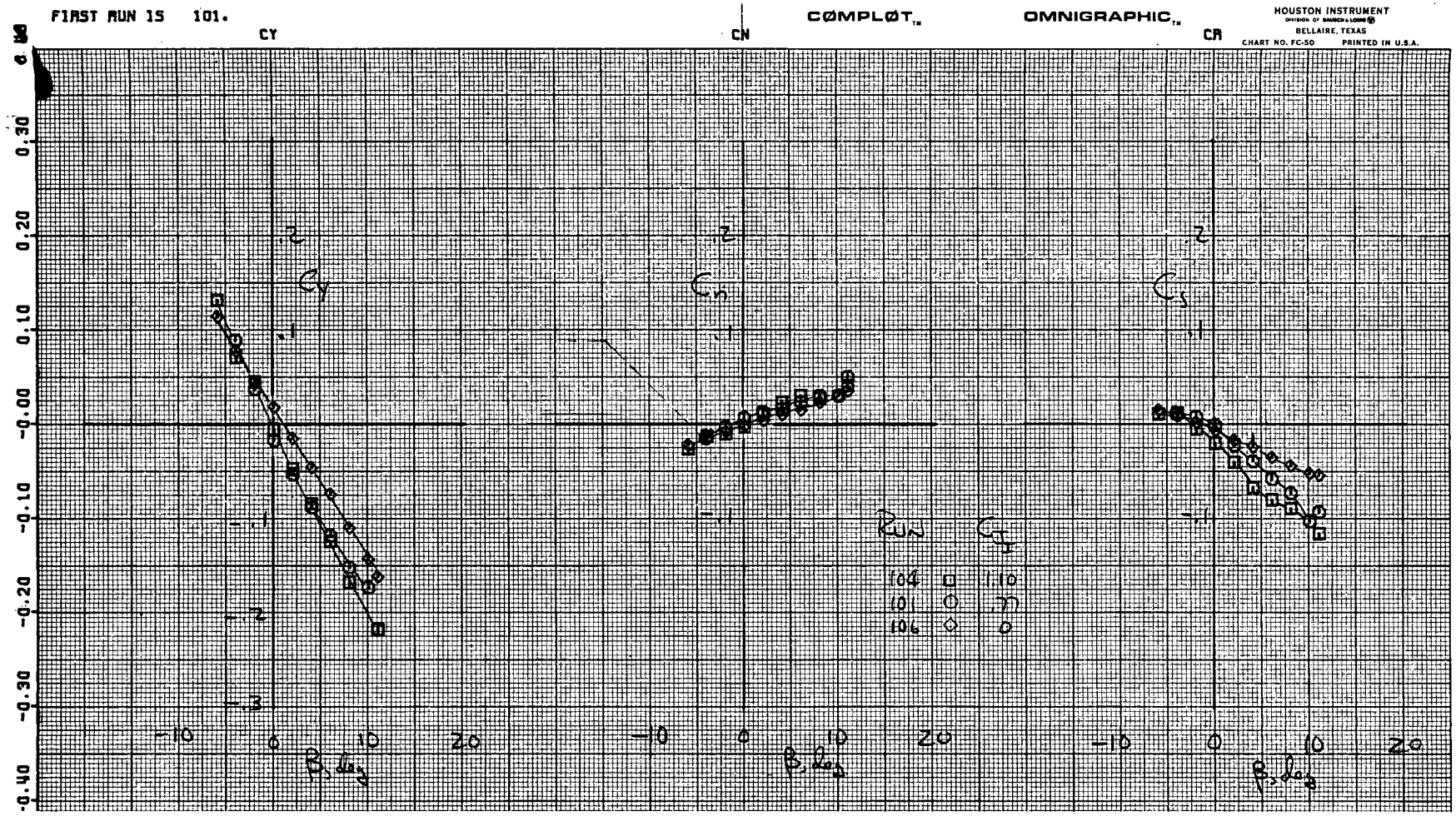

(a) Effect of C_{J_I}; $\alpha = 4°$

Figure 37.- Lateral-directional characteristics; $\delta_f = 41.1$.

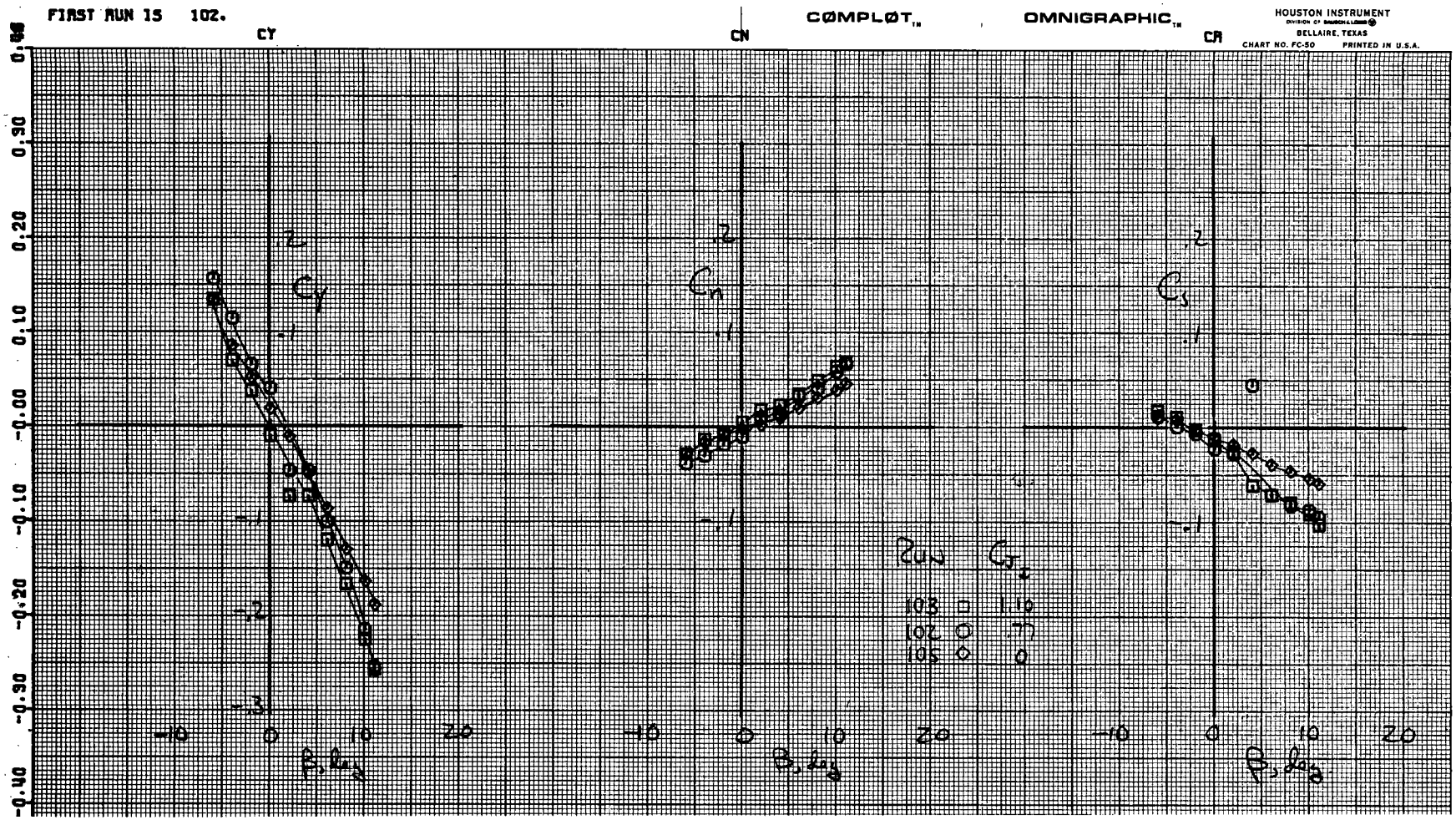

(b) Effect of C_{J_I}; α = 12°

Figure 37.- Continued.

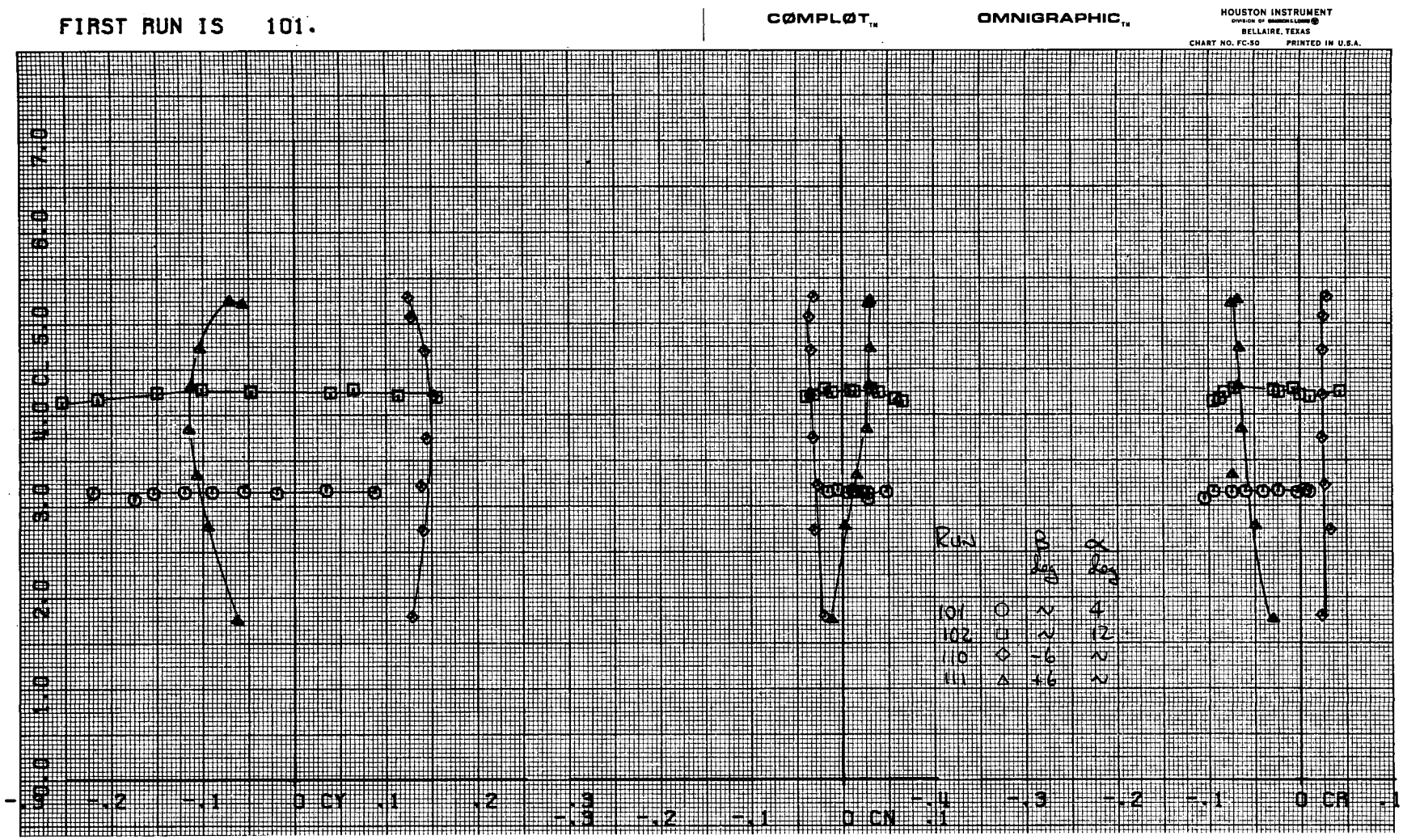

(c) Effect of α and β

Figure 37.- Concluded.

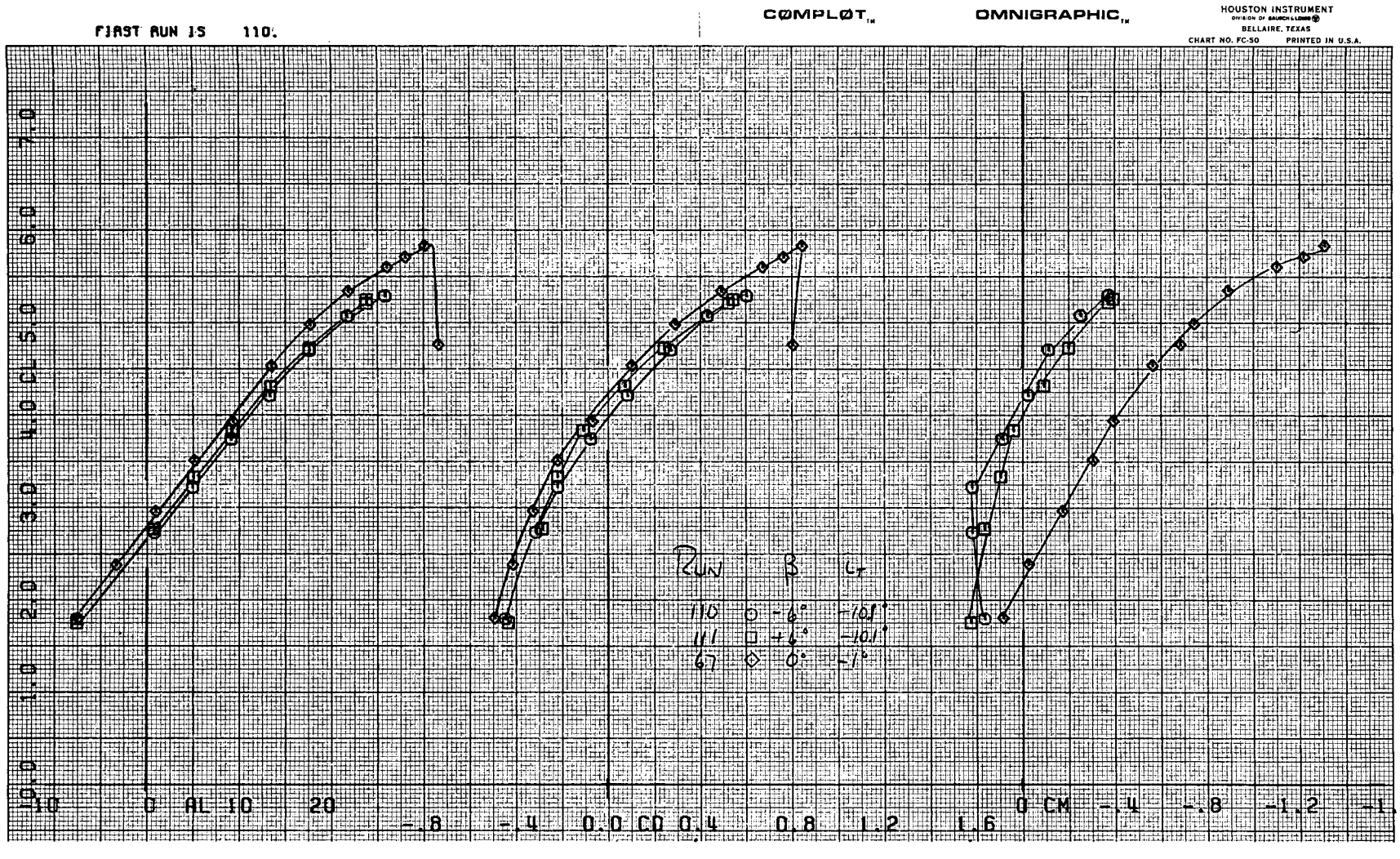

Figure 38.- Effect of sideslip on longitudinal aerodynamic characteristics with horizontal tail installed; δ_f = 41.1, δ_s = 60° (mod to stb'd).

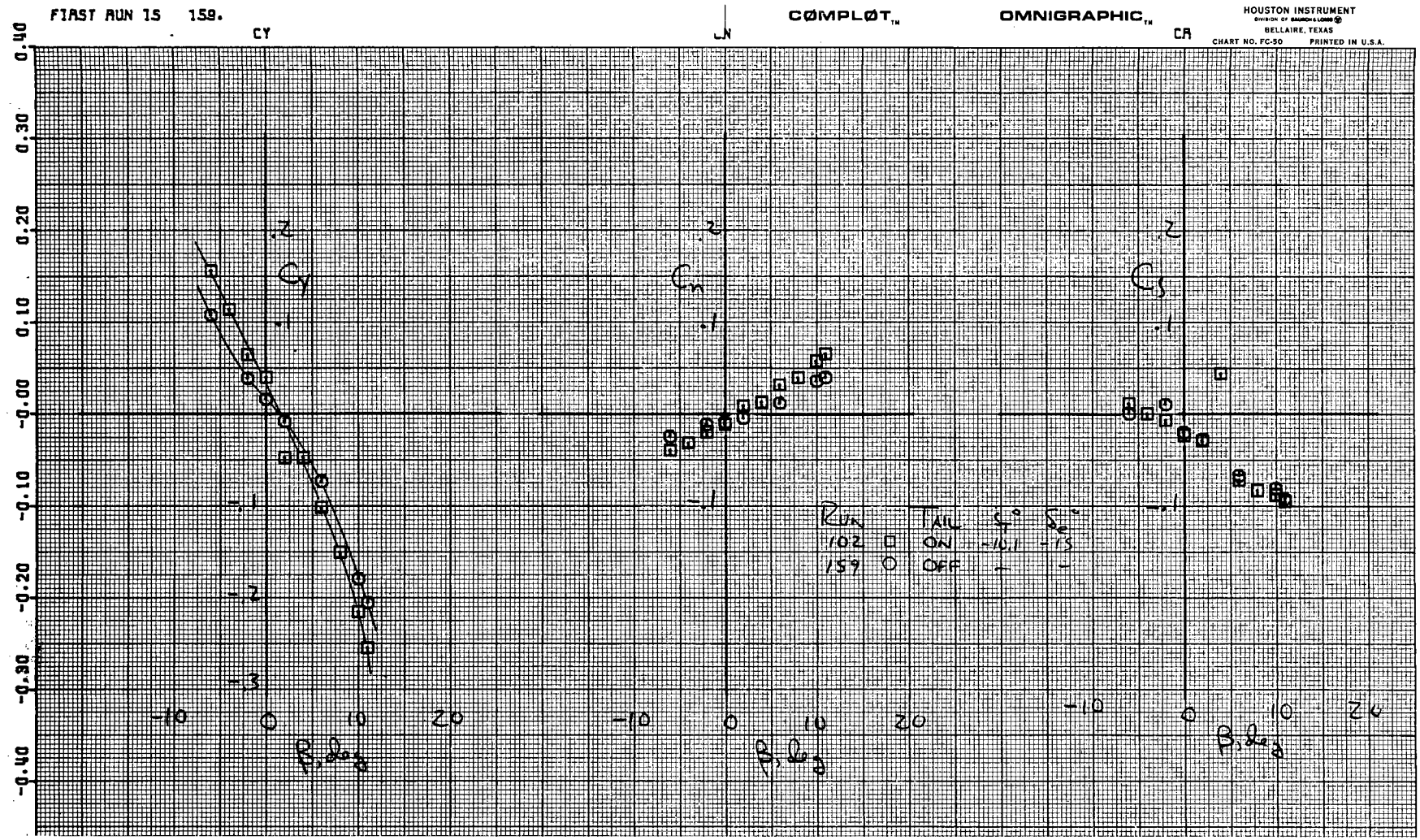

Figure 39.- Effect of horizontal tail on lateral-directional characteristics; $\delta_f = 41.1°$.